www.sciencemag.org/cgi/content/full/332/6034/1196/DC1

Supporting Online Material for

Scaling Up Digital Circuit Computation with DNA Strand Displacement Cascades

Lulu Qian and Erik Winfree*

*To whom correspondence should be addressed. E-mail: winfree@caltech.edu

Published 3 June 2011, *Science* **332**, 1196 (2011)
DOI: 10.1126/science.1200520

This PDF file includes:

Scaling up digital circuit computation with DNA strand displacement cascades

Supplementary information

Lulu Qian[1] and Erik Winfree[1,2,3]

[1] *Bioengineering,* [2] *Computer Science,* [3] *Computation and Neural Systems*
California Institute of Technology, Pasadena, CA 91125, USA

Contents

S1. Materials and methods

S1.1. Sequence design

All DNA strands in seesaw circuits consist of long recognition domains and short toehold domains, and these domains are functionally independent. Thus, sequence design was done at the domain level.

Software was written to generate distinct domain pools of the requested length according to the criteria proposed in Ref. [17]. These domain sequences use a three letter code (A, C and T) to reduce secondary structures and interactions [35, 36, 37], no more than 4 A's or T's in a row and no more than 3 C's in a row to reduce synthesis errors, and 30% to 70% C-content to ensure comparable melting temperatures [38]. For any two sequences in the pool, we require at least 30% of bases are different, and the longest run of matches is at most 35% of the domain length. As a result, undesired displacement by mismatched invading strands is unlikely. To build circuits that were demonstrated in this work, a pool of 15 nt recognition domains was generated. Each seesaw gate i was assigned with one recognition domain Si from the pool.

Because toehold domains cannot initiate branch migration without matching recognition domains, we use a universal toehold for all DNA strands. The only constraints on this toehold sequence are that it also uses the three letter code, it is strong enough to make seesawing as fast as possible, but weak enough to enable thresholding. The strand displacement rate reaches its maximum when the toehold length is 6 and decreases exponentially with toehold length (more accurately, free energy of the toehold) [7, 8]. Thus, ideally a toehold of 4 to 5 nt with an average number of C's provides thresholding with a 10- to 100-fold speed up compared to seesawing. In our initial experiments, a 4 nt universal toehold domain T with 2 C's was chosen (Figs. S14D and S17BC only; thereafter, we used a 5 nt universal toehold).

Given Si and T, all DNA strands were generated by directly concatenating these domains together. The two choices of strand orientation (e.g. $w_{2,5}$ could be either 5' $S2\ T\ S5$ 3' or 3' $S2\ T\ S5$ 5') should result in the same circuit function, if used consistently throughout the circuit. However, we chose the latter (as illustrated in Fig. 1C and other domain level specifications) because it matches the HgaI restriction enzyme cleaving site used to produce seesaw gates from hairpins (Fig. S20A). Incidentally, this choice might also have the benefit of reducing leak that is caused by chemical DNA synthesis errors such as truncations at the 5' end [39]. More detailed concatenating principles are shown in Fig. S15.

After we discovered a gate-gate leak caused by blunt end stacking initiated strand displacement (see SOM text S8 and Fig. S14), we added 'clamps' to the sequence design to reduce undesired strand displacement. Another pool of 15 nt recognition domains Si was generated, this time with a specified 2 nt clamp sequence c on both 5' and 3' ends. All the constraints for distinct domains remained the same. The clamp sequence was a random choice of the first two nucleotides of a recognition domain from the original pool. With clamps, the 5 nt universal toehold T becomes a variable element, containing a 3 nt toehold core t and the 2 nt clamp c on one side or the other. Considering the constraints of toehold domains, the 3 nt toehold core was randomly chosen with 1 C. All DNA strands were then generated by concatenating Si and T domains, with a different interpretation of T depending on whether it is on the left, right, or middle of recognition domains. Detailed concatenating principles are shown in Fig. S16.

For small circuits, designed DNA strands were verified by NUPACK [40] to ensure that no undesired secondary structures were found. Notice that the bottom strands of gates and thresholds are complementary domains of Si and T and thus contain A, G and T. However, except for the short toehold domains, they are always double-stranded throughout the computation. This three letter coding strategy efficiently reduces undesired interactions between single-stranded domains and enables faster circuit behavior compared to four letter coding [35, 39].

S1.2. Circuit preparation

After being designed, DNA oligonucleotides were purchased from Integrated DNA Technologies (IDT). All gate, threshold and fuel strands were ordered unpurified (standard desalting); all input strands were ordered purified by polyacrylamide gel electrophoresis (PAGE); and all reporter strands with fluorophore / quencher modifications were ordered purified by high-performance liquid chromatography (HPLC).

After being chemically synthesized and shipped as powder, DNA oligonucleotides were suspended in Milli-Q water (Millipore) and stored at 4 °C at ∼100 μM. For more accurate concentrations, input strands and reporter strands were first quantified using a BioPhotometer (Eppendorf). Absorbance at 260 nm ($OD260$)

was measured for each strand. We typically took the average of three measurements where a 1 μL sample was diluted with 99 μL Milli-Q water. Using the extinction coefficient (e, units: L/(mole·cm)) provided by IDT, the concentration (c, units: μM) of each strand was calculated as $c = 100 \times OD260/e \times 10^6$.

Reporter complexes were then annealed together at 20 μM, with a 20% excess of top strands (e.g. [Rep_6-t] / [Rep_6-b] = 1.2), in Tris-acetate-EDTA buffer containing 12.5 mM Mg^{2+} (1× TAE/Mg^{2+}). Because reporter top strands have no toehold domains and are modified with quenchers, this excess will ensure the formation of complexes even with somewhat imperfect stoichiometry, without leaving active single-stranded DNA or changing the fluorescence baseline. Annealing was performed in a PCR machine (Thermal Cycler, Eppendorf), first heating up to 95 °C, and then slowly cooling down to 20 °C at the rate of 1 °C/min.

Gate and threshold complexes need purification in addition to annealing, because either top strands or bottom strands in excess will cause undesired activities in a circuit. PAGE purification was employed to remove single-stranded DNA and poorly formed double-stranded complexes. Because of this extra step, gate and threshold complexes were quantified after purification, rather than for each unpurified strand before annealing. To obtain better yields in gel purification, gate and threshold strands were annealed together at higher concentrations of ∼45 μM, following the same procedure described above. 12% non-denaturing PAGE gels of 1.5 mm thickness were made by mixing 12 mL 19:1 40% acrylamide/bis, 4 mL 10× TAE/Mg^{2+} and Milli-Q water to 40 mL, then adding 240 μL APS and 24 μL TEMED to help polymerization. 10× BB non-denaturing dye (Bromophenol Blue 0.08 g, glycerol 10 mL and Milli-Q water to 20 mL) was added before annealed samples were loaded into the gels in a SE600 Vertical Electrophoresis Unit, 18×16 cm (Hoefer). We typically loaded 180 μL sample per lane, 2 lanes per sample, and kept one empty lane between different samples. Purification gels were run at 150 V for ∼6 hours at room temperature. We usually refresh the 1× TAE/Mg^{2+} running buffer every 1.5 hours. The proper bands (under UV light, only one clear dark band should be seen for each sample) were then cut from the gels, and the cut gel pieces were soaked in 1× TAE/Mg^{2+} solution (typically 1 mL prepared in a 1.7 mL test tube) for at least 12 hours at room temperature. After most DNA molecules presumably had come out from the gel pieces, the solution was extracted and the gel pieces were discarded. Finally, the purified gate and threshold complexes were quantified with the same protocol discussed above, except that we used 5 μL sample diluted with 95 μL Milli-Q water here because the purified samples had much lower concentrations compare to the single-stranded DNA in stock. Also, calculating extinction coefficients for double-stranded complexes was slightly different than for single-stranded species. We use $e = e(\text{top strand}) + e(\text{bottom strand}) - 3200N_{AT} - 2000N_{GC}$, where N_{AT} and N_{GC} are the number of AT pairs and GC pairs in the double-stranded domain, respectively [41].

To demonstrate the basic idea of parallel circuit preparation, a single seesaw gate and threshold were also generated from one single-stranded DNA each. Those two strands were first annealed to form hairpins at 20 μM, and then incubated with restriction enzymes at 37 °C overnight (in the manufacturer's recommended reaction buffers) to remove the undesired parts before gel purification (after which eluted complexes were in 1× TAE/Mg^{2+}). Restriction enzymes HgaI and MlyI were purchased from New England Biolabs (NEB). For more details see text S12 and Figs. S20 and S21.

S1.3. Kinetics experiments

Kinetics experiments were performed with a spectrofluorimeter (SPEX Fluorolog-3, Horiba). A maximum of four experiments can run in parallel on the instrument. 1.5 mL cuvettes were purchased from Hellma, either 119.004F-QS(round top) or 109.004F-QS(square top) with matching transmission numbers. Each set of four cuvettes was tested in our hands to show very little difference in fluorescence readout between cuvettes. The instrument also allows measuring with multiple excitation / emission pairs in one experiment. For circuits using only one reporter with the ROX fluorophore, excitation / emission was at 584 nm / 602 nm. For circuits using multiple reporters including the ROX fluorophore, excitation / emission at 588 nm / 608 nm was included. For circuits using reporter with the FAM fluorophore, excitation / emission at 495 nm / 520 nm was included. For circuits using reporter with the TYE563 fluorophore, excitation / emission at 549 nm / 563 nm was included. For circuits using reporter with the TYE665 fluorophore, excitation / emission at 647 nm / 664 nm was included. For circuits using reporter with the Cy5.5 fluorophore, excitation / emission at 685 nm / 706 nm was included. The fluorescence signals of the above five fluorophores were tested to have no noticeable interference with each other when used in the same circuit. For circuits using a reporter with TET fluorophore, excitation / emission was at 524 nm / 541 nm. Both

excitation and emission bandwidths were 2 nm and the integration time was 10 s for all experiments. In single reporter experiments, data was taken every minute; in multiple reporter experiments, data points decreased proportionally with the number of reporters because the reading for each wavelength required 1 min. Experiments for the square root circuit were done at 25 °C while all other experiments were done at 20 °C, except the study of temperature and circuit behavior (see text S11 and Fig. S19). Cuvettes were thoroughly cleaned with distilled water and 70% ethanol between experiments.

S1.4. Fluorescence data normalization

All raw data of fluorescence signals were normalized to relative concentrations of output signals when plotted. As mentioned above, our spectrofluorimeter can run four parallel kinetics experiments and the difference in fluorescence readout caused by the instrument is neglectable among these parallel experiments. Each set of parallel experiments we performed was of the same circuit with different inputs, and had at least one experiment in which a given output signal stayed OFF and one in which that output signal went ON.

For a given fluorophore, most sets of parallel experiments had at least one of the four output signals that went all the way to completion (maximally ON). In this case, the minimum level (output=0) was determined by the minimum of all four parallel data points at t=0; while the maximum level (output=1) was determined by the average of the last 5 data points if the fluorescence level went high and flattened out at the end of the experiment, and otherwise it was determined by the maximum level of a parallel experiment. For example, the four experiments of the two-input OR gate with inputs 00, 01, 10 and 11 shown in Fig. 2C were performed in parallel. All four trajectories were normalized to a minimum level determined by the data point at t=0 with input 00, and a maximum level determined by the average of the last 5 data points with input 11. Fluorescence data shown in Figs. 1E, 3CED, S2E, S5B, S6BD, S7B, S8BC, S9BC, S14DE, S17BD, S18C, S19D and S21DE were also normalized in this way. Note that the experiments were usually longer than plotted, thus the trajectories that do not look flattened out in these figures but actually flattened out at the end of the experiments were still used to determine the maximum level.

In the sets of experiments where none of the four output signals went all the way to completion (maximally ON) at the end of the experiments, we performed a post-experiment triggering step in which we added an excess of the inputs to the gates that directly generate the circuit outputs (i.e., the gates immediately upstream of the reporters), and then stopped data collection after the signals flattened out. In this case, the maximum level was determined by the average of the last 5 data points after the output signals were triggered to completion. (This post-experiment triggering protocol was chosen, rather than for example directly triggering the reporter, in order to reduce variability: the 1× concentration of strands released from an upstream gate is exactly the same whether triggered manually or by further upstream circuitry, whereas normalizing based on the 1.5× of directly triggered reporter introduces error due to reporter and gate stock concentrations measurement inconsistencies.) For example, the four experiments of the square root circuit with inputs 0001, 1000, 1100 and 1110 shown in Fig. S11 were performed in parallel. All four trajectories of output y_1^0 (dotted red lines) and y_2^0 (dotted black lines) were normalized in this way. At least one of the four trajectories of output y_1^1 (solid red lines) and y_2^1 (solid black lines) went all the way ON at the end of the experiment, thus these two sets of data were normalized with the first method. Similarly, fluorescence data shown in Figs. 4CD, S11 and S13 were also half normalized with the first method and half with the second.

S1.5. Gel electrophoresis

To examine the gate and threshold prepared from enzyme cutting hairpins, non-denaturing PAGE was run using a 15% gel at 100 V for 2.5 hours. After staining with SybrGold (Invitrogen) for 15 to 20 min, the gel was scanned on a Molecular Imager FX Pro Plus (Bio-Rad).

S1.6. Summary of a typical square root experiment

We annealed and purified all the double-stranded complexes in a week (preparing the gate components); pipetted and mixed all the DNA molecules into one cuvette in an hour (wiring the gates into a circuit); added the input strands in 5 minutes (setting the input signals); and waited for the fluorescence signal to go up in 10 hours (running the circuit and reading the output signals).

S2. A seesaw DNA catalyst

In strand displacement circuit designs, the structure of the DNA double helix is often neglected, and the sequence design is usually independent of the intended circuit function. Thus, instead of showing the DNA implementations at the helix level or sequence level, we prefer illustrations at the domain level (Fig. S1A). Furthermore, to enable complex circuit design, we present seesaw circuits using a systematic abstraction (Fig. S1B). The initial state of a circuit is specified by the relative concentrations of all DNA species. The final state, which reflects the circuit function, can be roughly estimated, more accurately calculated, or determined by simulation. When there is initially a threshold of 0.5× in the single seesaw gate circuit, the input, at 0.6×, first has to overcome the threshold before it can react with the gate:output complex (top pathway in Fig. S1C). Then the remaining 0.1× of the input serves as a catalyst for the exchange of fuel and output (bottom pathway in Fig. S1C). In this catalytic cycle, input initially reacts with the gate:output complex, releasing the output and in turn producing the input:gate complex (bottom right pathway in Fig. S1C). Because there is much more fuel than output, the input:gate complex will prefer to react with the fuel, generating the gate:fuel complex while freeing the input (bottom left pathway in Fig. S1C). At this point, the input has a choice to either react with the gate:output complex or the gate:fuel complex, but it will always get bounced back by the fuel (because there is always a lot more fuel than output), resulting in accumulation of the gate:fuel complex and consumption of the gate:output complex until the circuit reaches its equilibrium. At the final state (equilibrium), detailed balance requires every wire connected to the same gate to have the same ratio of free signal and gate:signal complexes. For example, with the specific circuit and initial concentrations shown in Fig. S1B, given that the free and bound fuel has to be 10× total (constrained by the initial amount of free fuel) and at most 1× fuel can bind to the gate (constrained by the amount of gate base strand which is equal to the initial amount of bound output), the ratio of free and bound fuel can't be less than 9×. Because this same ratio must apply to both input and output, almost all input and output will stay free. In summary, if there is a large amount of fuel relative to the gate species, then the ratio on that wire must always remain high, so at equilibrium the output wire must also have a large fraction of signal strands free. Accurate calculation of equilibria for arbitrary seesaw circuits was discussed in [17].

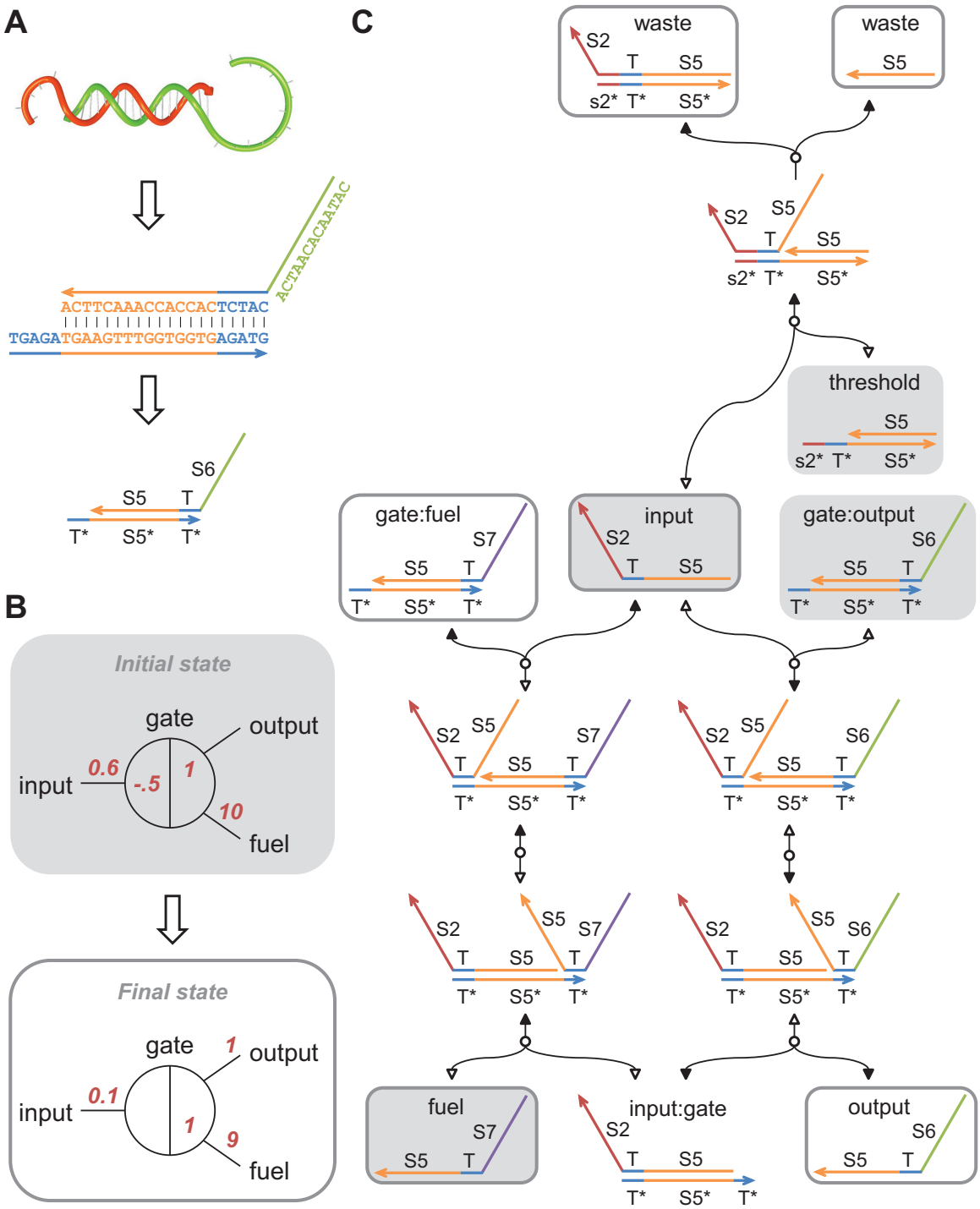

Figure S1: Representation and mechanism of a seesaw DNA motif. (A) Helix level, sequence level and domain level illustrations of a seesaw DNA gate. $S5$ and $S6$ are long recognition domains. T is a short toehold domain. T^* is the Watson-Crick complement of T, etc. (B) Abstract diagram of a seesaw gate motif with an example of an initial state and its final state. Red numbers indicate relative concentrations of initial species (0.6× input, 0.5× threshold, 1× gate:output complex and 10× fuel) and final species (0.1× input, 1× gate:fuel complex, 1× output and 9× fuel). Numbers in the final state are approximations. (C) Reaction pathways of a seesaw catalyst with threshold. Shaded boxes highlight the initial species and transparent boxes outline the final species. Solid arrows indicate flows of the forward reactions and outlined arrows indicate flows of the respective backward reactions. Matching colors and domain names suggest where binding or branch migration can occur. $s2^*$ is the first few nucleotides of $S2^*$ from the 3' end, forming a longer toehold together with T.

Given an abstract diagram (e.g. Fig. S2C), DNA implementations of the seesaw circuit can be easily translated (e.g. Fig. S2D). Each red number on a wire from the right side of gate i to the left side of gate (or reporter) j indicates the initial relative concentration of $w_{i,j}$ (e.g. $w_{2,5}$ and $w_{5,7}$), which is implemented as a free signal strand with sequence $SiTSj$. Each positive red number within a gate node i at the end of a wire from the right side of gate i to the left side of gate (or reporter) j indicates the initial relative concentration of $G_{i:i,j}$ (e.g. $G_{5:5,6}$), which is implemented as the gate i base strand $T^*Si^*T^*$ bound to the left side of signal strand $SiTSj$. Not shown in this figure, each negative red number at the same place as $G_{i,j:j}$ indicates the initial relative concentration of $Th_{i,j:j}$. Each negative red number within a reporter half node i indicates the initial relative concentration of Rep_i (e.g. Rep_6), which is implemented as strand Si modified with a quencher bound to strand T^*Si^* modified with a fluorophore. Thresholds and reporters are indicated by negative numbers because they both absorb free signal strands.

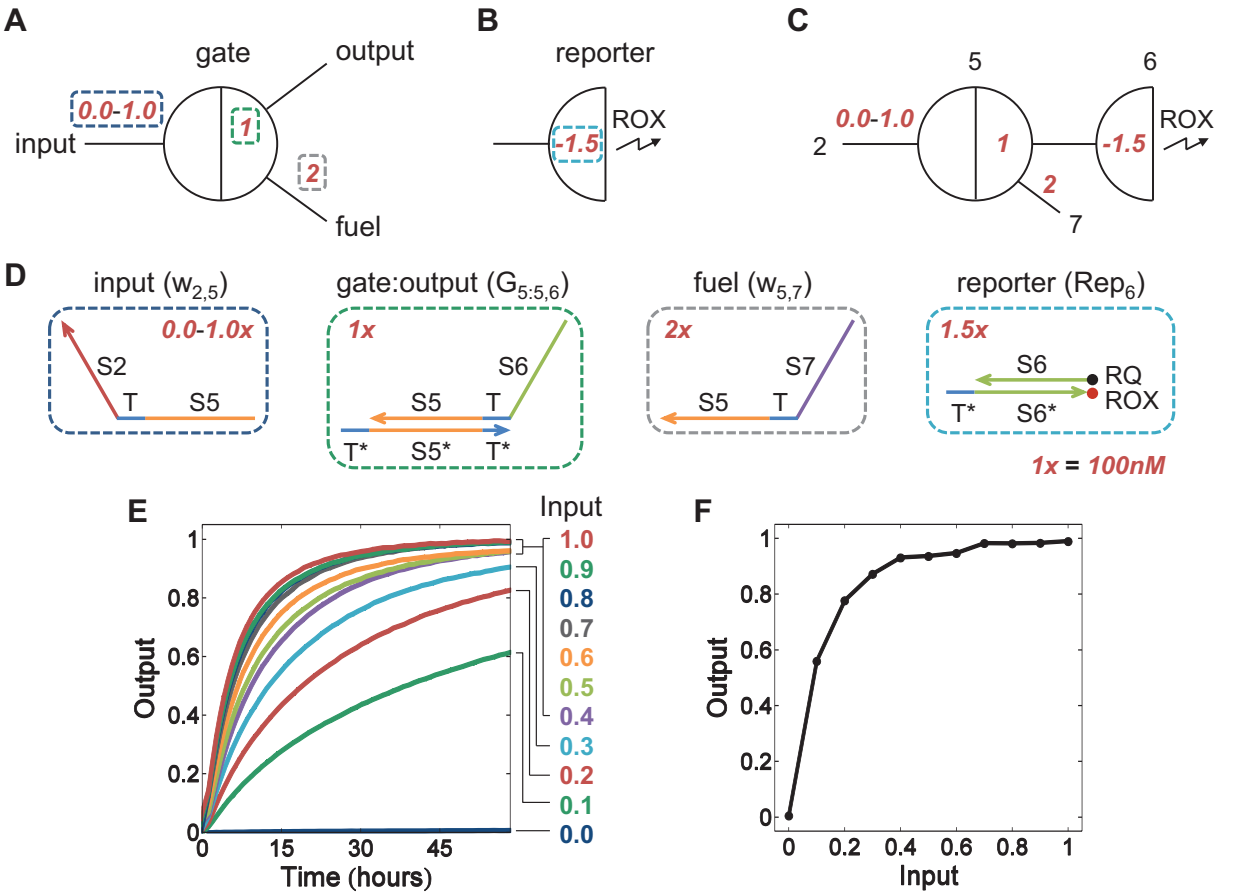

Figure S2: Demonstration of a seesaw catalyst. (A) Abstract diagram of a seesaw catalyst with relative concentrations of initial species highlighted in colored boxes. (B) Abstract diagram of a reporter with its initial relative concentration highlighted in a colored box. (C) Abstract diagram of the seesaw catalyst connected with the reporter. Black numbers identify seesaw gates. (D) DNA implementations of the seesaw catalyst and the fluorophore-labeled reporter. Matching colored boxes highlight DNA species represented in the abstract diagrams. Text in parentheses are names of these species following a systematic naming scheme for seesaw networks. (E) Kinetics experiments of the seesaw catalyst. Gate:output complex, fuel strand and reporter complex were mixed in solution with relative concentrations of 1×, 2× and 1.5× respectively (1×=100 nM). Input strands were then added with concentrations varying from 0.0× to 1.0× in increments of 0.1×. The top strand of the reporter complex was modified with a 5' Iowa Black RQ quencher; the bottom strand was modified with a 3' ROX fluorophore. Sequences of strands are listed in Tables S2 and S3, circuit 1. Experiments were performed at 20 °C in Tris-acetate-EDTA buffer containing 12.5 mM Mg^{2+}. Output signals were inferred by fluorescence signals normalized to a fraction of the maximum completion level. (F) Input vs. output plot of E. The output at ∼1 hour is re-plotted against the relative concentrations of the initial input.

S3. Design constraints in amplifying gates and integrating gates

Note that only one input is allowed in amplifying gates and no threshold is allowed in integrating gates. This is because multiple inputs with thresholds will raise the issue of 'threshold crosstalk' (Fig. S3), meaning that one input (e.g. $w_{1,5}$) can be absorbed by the threshold of another input (e.g. $Th_{2,5:5}$) due to the same initial toehold sequence T^* even if the extra bases are different. Consequently, after one input exceeds its own threshold, having reacted at a fast rate, it will continue to be absorbed by the other threshold – at roughly the same slower rate with which it reacts with the gate:output complex.

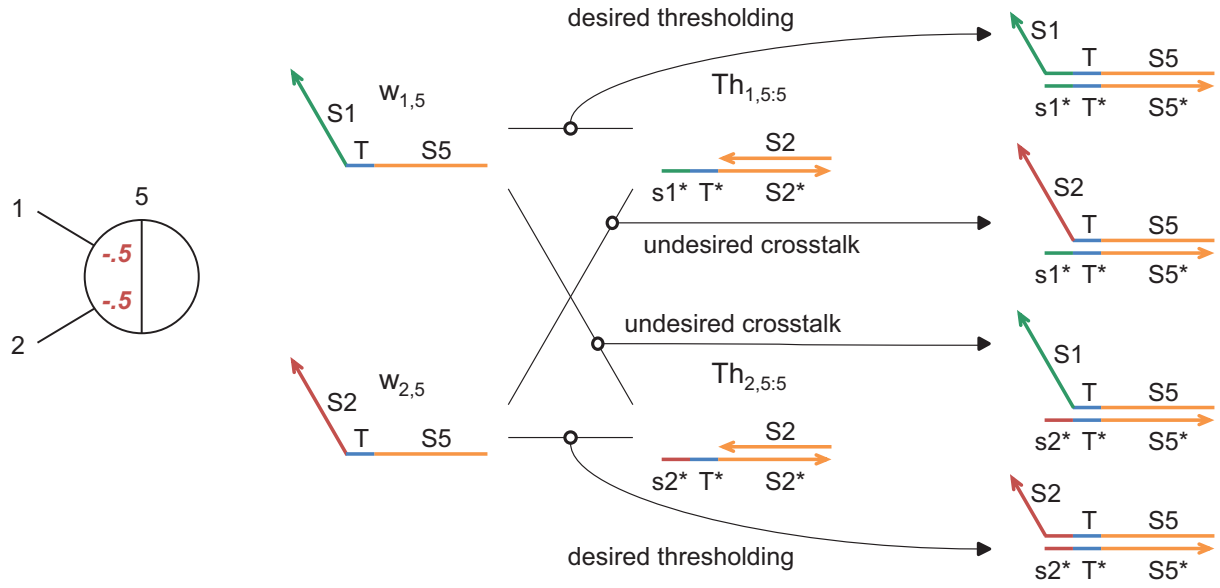

Figure S3: Threshold crosstalk – the issue of multiple inputs with thresholds.

Also, no fuel is allowed in integrating gates and no amplifying gate is allowed to connect to a directly downstream amplifying gate. This is because an upstream fuel (e.g. $w_{2,7}$) can inhibit a directly downstream threshold (e.g. $Th_{2,5:5}$) by binding to it via the same extended toehold (e.g. $s2^*T^*$) that the input (e.g. $w_{2,5}$ released from $G_{2:2,5}$) uses to bind to the threshold. Such interactions will take significantly longer to resolve, because nucleic acid dissociation rates decrease exponentially with the number (more accurately, free energy) of base pairs that must be broken [42]. As a consequence, these threshold reactions will be slowed down more than gate reactions, decreasing their effectiveness as thresholds. We call this 'threshold inhibition' (Fig. S4).

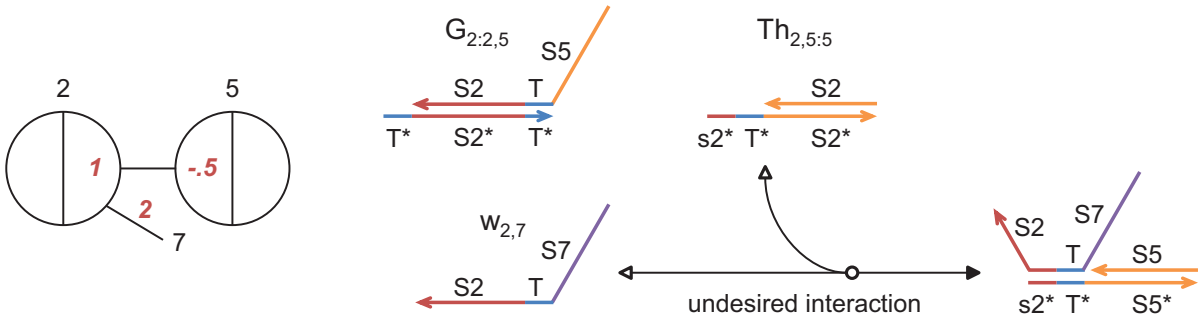

Figure S4: Threshold inhibition – the issue of fuel with a directly downstream threshold.

S4. Logic computation cascades

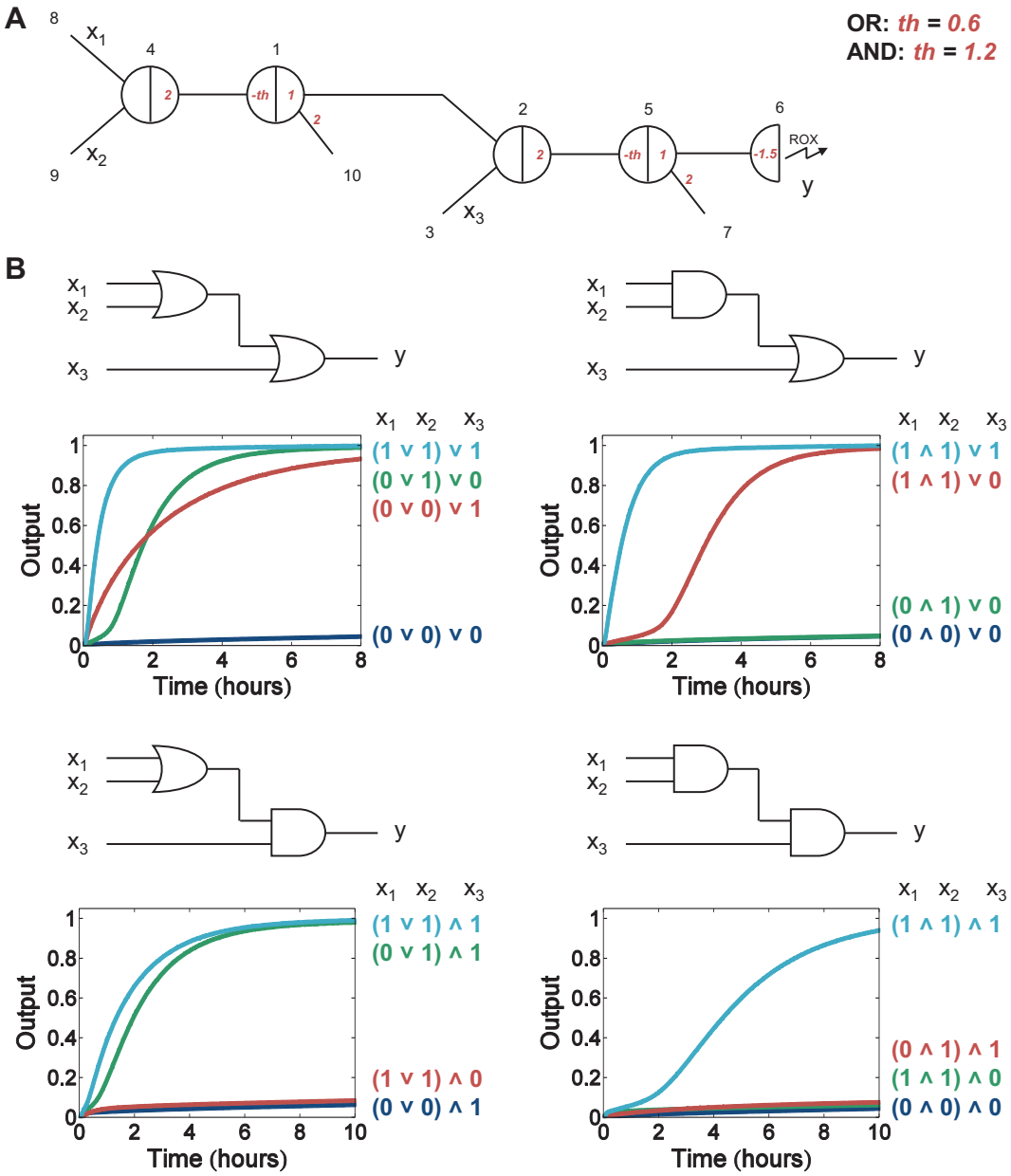

Figure S5: Two-layer AND/OR cascades. (A) Abstract diagram of two-layer seesaw AND/OR cascades. Functions depend on the initial concentration of the threshold. (B) Kinetics experiments of the two-layer AND/OR cascades. Sequences of strands are listed in Tables S2 and S3, circuit 4. Trajectories and their corresponding inputs have matching colors. Inputs were added with relative concentrations of 0.1× (0, logic OFF) or 0.9× (1, logic ON) where the standard concentration 1×=100 nM. Experiments were performed at 20 °C in Tris-acetate-EDTA buffer containing 12.5 mM Mg^{2+}.

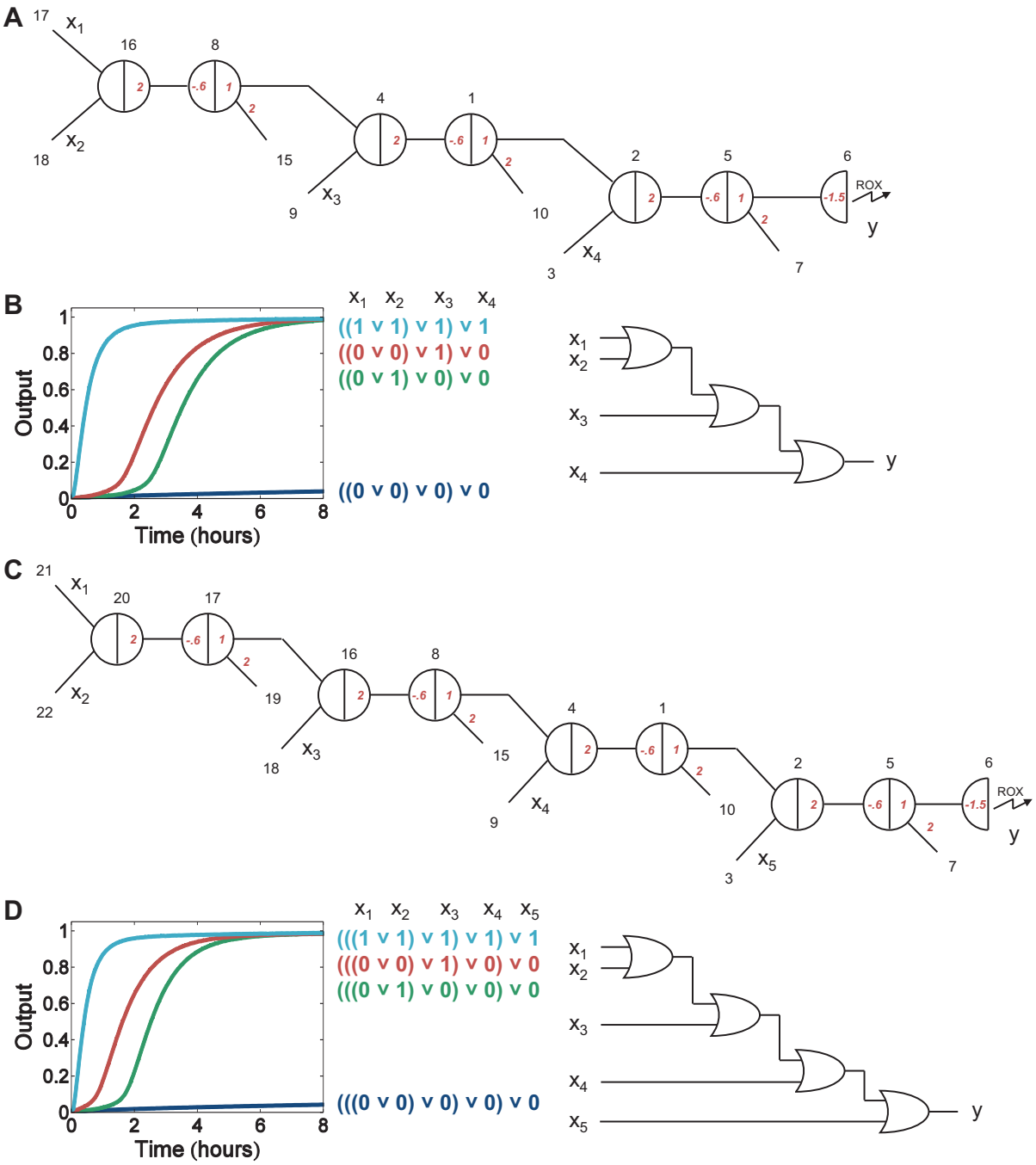

Figure S 6: Multi-layer OR cascades. (A) Abstract diagram of a three-layer seesaw OR cascade. (B) Kinetics experiments of the three-layer OR cascade. Sequences of strands are listed in Tables S2 and S3, circuit 5. (C) Abstract diagram of a four-layer seesaw OR cascade. (D) Kinetics experiments of the four-layer OR cascade. Sequences of strands are listed in Tables S2 and S3, circuit 6. Trajectories and their corresponding inputs have matching colors. For the OR cascade delay and switching time plots (Fig. 3AB), data from all-OR cascades in Figs. 2, S5, and S6 were used whenever the input consisted of exactly one ON state signal, with the exception of the red trace of Fig. S5B, which was anomalously slow (presumably due to sequence design problems). Inputs were added with relative concentrations of 0.1× (0, logic OFF) or 0.9× (1, logic ON) where the standard concentration 1×=100 nM. Experiments were performed at 20 °C in Tris-acetate-EDTA buffer containing 12.5 mM Mg^{2+}.

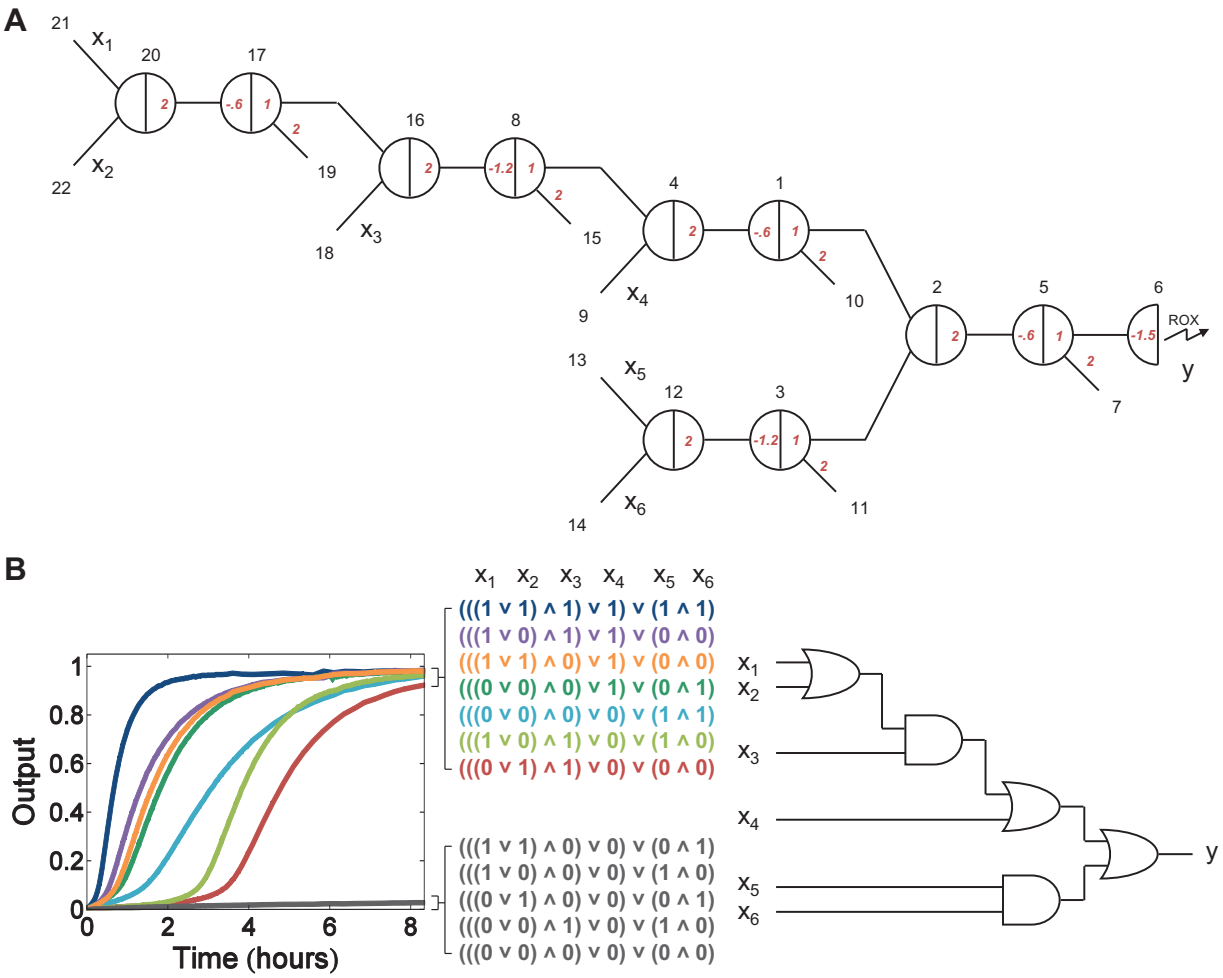

Figure S7: A circuit with five AND/OR gates and four layers. (A) Abstract diagram of the seesaw circuit. (B) Kinetics experiments of the seesaw circuit. This is the same data as is plotted in Fig. 3C. Note that the three slowest traces are for inputs that require the circuit to wait for a slow AND gate. Sequences of strands are listed in Tables S2 and S3, circuit 7. Trajectories and their corresponding inputs have matching colors. Inputs were added with relative concentrations of 0.1× (0, logic OFF) or 0.9× (1, logic ON) where the standard concentration 1×=100 nM. Experiments were performed at 20 °C in Tris-acetate-EDTA buffer containing 12.5 mM Mg^{2+}.

S5. Fan-in and fan-out

In AND gates, additional fan-in requires increasing the threshold, which results in a slowdown for the same reason that a two input AND gate is slower than an OR gate (Fig. S8). In contrast, in both AND and OR gates, increasing the fan-out has no discernible effect on speed (Fig. S9). This can be explained by the linearity of reaction rates on concentration: the same catalytic input reacts with more gate complexes and more fuel, both of which scale with fan-out.

For an n-input AND/OR gate, there are two initial concentrations that increase with n: (1) In the integrating gate, the bound output concentration is n times $1\times$, which is the maximum input sum, for each input being ON. (2) In the amplifying gate, when it is OR fan-in, the threshold is above the maximum of n inputs being OFF and below the minimum of one input being ON; when it is AND fan-in, the threshold is above the maximum of $n-1$ inputs being ON and below the minimum of n inputs being ON. For an n-output AND/OR, the initial bound output is still $1\times$ for each fan-out wire and the initial free fuel is n times $2\times$ in the amplifying gate.

The AND/OR fan-out mechanism is not limited by the degree of fan-out, but the fan-in mechanism has a limiting constraint. For example, consider a digital abstraction with the OFF state range being $0\times$-$0.1\times$ and the ON state range being $0.9\times$-$1\times$. In order to satisfy the threshold inequalities described above, the lower bound has to be smaller than the upper bound. That gives $0.1n < 0.9$ for OR and $(n-1)+0.1 < 0.9n$ for AND, so the maximum fan-in number is 8 in both cases. As an alternative, fan-in can also be implemented as a binary tree of two-input AND/OR gates.

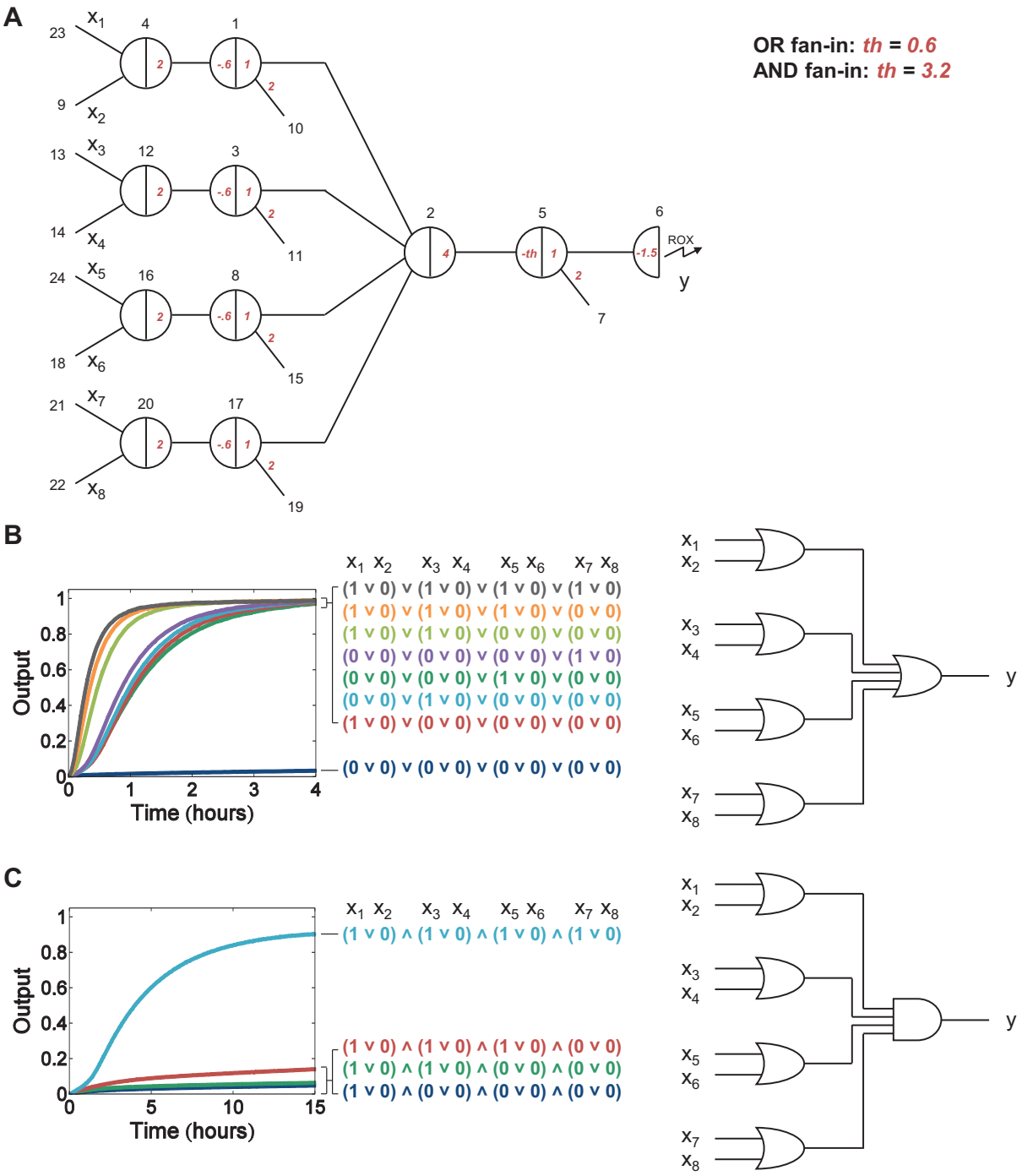

Figure S 8: Circuits with four-input AND or OR gates. (A) Abstract diagram of a seesaw circuit with a four-input AND or OR gate, depending on the initial concentration of the threshold. (B) Kinetics experiments of the circuit with an OR gate with fan-in from four OR gates. This is the same data as is plotted in Fig. 3D. (C) Kinetics experiments of the circuit with an AND gate with fan-in from four OR gates. Sequences of strands are listed in Tables S2 and S3, circuit 8. Trajectories and their corresponding inputs have matching colors. Inputs were added with relative concentrations of 0.1× (0, logic OFF) or 0.9× (1, logic ON) where the standard concentration 1×=100 nM. Experiments were performed at 20 °C in Tris-acetate-EDTA buffer containing 12.5 mM Mg^{2+}.

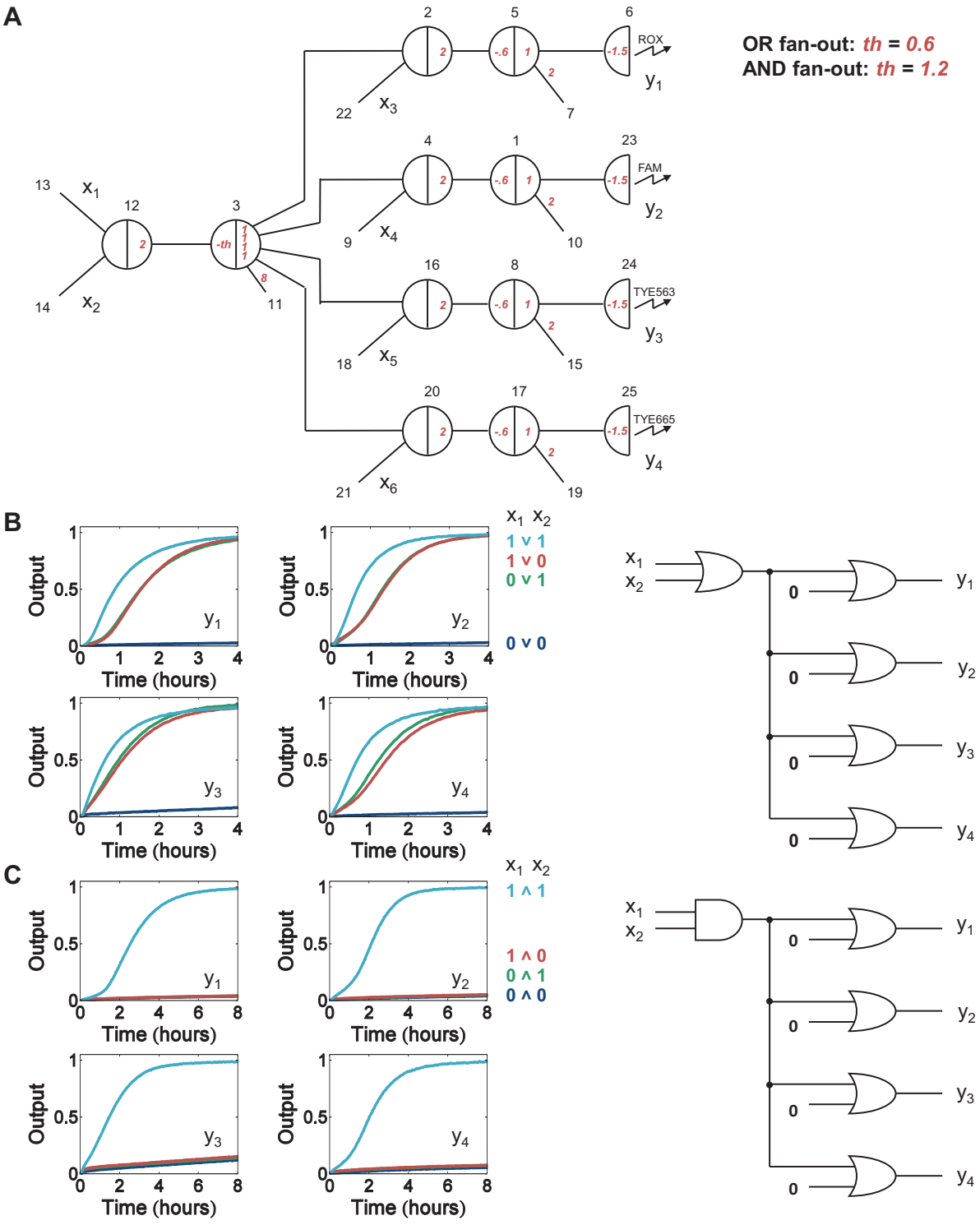

Figure S9: Circuits with four-output AND or OR gates. (A) Abstract diagram of a seesaw circuit with a four-output AND or OR gate, depending on the initial concentration of the threshold. (B) Kinetics experiments of a seesaw circuit with an OR gate with fan-out to four OR gates. This is the same data as is plotted in Fig. 3E. (C) Kinetics experiments of the circuit with an AND gate with fan-out to four OR gates. Sequences of strands are listed in Tables S2 and S3, circuit 9. Trajectories and their corresponding inputs have matching colors. Inputs were added with relative concentrations of 0.1× (0, logic OFF) or 0.9× (1, logic ON) where the standard concentration 1×=100 nM. Experiments were performed at 20 °C in Tris-acetate-EDTA buffer containing 12.5 mM Mg^{2+}.

S6. A square root circuit

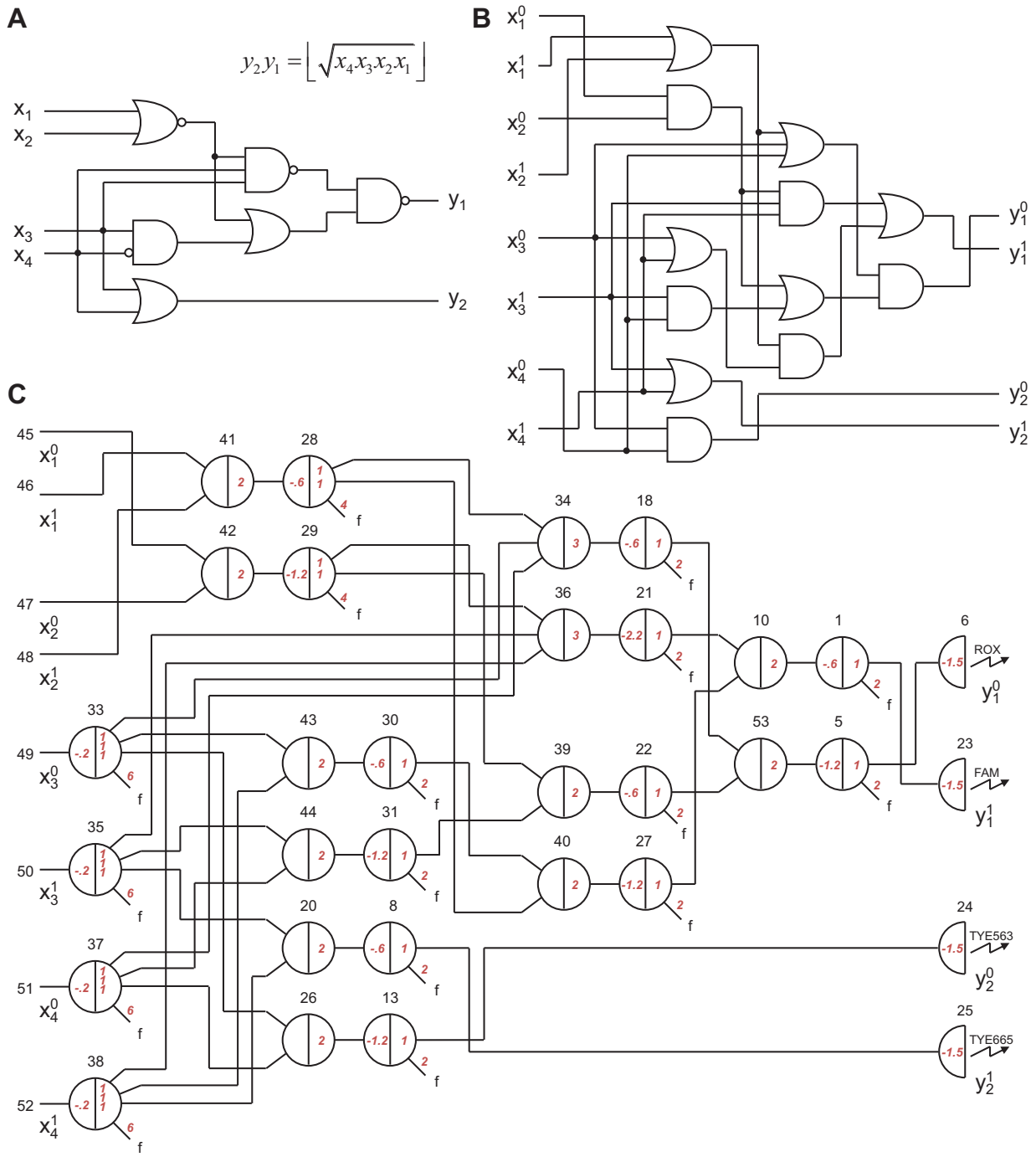

Figure S10: Abstract diagrams of a square root circuit. (A) A digital logic circuit that computes the floor of the square root of a four-bit binary number. (B) Abstract diagram of the dual-rail circuit that is equivalent to the square root circuit. (C) Abstract diagram of the seesaw circuit that is equivalent to the dual-rail circuit.

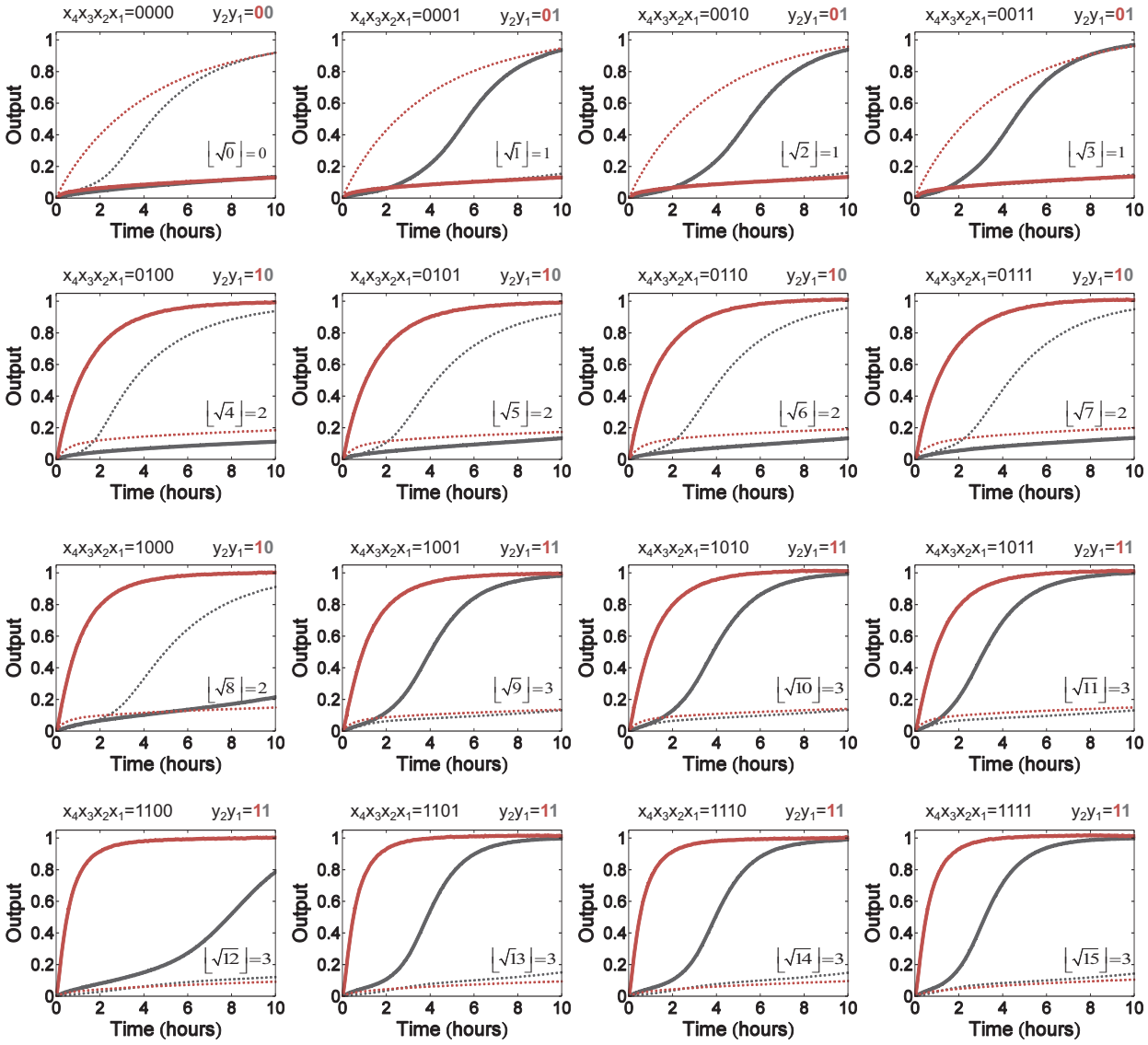

Figure S11: Kinetics experiments of the square root circuit with all 16 combinations of inputs from 0000 to 1111. This is the same data that is presented in a condensed form (superimposed) in Fig. 4C. Sequences of strands are listed in Tables S4 to S7. Trajectories and their corresponding outputs have matching colors. Dotted lines indicate dual-rail outputs that represent logic OFF; solid lines indicate dual-rail outputs that represent logic ON. ROX, FAM, TYE563 and TYE665 fluorophores were used to simultaneously report the two pairs of dual-rail outputs. Inputs were added with relative concentrations of 0.1× (0, logic OFF) or 0.9× (1, logic ON) where the standard concentration 1×=50 nM. Experiments were performed at 25 °C in Tris-acetate-EDTA buffer containing 12.5 mM Mg^{2+}.

S7. Internal readout

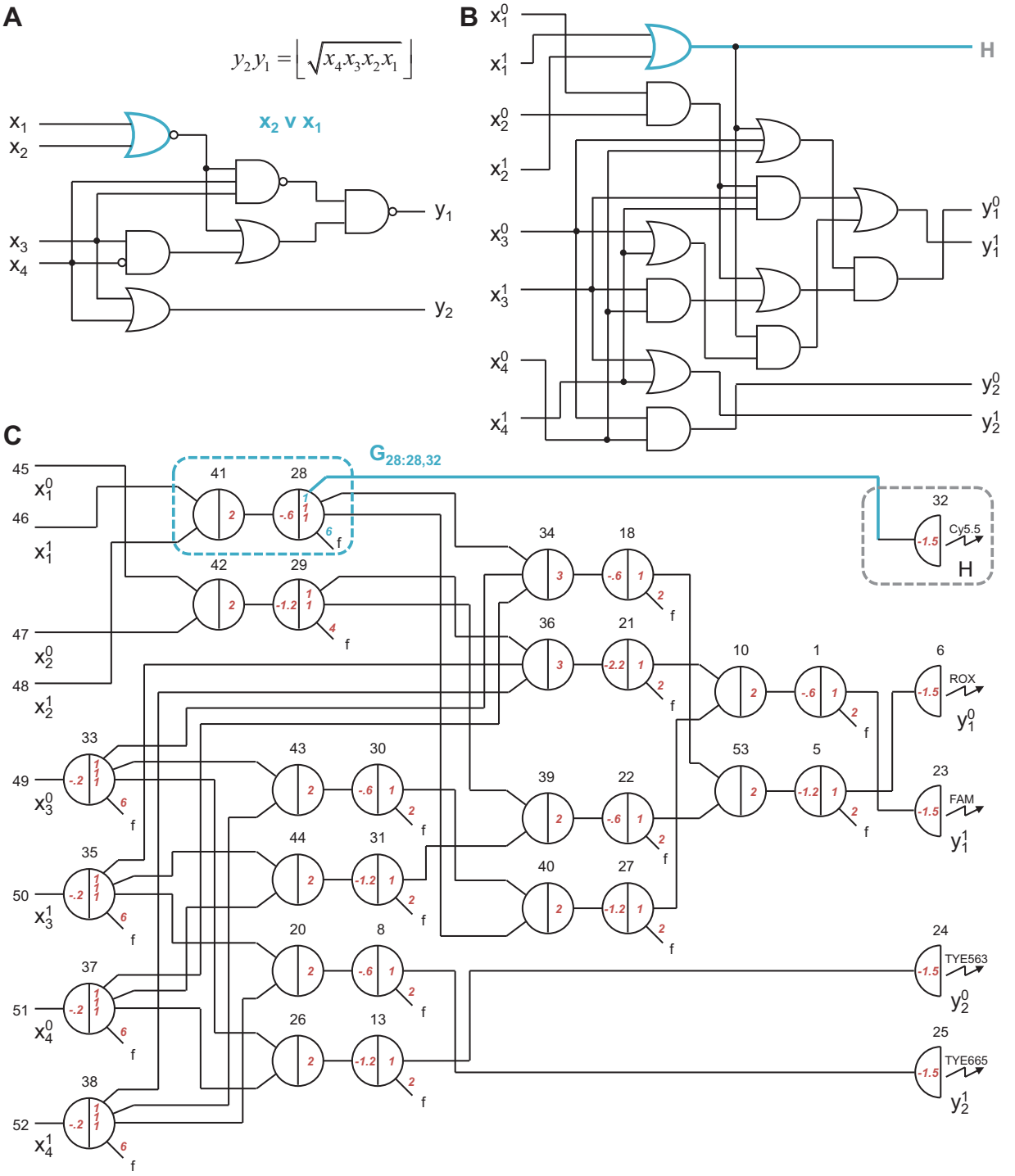

Figure S 12: Abstract diagrams of the square root circuit with the fifth reporter wired to an internal gate. (A) Original digital logic diagram with the targeted gate highlighted in blue. (B) Dual-rail logic diagram with the target gate highlighted in blue. Note that with a single debugging reporter, only one of the dual-rail signals for the NOR gate can be read out at a time. Here we choose the signal representing logic OFF, which is actually the internal output of x_1 OR x_2. (C) Seesaw circuit diagram with the targeted gate highlighted in blue and the debugging reporter explicitly shown.

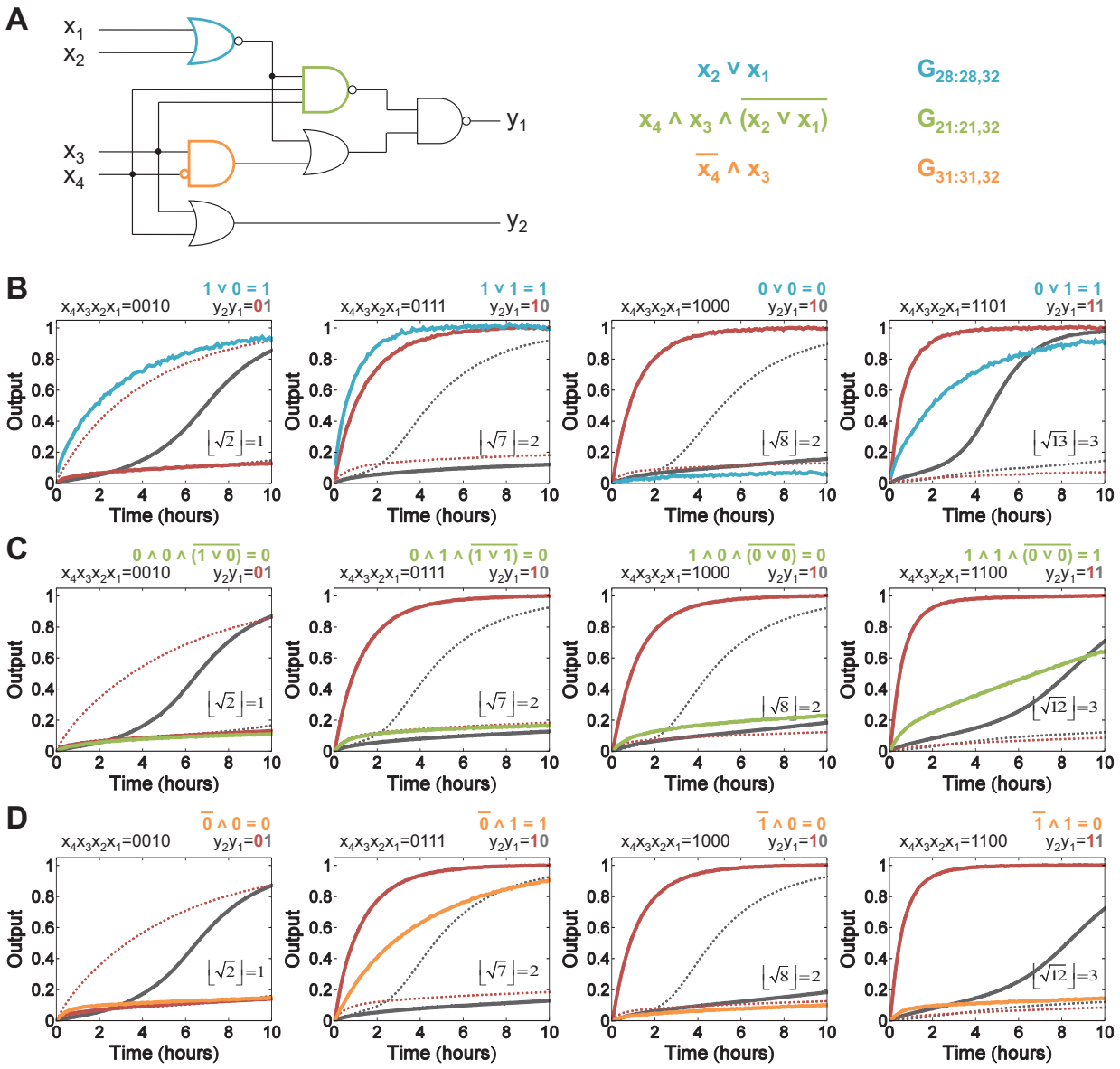

Figure S13: Kinetics experiments of the square root circuit with the fifth reporter wired to three internal gates (three distinct configurations). (A) The square root circuit with targeted internal gates identified, along with their associated (and color-coded) logic formulas and the gate:signal complex required to wire the targeted gate to the debugging reporter. (B) Reading out gate 28 (blue) while simultaneously reading out y_1^0, y_1^1, y_2^0, and y_2^1 for comparison with experiments of Fig. S11 using the same inputs. (C) Reading out gate 21 (green). (D) Reading out gate 31 (orange). Sequences of strands are listed in Tables S4 to S7. The Cy5.5 fluorophore was used for the fifth reporter. Inputs were added with relative concentrations of 0.1× (0, logic OFF) or 0.9× (1, logic ON) where the standard concentration 1×=50 nM. Experiments were performed at 25 °C in Tris-acetate-EDTA buffer containing 12.5 mM Mg^{2+}.

S8. System leak and other side reactions

In addition to the three basic reactions (seesawing, thresholding and reporting) intended in a seesaw circuit, a number of side reactions also occur.

First, even without a toehold, a single-stranded DNA domain can displace an identical domain from a double helix, albeit at a rate five or six orders of magnitude slower than the fastest rate for toehold-mediated strand displacement [7, 8]. Examples include (1) 'fuel-gate leak' where, with reference to Fig. S2D, fuel $w_{5,7}$ reacts directly with $G_{5:5,6}$, yielding output $w_{5,6}$ and $G_{5:5,7}$ even in the absence of input $w_{2,5}$, and (2) 'gate-gate leak' where, as shown in Fig. S14A, the single-stranded $S5$ domain of $G_{2:2,5}$ directly interacts with the downstream gate $G_{5:5,6}$, causing it to release its top strand $w_{5,6}$. Gate-gate leak can be explained by DNA blunt end stacking, which occurs between the base pairs on the end of two double helices, creating a stacking energy to initiate strand displacement. In some initial experiments, we discovered that gate-gate leak ($\sim 20\ \mathrm{M^{-1}s^{-1}}$) is significantly larger than fuel-gate leak ($\sim 1\ \mathrm{M^{-1}s^{-1}}$), and cannot be efficiently cleaned up with thresholds (Fig. S14D).

To reduce gate-gate leak, 'clamps' were added in our circuit design (Fig. S14B and Fig. S16). The first two nucleotides on both sides of each recognition domain were specified to be the clamp c. Gate base strands were extended on both sides to cover the clamps on signal strands bound to one side or the other. Since the extended short domains (black-blue and blue-black) serve as the real toeholds, the short domain (blue) that is now surrounded by two clamps is now called the 'toehold core' t. While blunt end stacking still occurs, the single-stranded domain of $G_{2:2,5}$ (now starting with the third nucleotide of $S5$) is no longer identical with the double-stranded domain of $G_{5:5,6}$, thus preventing the undesired strand displacement. On the other hand, the desired strand displacement reactions still take place efficiently. After single strand $w_{2,5}$ gets released from gate 2, the 2 nt clamp on the right side of domain $S2$ together with the 3 nt toehold core t will bind to the exposed toehold c^*t^* on $G_{5:5,6}$, and enable strand displacement through the entire $S5$ domain. The same circuit modified with clamps behaved much more cleanly (Fig. S14E). Based on this result, we made clamps the default design for all seesaw circuits.

Note that in systems designed with clamps, the real toeholds are different on the left and right of a gate, and signal strands therefore bind to the left and right toeholds of a gate via slightly (2 nt) offset subsequences. Nonetheless, every diagram (except Figs. S14B and S16) is drawn as if there were no clamps, with both left and right toeholds labeled 'T'. It is understood that these simplified diagrams must be re-interpreted with clamps as shown in Fig. S16, where 'T^*' on the left of a base strand indicates c^*t^*, and 'T^*' on the right of a base strand indicates t^*c^*.

Second, because we use a universal toehold sequence T, *any* signal strand can bind to the toehold of *any* gate complex. However, the uniqueness of the recognition domains Si ensures that no such binding will lead to strand displacement, and the invading signal strand will quickly fall off. While this 'universal toehold binding' will not result in an incorrect strand displacement reaction, it will change the effective reaction rates by temporarily disabling some fraction of gate and threshold complexes and reducing the free signal strand concentrations. If all reactions are slowed down to the same degree, then the behavior changes are inconsequential. Furthermore, the disruption is less at higher temperatures and lower concentrations, and therefore can be avoided at the cost of overall speed. This is discussed further in SOM text S15.

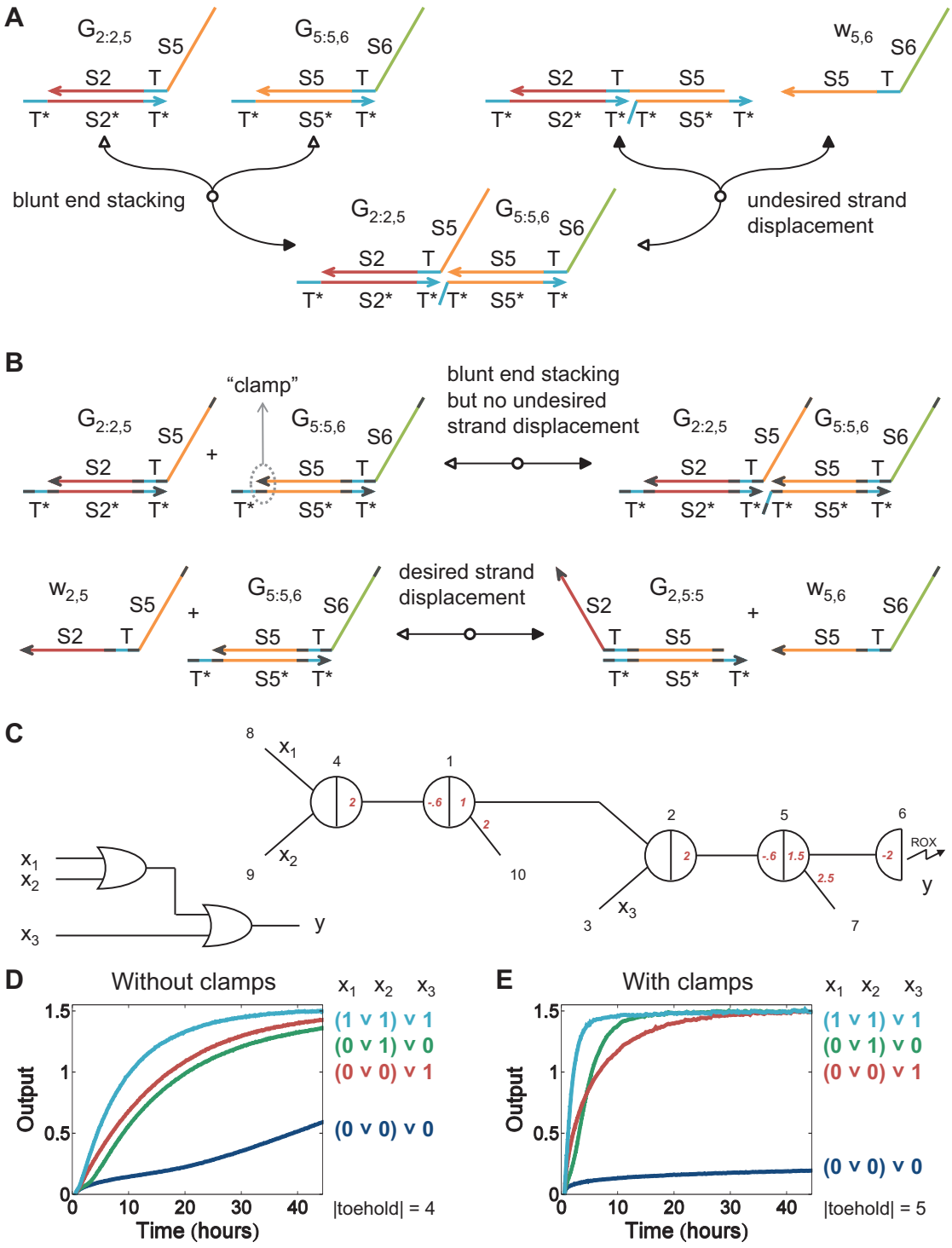

Figure S 14: Motivation and mechanism for seesaw clamps. (A) Mechanism of seesaw gate-gate leak in DNA implementations lacking clamps (c.f. Fig. S15). (B) Mechanism of seesaw clamps for rejecting gate-gate leak while preserving the desire stand displacement reactions (c.f. Fig S16). (C) Abstract diagram of a seesaw OR cascade. (D) Kinetics experiments of the seesaw OR cascade without the clamps. Sequences of strands are listed in Table S8. (E) Kinetics experiments of the seesaw OR cascade with the clamps. Sequences of strands are listed in Tables S2 and S3, circuit 4. Trajectories and their corresponding inputs have matching colors. Inputs were added with relative concentrations of 0.2× (0, logic OFF) or 0.8× (1, logic ON) where the standard concentration 1×=30 nM and experiments were performed at 20 °C in Tris-acetate-EDTA buffer containing 12.5 mM Mg^{2+}.

4 nt toehold	T	=	[....]
15 nt recognition domain	Si	=	[.....] ($\forall\ i$)
5 nt of Si on the 5' end	si	=	[.....] ($\forall\ i$)
$w_{i,j}$ $= Sj\ T\ Si$	$G_{i:i,j}$	=	$w_{i,j} + G_i$-b
G_i-b $= T^*\ Si^*\ T^*$			
$Th_{k,i:i}$-t $= Si$	$Th_{k,i:i}$	=	$Th_{k,i:i}$-t + $Th_{k,i:i}$-b
$Th_{k,i:i}$-b $= sk^*\ T^*\ Si^*$			

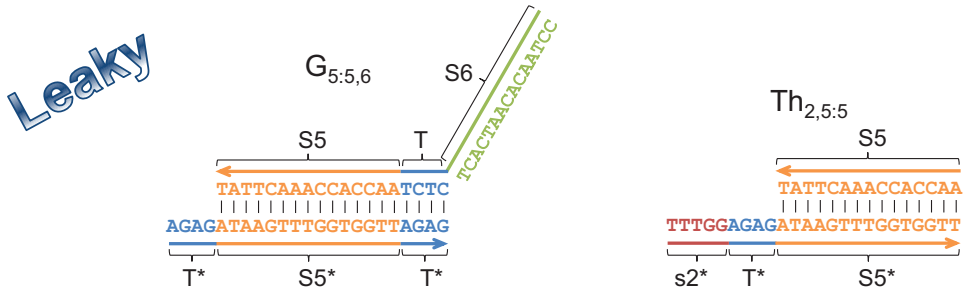

Domain level sequences					
T	= CTCT	T*	= AGAG		
S2	= CCAAACAAAACCTAT	S5	= AACCACCAAACTTAT	S6	= CCTAACACAATCACT
S2*	= ATAGGTTTTGTTTGG	S5*	= ATAAGTTTGGTGGTT		
Top and bottom strands of $G_{5:5,6}$					
$w_{5,6}$	= S6 T S5	= CCTAACACAATCACT CTCT AACCACCAAACTTAT			
G_5-b	= T* S5* T*	= AGAG ATAAGTTTGGTGGTT AGAG			
Top and bottom strands of $Th_{2,5:5}$					
$Th_{2,5:5}$-t	= S5	= AACCACCAAACTTAT			
$Th_{2,5:5}$-b	= s2* T* S5*	= TTTGG AGAG ATAAGTTTGGTGGTT			

Figure S15: Example of sequence design without clamps.

2 nt clamp	c	=	[..]
3 nt toehold core	t	=	[...]
15 nt recognition domain	Si	=	c [.....] c $(\forall\ i)$
7 nt of Si on the 5' end	si	=	c [.....] $(\forall\ i)$

	shorthand	explicit			
$w_{i,j}$	$= Sj\ T\ Si$	$= Sj\ t\ Si$	$G_{i:i,j}$	=	$w_{i,j} + G_i$-b
G_i-b	$= T^*\ Si^*\ T^*$	$= c^*\ t^*\ Si^*\ t^*\ c^*$			
$Th_{k,i:i}$-t	$= Si$		$Th_{k,i:i}$	=	$Th_{k,i:i}$-t + $Th_{k,i:i}$-b
$Th_{k,i:i}$-b	$= sk^*\ T^*\ Si^*$	$= sk^*\ t^*\ Si^*$			

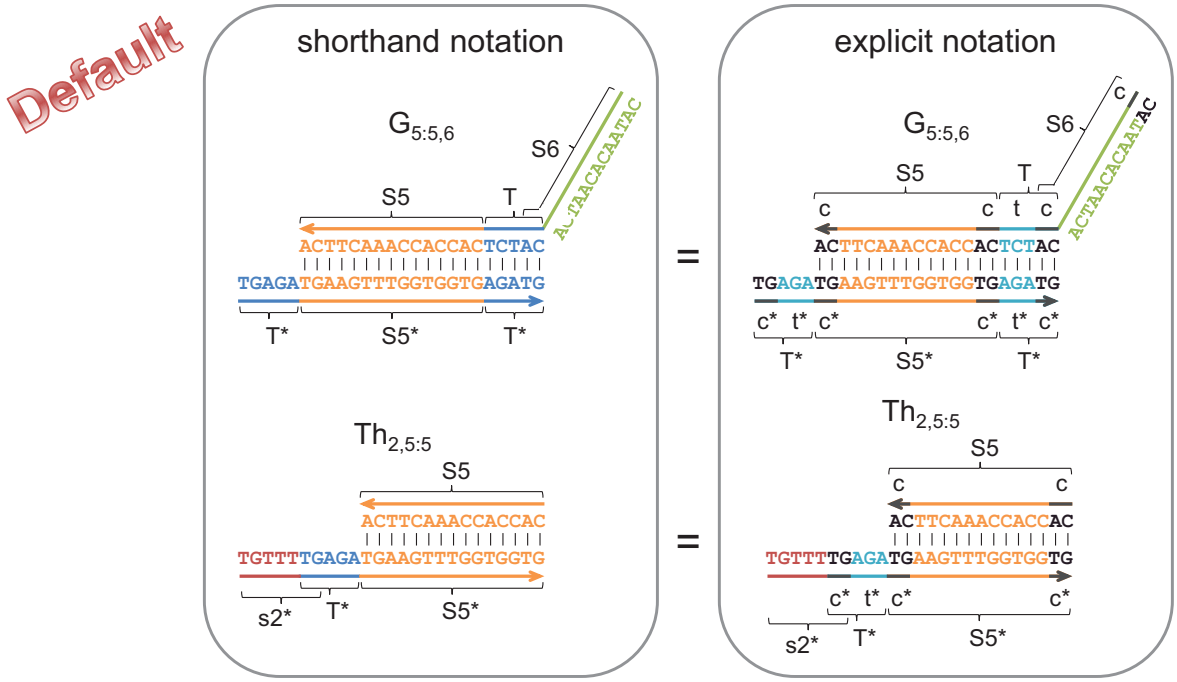

Domain level sequences					
c	= CA	t	= TCT		
c*	= TG	t*	= AGA		
S2	= CAAAACAAAACCTCA	S5	= CACCACCAAACTTCA	S6	= CATAACACAATCACA
S2*	= TGAGGTTTTGTTTTG	S5*	= TGAAGTTTGGTGGTG		

Top and bottom strands of $G_{5:5,6}$			
$w_{5,6}$	= S6 T S5	= S6 t S5	= CATAACACAATCACA TCT CACCACCAAACTTCA
G_5-b	= T* S5* T*	= c* t* S5* t* c*	= TG AGA TGAAGTTTGGTGGTG AGA TG

Top and bottom strands of $Th_{2,5:5}$			
$Th_{2,5:5}$-t	= S5		= CACCACCAAACTTCA
$Th_{2,5:5}$-b	= s2* T* S5*	= s2* t* S5*	= TGTTTTG AGA TGAAGTTTGGTGGTG

Figure S16: Example of sequence design with clamps.

S9. Toehold length and circuit behavior

Performance of thresholding with different toehold lengths was studied (Fig. S17). The shorter toehold system is roughly 10 times slower, but it is more effective at suppressing OFF state leak (flatter output response for inputs less than the threshold), presumably because of the increased ratio of rate constants for reacting with threshold complexes, relative to reacting with gate complexes. We expect that the shorter toehold system would be equally effective for suppressing ON state deviations as the longer toehold system, if it were run for $\sim$ 30 hours (i.e. 10 times as long as the longer toehold system was run). Aiming for fast circuit behavior with reasonable thresholding, we chose toehold length 5 for all seesaw circuits demonstrated in this paper (except where explicitly mentioned otherwise).

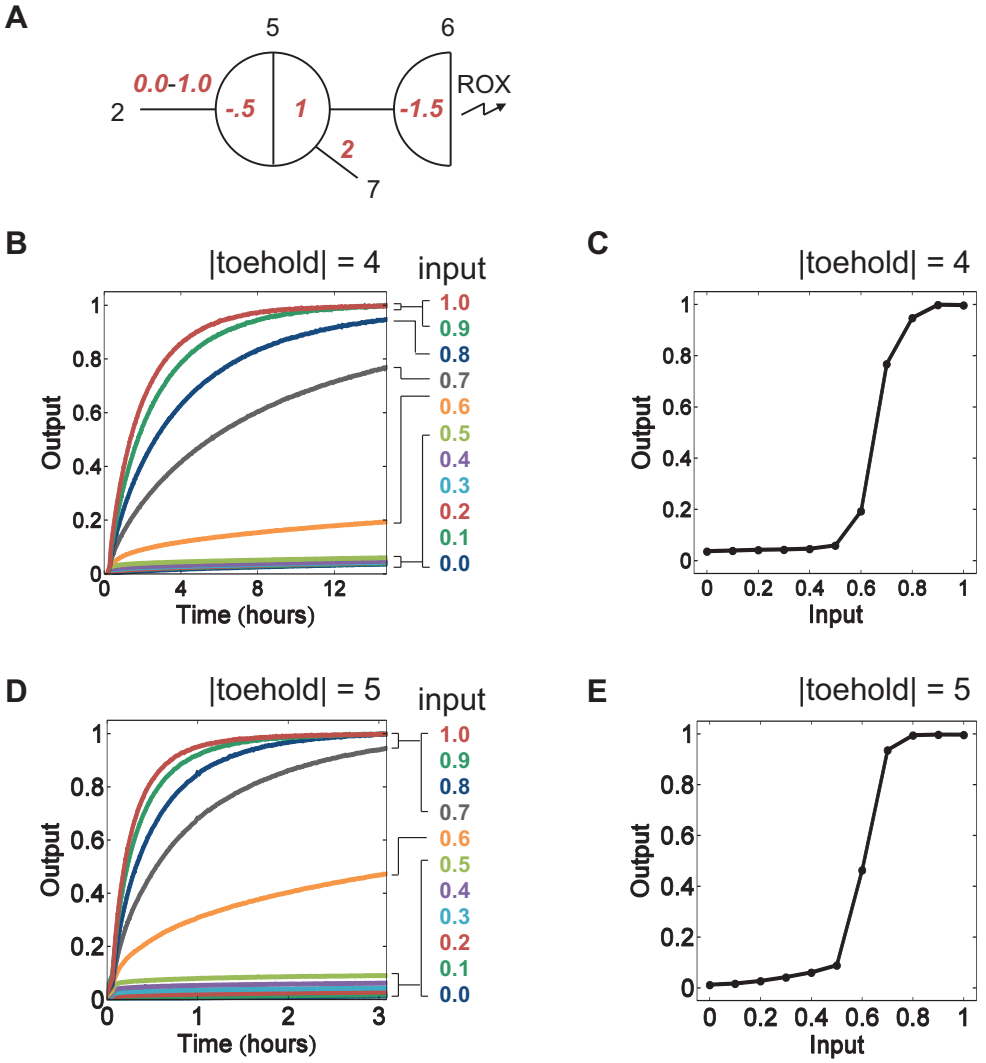

Figure S17: Performance of thresholding with different toehold lengths. (A) Abstract diagram of a seesaw catalyst with a threshold. (B) Kinetics experiments of a seesaw thresholding with toehold length 4. Sequences of strands are included in Table S8. The standard concentration 1×=100 nM and experiments were performed at 20 °C in Tris-acetate-EDTA buffer containing 12.5 mM Mg^{2+}. The same experimental conditions apply to D. (C) Input vs. output plot of B after $\sim$ 15 hours. (D) Kinetics experiments of a seesaw thresholding with toehold length 5. Sequences of strands are listed in Tables S2 and S3, circuit 2. (E) Input vs. output plot of D after $\sim$ 3 hours.

S10. DNA synthesis method and circuit behavior

Circuit performance with different purification methods for chemical synthesis of DNA was studied (Fig. S18). In all three cases, gate complexes were annealed, gel purified, and quantified according to the same procedure. It is surprising that leak was greatest when using IDT (Integrated DNA Technologies) PAGE purified strands, but this result has been observed consistently in our lab. The best results were obtained with IDT unpurified gate strands and IDT PAGE purified inputs, so this combination was used for all experiments in this paper (except where explicitly mentioned otherwise).

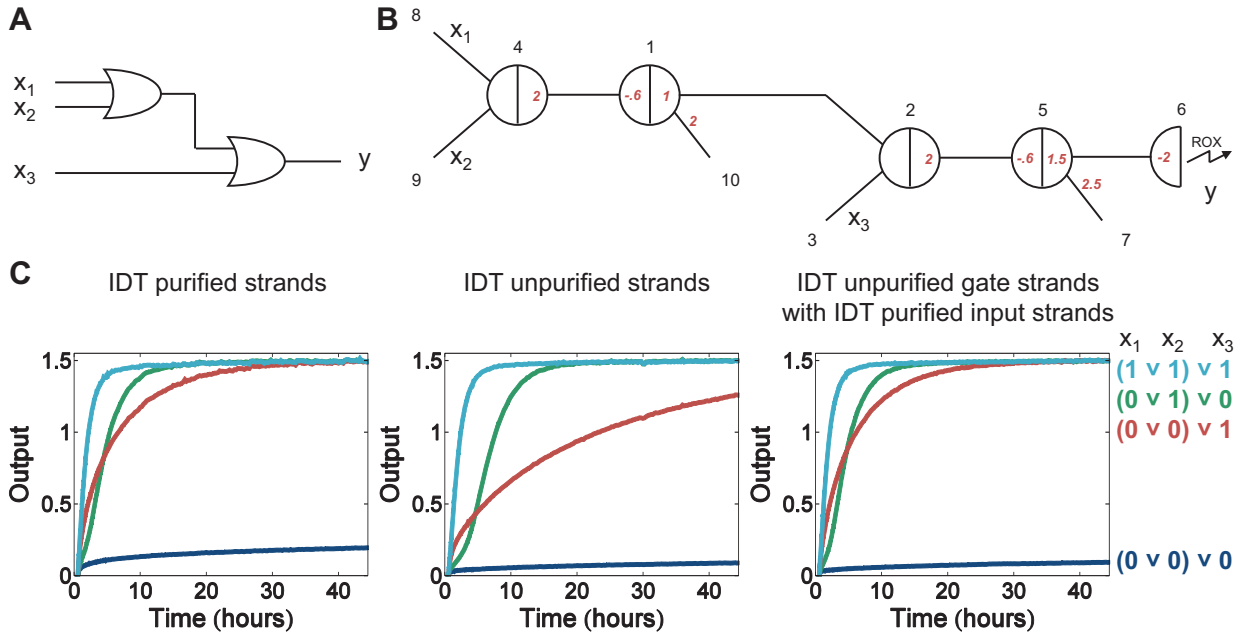

Figure S18: Circuit performance with different purification methods for chemical synthesis of DNA. (A) Digital logic diagram of a two-layer OR cascade. (B) Seesaw circuit diagram of the two-layer OR cascade. (C) Kinetics experiments of the two-layer OR cascade with IDT PAGE purified strands, IDT unpurified strands, IDT unpurified gate strands with IDT PAGE purified input strands. Sequences of strands are listed in Tables S2 and S3, circuit 4. The standard concentration was 1×=30 nM and experiments were performed at 20 °C in Tris-acetate-EDTA buffer containing 12.5 mM Mg^{2+}.

S11. Temperature and circuit behavior

Circuit performance at different temperatures was studied (Fig. S19). In this circuit, we observed a minimum of leak at 25 °C, which is why the square root circuit was run at this temperature. The number of side reactions for universal toehold binding grows quadratically with circuit size, and they affect the threshold more than the gate complex because of the increased chance that a free single strand shares a longer toehold with the threshold. Thus, circuits using universal toeholds are more sensitive to temperature when the circuit is larger.

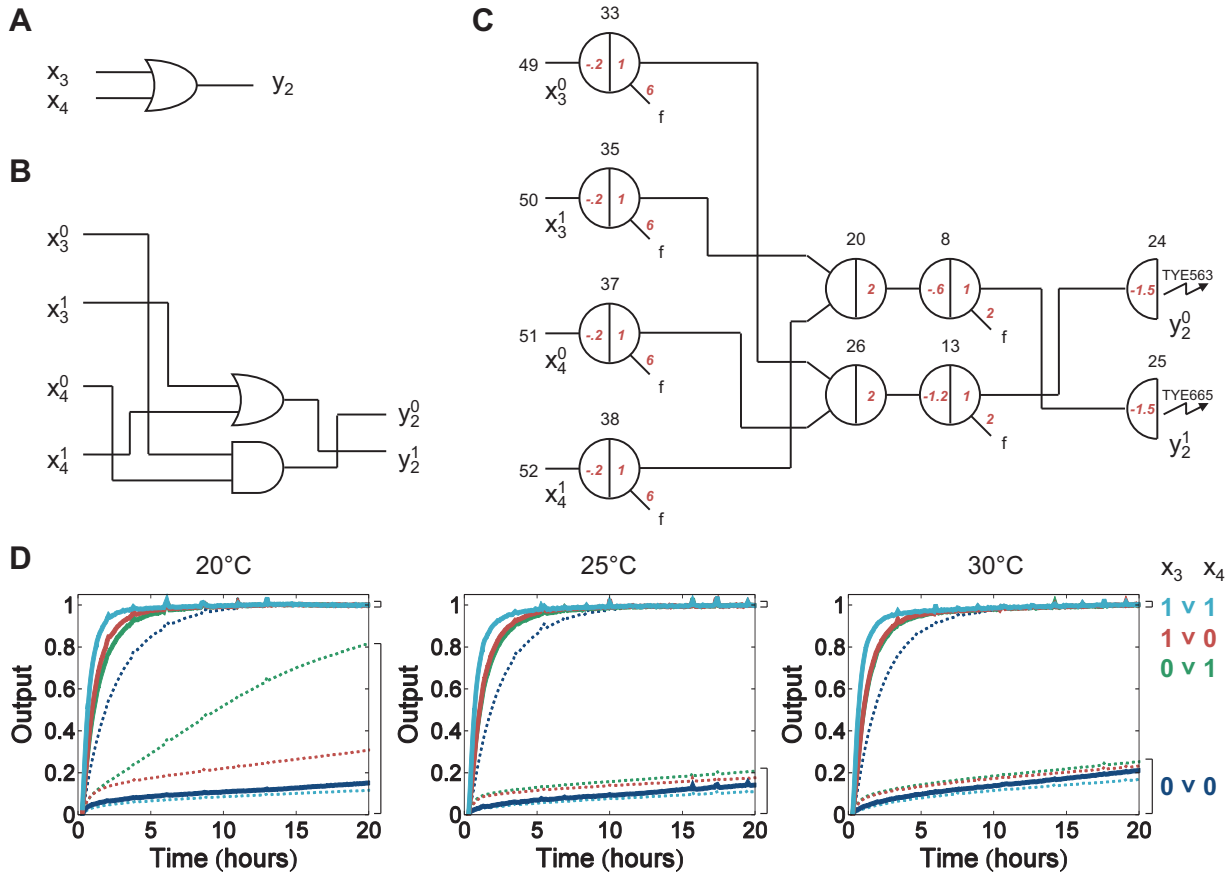

Figure S19: Circuit performance at different temperatures. (A) Digital logic diagram of an OR gate from the square root circuit. (B) Dual-rail circuit diagram of the OR gate. (C) Seesaw circuit diagram of the dual-rail circuit. Fuels of gate 33, 35, 37 and 38 are as high as in the full square root circuit. (D) Kinetics experiments of the square root subcircuit at 20 °C, 25 °C and 30 °C. Sequences of strands are included in Tables S4 to S7. The standard concentration was 1×=50 nM and experiments were performed in Tris-acetate-EDTA buffer containing 12.5 mM Mg^{2+}.

S12. Parallel gate synthesis and preparation

Annealing and purifying DNA gate complexes are the most time-consuming steps in the experiments. This is because: (1) Each gate complex (or at least each layer of gate complexes) has to be annealed separately, otherwise each signal strand will bind both to the upstream gate base strand and to the downstream gate base strand – rather than only bind to the upstream gate base strand such that the bound signal strand will be released only when the input arrives. (2) Each gate complex has to be purified in order to remove extra top or bottom strands when the stoichiometry is not perfect, otherwise the extra strands will cause undesired reactions with other components in the circuit.

Interestingly, for the seesaw DNA motif, there is a way to get around this complexity. As shown in Fig. S20A, a signal strand and its upstream gate base strand can be designed to be connected by a stem-loop fragment, thus becoming a single strand of DNA. During annealing, intramolecular hairpins form first and become kinetically trapped before other intermolecular reactions occur [20], thus the correct signal strand domain will bind to the correct gate domain. Then, the undesired stem-loop fragment can be removed by restriction enzyme digestion or photocleavage. The threshold complex can also be prepared in a similar way (Fig. S20B). Gel analysis showed that the gate:signal complex and the threshold complex were formed properly after annealing and enzyme cutting (Fig. S20C). This method appears to be more promising than parallel gate annealing of alternate layers, because the latter introduces additional sequence design difficulties: As top strands and bottom strands are mixed in single-stranded form, there is considerable opportunity for a top strand (e.g., $SiTSj$) to bind with mismatches to an unrelated gate base strand (e.g., $T^*Sk^*T^*$). Our sequence design criteria were formulated to prevent branch migration through unrelated recognition domains, but are not stringent enough to prevent spurious hybridization between unrelated top and bottom strands.

Fluorescence kinetics experiments showed that seesaw catalysis and thresholding worked with DNA complexes prepared from hairpins (Fig. S21). Since all components in seesaw circuits can be prepared from single-stranded DNA, parallel synthesis of hairpin precursors is possible using DNA microarrays and annealing. Parallel preparation of mature gate and threshold complexes is also possible using the above method. Hairpins will prevent incorrect binding, and the stoichiometry will be perfect because the two parts are on one strand. This manufacturing process could be crucial for making large-scale circuits.

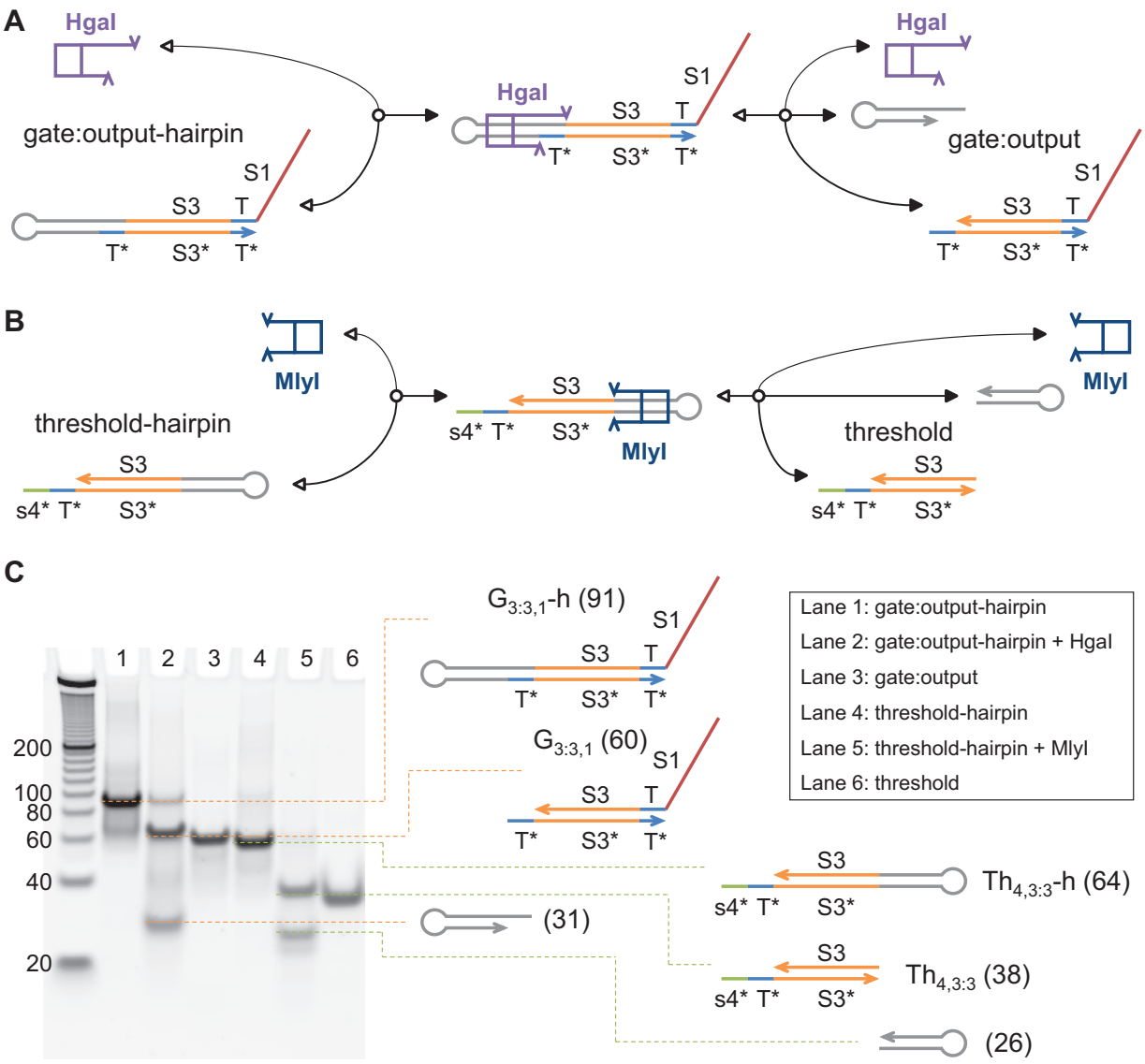

Figure S20: Seesaw gate and threshold generated from hairpins. (A) Mechanism of gate production using type IIs restriction enzymes HgaI and MlyI. (B) Mechanism of threshold production. (C) Non-denaturing PAGE analysis of restriction enzyme cutting of seesaw hairpin precursors to form mature gate and threshold complexes. The number of nucleotides within each molecular species is given in parentheses. Sequences of strands are included in Table S9.

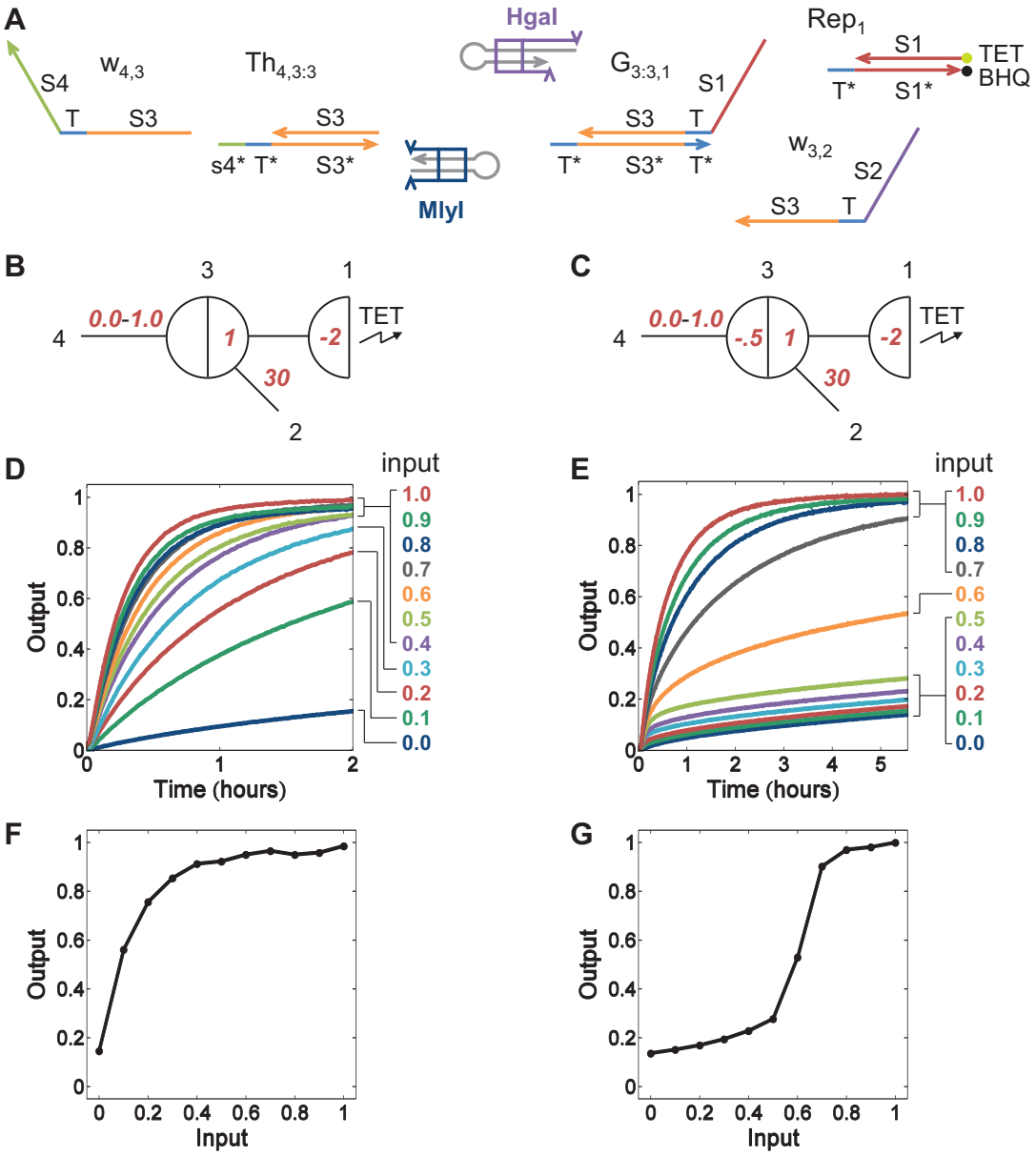

Figure S21: A seesaw catalyst and threshold demonstrated with gate and threshold complexes prepared from seesaw hairpins. (A) DNA molecules of the seesaw catalyst with threshold. Note that stem-loop fragments were not present during the kinetics experiments, since gate and threshold complexes were gel purified and quantified after restriction enzyme digestion. Also note that the reporter was prepared separately by the usual procedure of annealing its two strands together. (B) Abstract diagram of the seesaw catalyst. (C) Abstract diagram of the seesaw catalyst with threshold. (D) Kinetics experiments of the seesaw catalyst. (E) Kinetics experiments of the seesaw catalyst with threshold. (F) Input vs. output plot of D. The output at ∼2 hours is re-plotted against the relative concentrations of the initial input. (G) Input vs. output plot of E. The output at ∼5.5 hours is re-plotted against the relative concentrations of the initial input. Input strands were added with concentrations varying from 0.0× to 1.0× in increments of 0.1×. (The high leak in these experiments, relative to those in Fig. 1E and Fig. S2E, is likely due to the 15 times higher fuel concentration, which was used for historical reasons.) The top strand of the reporter complex was modified with a 5' TET fluorophore; the bottom strand was modified with a 3' Black Hole Quencher. Sequences of strands are listed in Table S9. The standard concentration 1×=30 nM and experiments were performed at 20 °C in Tris-acetate-EDTA buffer containing 12.5 mM Mg^{2+}.

S13. Modeling and simulations

Seesaw networks are modeled with the following chemical reactions: $\forall i, j, k, x, y$

Designed reactions	Seesawing reactions	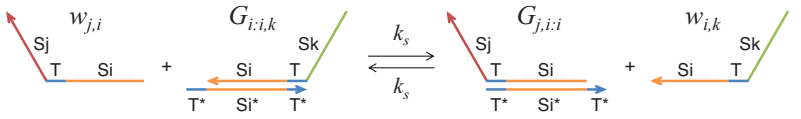
	Thresholding reactions	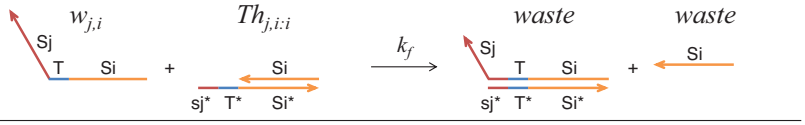
	Reporting reactions	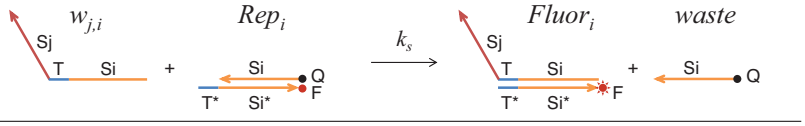
Side reactions	Universal toehold binding reactions	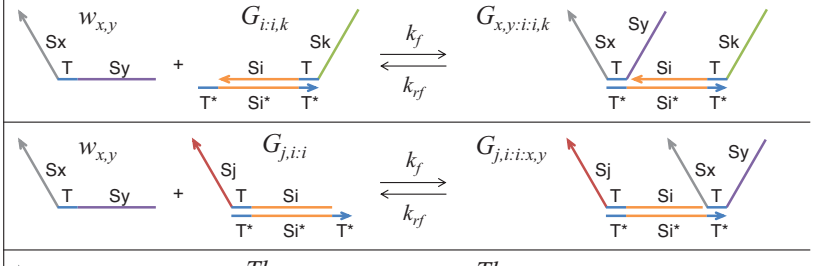
	Leak reactions	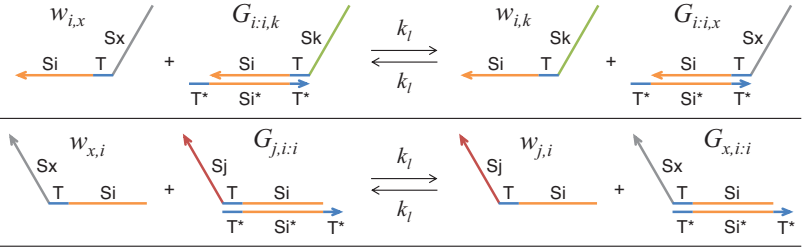

The designed reactions include: (1) Seesawing reactions that are reversible strand displacement reactions with slow forward and backward rates k_s associated with 5-nucleotide toeholds. (2) Thresholding reactions that are irreversible strand displacement reactions with fast rates k_f associated with 10-nucleotide extended toeholds. One of the two waste products will be omitted later. (3) Reporting reactions that are irreversible strand displacement reactions with slow rates k_s associated with 5-nucleotide toeholds. The fluorescent product named "F-waste" in the main paper is renamed as "Fluor$_i$" here for simulating the output fluorescence signals. The waste product will be omitted later.

It is only necessary to include designed reactions in the model for index combinations that actually occur within the network. For example, seesawing reactions may be omitted if $w_{j,i}^{tot} = 0$ or $G_i^{tot} = 0$ or $w_{i,k}^{tot} = 0$, where $w_{j,i}^{tot} = [G_{j:j,i}](t=0) + [w_{j,i}](t=0) + [G_{j,i:i}](t=0)$ and $G_i^{tot} = \sum_n [G_{i:i,n}](t=0) + \sum_m [G_{m,i:i}](t=0)$ and $w_{i,k}^{tot} = [G_{i:i,k}](t=0) + [w_{i,k}](t=0) + [G_{i,k:k}](t=0)$. Similarly, thresholding reactions may be omitted if $w_{j,i}^{tot} = 0$ or $[Th_{j,i:i}](t=0) = 0$; and reporting reactions may be omitted if $w_{j,i}^{tot} = 0$ or $[Rep_i](t=0) = 0$. Also note that in general seesaw networks, threshold and reporter complexes with the opposite orientation may also appear and must be modeled, but they are not used in our construction for feedforward digital logic circuits.

Side reactions due to spurious binding and spontaneous leak are also included in the model: (1) Universal toehold binding reactions that temporarily occur between *any* free signal and *any* bound signal, threshold, or reporter. These spurious binding are caused by a universal sequence used for all toeholds in seesaw circuits. The forward rate (toehold binding rate) k_f is the same as the fast strand displacement rate because they both reach the maximum rate for DNA hybridization. The backward rate (toehold disassociation rate) is faster (k_{rf}) between free and bound signals, and is slower (k_{rs}) between free signals and threshold complexes because the sequence similarity of the first few nucleotides among recognition domains is inevitable in large circuits. (2) Leak reactions due to zero-toehold strand displacement occur with very slow forward and backward rates k_l. These spontaneous leaks occur between free and bound signals that are connected to the same side of the same gate (e.g. in 'fuel-gate leak', a fuel displaces a bound output and releases a free output). To avoid counting the same reaction twice, it is only necessary to include the reversible reaction for $x < k$ in computer simulations (for the first case) and for $x < j$ (for the second case).

Note that we do not include universal toehold binding reactions in cases that correspond to designed reactions, such as for $y = i$ in the first reaction scheme and $x = i$ in the second reaction scheme. In the third reaction scheme, our construction guarantees that either $x = j$ and $y = i$, or else $x \neq j$ and $y \neq i$, because thresholds are only used on wires connecting nodes with no other connections on the relevant sides. In more detail, our digital logic circuit construction is 'clean' in the terminology of ref. [17], i.e. it has no threshold crosstalk and no threshold inhibition as discussed in SI text S3. This ensures that for universal toehold binding reactions with the thresholds, the sj^* domain will not bind to Sx by design; whatever binding is present must be due to unintentional sequence complementarity. Since it is impossible to avoid all such unintentional binding in large circuits, we set $k_{rs} < k_{rf}$; but we must note that using a single 'average' value for all domain sequences is a notable source of inaccuracy in our simple model, as we expect considerable sequence dependence for the true reaction rates.

Also note that several additional types of leak reaction are not modeled. We neglect gate-gate leak, for example, because it appears to be nearly eliminated when clamps are used, as described in SI text S8. There is also a potential reporter leak between Rep_i and $w_{i,j}$; thankfully, in our construction, no free signal strand will ever have a left side domain that matches a reporter. However, the Si waste could leak with reporter Rep_i, and $w_{i,j}$ could leak with threshold $Th_{j,i:i}$; these and other similar zero-toehold leaks are not modeled because we expect that they are much less significant than the modeled fuel-gate leaks.

After adjusting the model's five rate constant parameters by hand, this model could accurately fit experimental data for a single gate with a single reporter, with and without a threshold (figs. S22 and S23).

To simplify the modeling of universal toehold binding and improve the simulation efficiency for large networks, we employ an approximation for all systems larger than a single gate with a single reporter. Specifically, reactions between all free signals and a specific bound signal are replaced by one reaction between the bound signal and a lumped W species whose initial concentration is the total initial concentration of all free signals. Similarly, a lumped G species represents total bound signals, and a lumped TH species represents total thresholds. Dynamics of the lumped species approximately track the dynamics of the explicit (unsimplified) system, with the inaccuracy that (1) the lumped reactions effectively include universal toehold binding reactions for cases that correspond to designed reactions, which were not included in the explicit system, thus leading to a slight overestimate of the effect of universal toehold bind that becomes negligible in large networks; and (2) the lumped variables W and TH are not reduced as free signals and thresholds annihilate each other, thus also leading to a slight overestimate of the effect of universal toehold binding.

Mass action chemical reaction network models for seesaw networks can be constructed systematically using recursive formulas defined in Mathematica, as sketched in the following pages. For each seesaw node definition, formal chemical reactions are added for the designed reactions, leak reactions, and lumped universal toehold binding reactions involving the species at that node. To avoid over-counting, lumped reactions for wires on the right side of the node are not included; they will be included in the reactions for the downstream node. (An exception is that depletion of fuels by universal toehold binding is not model – and oversight that is likely to have little effect, as the fuels are always in excess anyway.) Also to avoid over-counting, leak reactions are tallied only for $j < j'$ and $k < k'$. The concentrations of species is also provided, with the variable c being the $1\times$ standard concentration. Once the full set of formal chemical reactions has been generated, a set of Mathematica routines developed by David Soloveichik [9] can be used to obtain a system of ordinary differential equations representing mass action dynamics, which can be simulated using the built-in numerical integration algorithms. A self-contained set of Mathematica files can be produced automatically using the seesaw compiler [21].

As experiments were performed at two temperatures, 20 °C and 25 °C, we defined a separate parameter set (five rate constants) for each temperature. After adjustment, the 20 °C parameter set yielded semiquantitative agreement with all experiments performed at that temperature (figs. S22 to S30), while the 25 °C parameter set agreed well with the square root circuit (fig. S31).

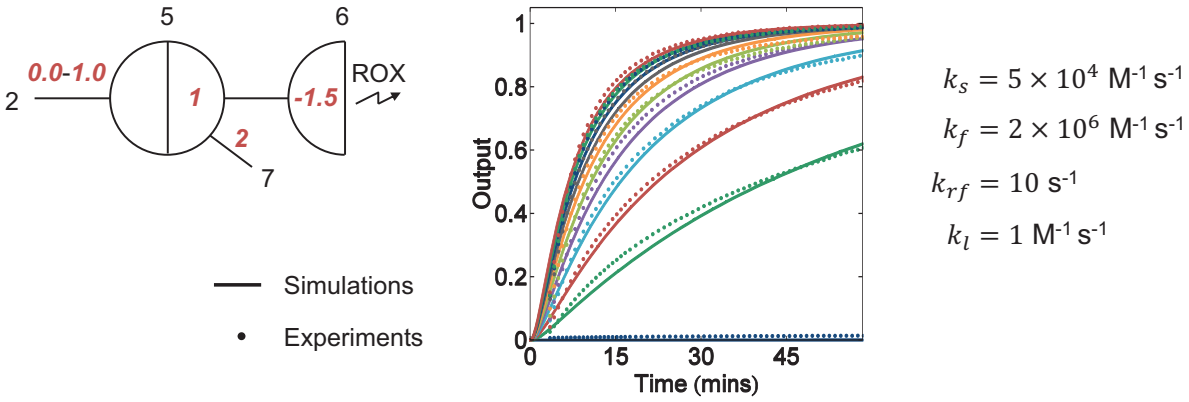

Figure S22: Modeling of a seesaw catalyst. (Experimental data is from Fig. S2E.) k_s is the slow strand displacement rate of seesawing and reporting reactions. k_f is the fast strand displacement rate of thresholding reactions, and the forward rate of spurious toehold binding reactions due to a universal toehold sequence, both of which reach the maximum DNA hybridization rate. k_{rf} is the backward reaction rate of spurious toehold binding between signal strands and gate:signal complexes – it is a fast toehold disassociation rate. k_l is the leak reaction rate of zero-toehold strand displacement.

Designed reactions:

Seesawing reactions:

$$w_{2,5} + G_{5:5,6} \underset{k_s}{\overset{k_s}{\rightleftharpoons}} G_{2,5:5} + w_{5,6}$$

$$w_{2,5} + G_{5:5,7} \underset{k_s}{\overset{k_s}{\rightleftharpoons}} G_{2,5:5} + w_{5,7}$$

Reporting reactions:

$$w_{5,6} + Rep_6 \xrightarrow{k_s} Fluor_6$$

Side reactions:

Universal toehold binding reactions:

$$w_{5,6} + G_{5:5,6} \underset{k_{rf}}{\overset{k_f}{\rightleftharpoons}} G_{5,6:5:5,6}$$

$$w_{5,7} + G_{5:5,6} \underset{k_{rf}}{\overset{k_f}{\rightleftharpoons}} G_{5,7:5:5,6}$$

$$w_{5,6} + G_{5:5,7} \underset{k_{rf}}{\overset{k_f}{\rightleftharpoons}} G_{5,6:5:5,7}$$

$$w_{5,7} + G_{5:5,7} \underset{k_{rf}}{\overset{k_f}{\rightleftharpoons}} G_{5,7:5:5,7}$$

$$G_{2,5:5} + w_{2,5} \underset{k_{rf}}{\overset{k_f}{\rightleftharpoons}} G_{2,5:5:2,5}$$

$$w_{2,5} + Rep_6 \underset{k_{rf}}{\overset{k_f}{\rightleftharpoons}} Rep_{2,5:6}$$

$$w_{5,7} + Rep_6 \underset{k_{rf}}{\overset{k_f}{\rightleftharpoons}} Rep_{5,7:6}$$

Leak reactions:

$$G_{5:5,6} + w_{5,7} \underset{k_l}{\overset{k_l}{\rightleftharpoons}} G_{5:5,7} + w_{5,6}$$

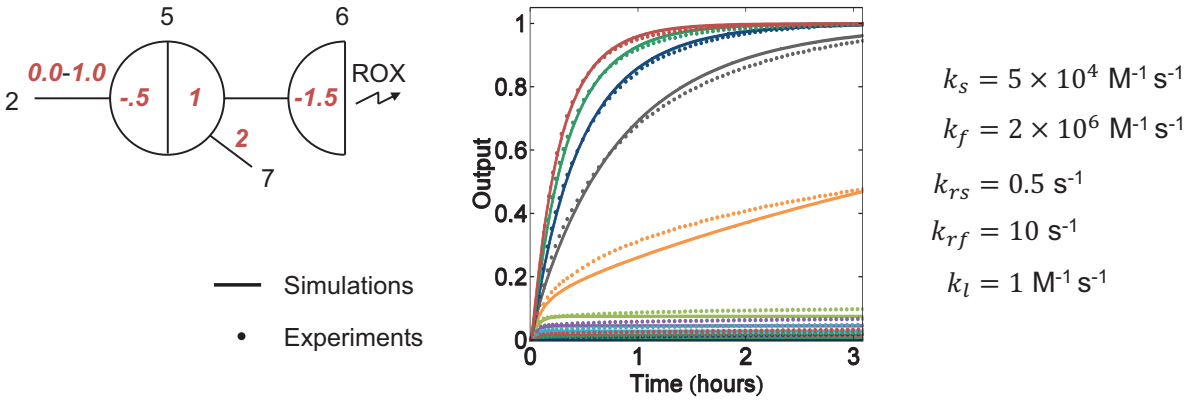

Figure S23: Modeling of a seesaw catalyst with threshold. (Experimental data is from Fig. 1E.) k_{rs} is the backward reaction rate of spurious toehold binding between signal strands and threshold complexes – it is a slow toehold disassociation rate because threshold complexes have extended toeholds that are likely to bind to the signal strands by more than the universal toehold domain. Here and elsewhere, nominal threshold concentrations were multiplied by 1.1 to account for empirically higher-than-expected concentrations.

Designed reactions:

Seesawing reactions:

$$w_{2,5} + G_{5:5,6} \underset{k_s}{\overset{k_s}{\rightleftharpoons}} G_{2,5:5} + w_{5,6}$$

$$w_{2,5} + G_{5:5,7} \underset{k_s}{\overset{k_s}{\rightleftharpoons}} G_{2,5:5} + w_{5,7}$$

Thresholding reactions:

$$w_{2,5} + Th_{2,5:5} \xrightarrow{k_f} waste$$

Reporting reactions:

$$w_{5,6} + Rep_6 \xrightarrow{k_s} Fluor_6$$

Side reactions:

Universal toehold binding reactions:

$$w_{5,6} + G_{5:5,6} \underset{k_{rf}}{\overset{k_f}{\rightleftharpoons}} G_{5,6:5:5,6}$$

$$w_{5,7} + G_{5:5,6} \underset{k_{rf}}{\overset{k_f}{\rightleftharpoons}} G_{5,7:5:5,6}$$

$$w_{5,6} + G_{5:5,7} \underset{k_{rf}}{\overset{k_f}{\rightleftharpoons}} G_{5,6:5:5,7}$$

$$w_{5,7} + G_{5:5,7} \underset{k_{rf}}{\overset{k_f}{\rightleftharpoons}} G_{5,7:5:5,7}$$

$$G_{2,5:5} + w_{2,5} \underset{k_{rf}}{\overset{k_f}{\rightleftharpoons}} G_{2,5:5:2,5}$$

$$w_{5,6} + Th_{2,5:5} \underset{k_{rs}}{\overset{k_f}{\rightleftharpoons}} Th_{5,6:2,5:5}$$

$$w_{5,7} + Th_{2,5:5} \underset{k_{rs}}{\overset{k_f}{\rightleftharpoons}} Th_{5,7:2,5:5}$$

$$w_{2,5} + Rep_6 \underset{k_{rf}}{\overset{k_f}{\rightleftharpoons}} Rep_{2,5:6}$$

$$w_{5,7} + Rep_6 \underset{k_{rf}}{\overset{k_f}{\rightleftharpoons}} Rep_{5,7:6}$$

Leak reactions:

$$G_{5:5,6} + w_{5,7} \underset{k_l}{\overset{k_l}{\rightleftharpoons}} G_{5:5,7} + w_{5,6}$$

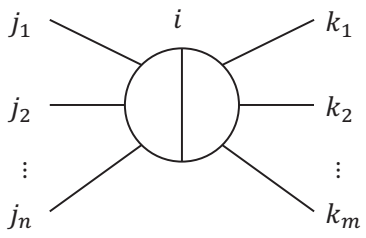

seesaw$[i, \{j_1, j_2, \cdots, j_n\}, \{k_1, k_2, \cdots, k_m\}]$

$$
= \left\{
\begin{array}{l}
\text{for all } j, j' \in \{j_1, j_2, \cdots, j_n\}, k, k' \in \{k_1, k_2, \cdots, k_m\} \\
\left.
\begin{array}{rcl}
w_{j,i} + G_{i:i,k} & \overset{k_s}{\underset{k_s}{\rightleftharpoons}} & G_{j,i:i} + w_{i,k}
\end{array}
\right\} \text{Seesawing reactions} \\
\left.
\begin{array}{rcl}
w_{j,i} + Th_{j,i:i} & \overset{k_f}{\rightarrow} & waste
\end{array}
\right\} \text{Thresholding reactions} \\
\left.
\begin{array}{rcl}
W + G_{i:i,k} & \overset{k_f}{\underset{k_{rf}}{\rightleftharpoons}} & G_{W:i:i,k} \\
G_{j,i:i} + W & \overset{k_f}{\underset{k_{rf}}{\rightleftharpoons}} & G_{j,i:i:W} \\
W + Th_{j,i:i} & \overset{k_f}{\underset{k_{rs}}{\rightleftharpoons}} & Th_{W:j,i:i} \\
w_{j,i} + G & \overset{k_f}{\underset{k_{rf}}{\rightleftharpoons}} & G_{j,i:G} \\
w_{j,i} + TH & \overset{k_f}{\underset{k_{rs}}{\rightleftharpoons}} & Th_{j,i:TH}
\end{array}
\right\} \text{Universal toehold binding reactions} \\
\left.
\begin{array}{rcl}
G_{j,i:i} + w_{j',i} & \overset{k_l}{\underset{k_l}{\rightleftharpoons}} & G_{j',i:i} + w_{j,i} \\
G_{i:i,k} + w_{i,k'} & \overset{k_l}{\underset{k_l}{\rightleftharpoons}} & G_{i:i,k'} + w_{i,k}
\end{array}
\right\} \text{Leak reactions}
\end{array}
\right.
$$

Total signal, gate and threshold			
$W(t=0)$	$=$	$\sum[w_{i,j}](t=0)$	for all i, j in the seesaw circuit
$G(t=0)$	$=$	$\sum[G_{j,i:i}](t=0) + [G_{i:i,k}](t=0) + [Rep_i](t=0)$	for all i, j, k in the seesaw circuit
$TH(t=0)$	$=$	$\sum[Th_{j,i:i}](t=0)$	for all i, j in the seesaw circuit

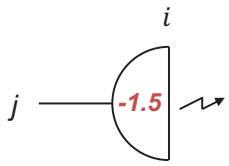

reporter$[i, j]$

$$
= \left\{ \begin{array}{rcll}
w_{j,i} + Rep_i & \stackrel{k_s}{\rightarrow} & Fluor_i & \left.\vphantom{\begin{array}{c}a\\a\\a\end{array}}\right\} \text{Reporting reactions} \\
W + Rep_i & \underset{k_{rf}}{\overset{k_f}{\rightleftharpoons}} & Rep_{W:i} & \left.\vphantom{\begin{array}{c}a\\a\\a\end{array}}\right\} \text{Universal toehold binding reactions} \\
w_{j,i} + G & \underset{k_{rf}}{\overset{k_f}{\rightleftharpoons}} & G_{j,i:G} & \\
w_{j,i} + TH & \underset{k_{rs}}{\overset{k_f}{\rightleftharpoons}} & Th_{j,i:TH} & \\
\text{conc}[Rep_i] & = & 1.5 \times c & \left.\vphantom{\begin{array}{c}a\\a\\a\end{array}}\right\} \text{Initial concentration of the reporter}
\end{array} \right.
$$

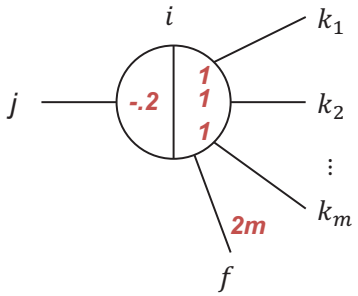

inputfanout$[i, j, \{k_1, k_2, \cdots, k_m\}]$

$$
= \left\{ \begin{array}{rcll}
\text{seesaw}[i, \{j\}, \{k_1, k_2, \cdots, k_m, f\}] & & & \\
\text{conc}[G_{i:i,k}] & = & 1 \times c \quad \text{for all } k \in \{k_1, k_2, \cdots, k_m\} & \\
\text{conc}[w_{i,f}] & = & 2 \times m \times c & \\
\text{conc}[Th_{j,i:i}] & = & 1.1 \times 0.2 \times c &
\end{array} \right.
$$

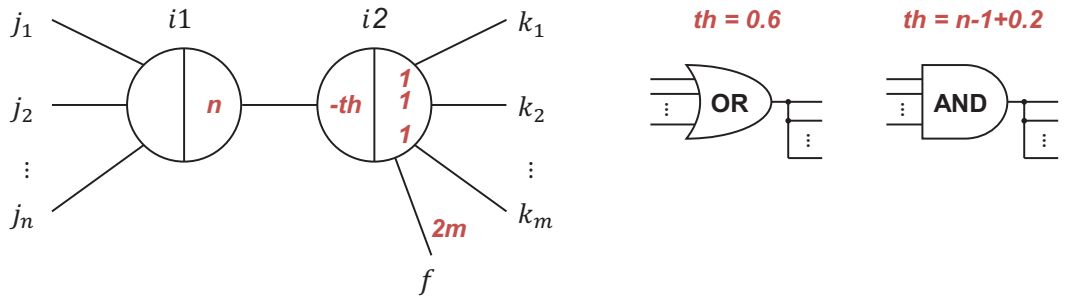

seesawOR$[i1, i2, \{j_1, j_2, \cdots, j_n\}, \{k_1, k_2, \cdots, k_m\}]$

$$
= \begin{cases}
\text{seesaw}[i1, \{j_1, j_2, \cdots, j_n\}, \{i2\}] \\
\text{seesaw}[i2, \{i1\}, \{k_1, k_2, \cdots, k_m, f\}] \\
\text{conc}[G_{i1:i1,i2}] = n \times c \\
\text{conc}[G_{i2:i2,k}] = 1 \times c \quad \text{for all } k \in \{k_1, k_2, \cdots, k_m\} \\
\text{conc}[w_{i2,f}] = 2 \times m \times c \\
\text{conc}[Th_{i1,i2:i2}] = 1.1 \times 0.6 \times c
\end{cases}
$$

seesawAND$[i1, i2, \{j_1, j_2, \cdots, j_n\}, \{k_1, k_2, \cdots, k_m\}]$

$$
= \begin{cases}
\text{seesaw}[i1, \{j_1, j_2, \cdots, j_n\}, \{i2\}] \\
\text{seesaw}[i2, \{i1\}, \{k_1, k_2, \cdots, k_m, f\}] \\
\text{conc}[G_{i1:i1,i2}] = n \times c \\
\text{conc}[G_{i2:i2,k}] = 1 \times c \quad \text{for all } k \in \{k_1, k_2, \cdots, k_m\} \\
\text{conc}[w_{i2,f}] = 2 \times m \times c \\
\text{conc}[Th_{i1,i2:i2}] = 1.1 \times (n - 1 + 0.2) \times c
\end{cases}
$$

Temperature: 20 °C		
k_s	=	5×10^4 $\mathrm{M}^{-1}\mathrm{s}^{-1}$
k_f	=	2×10^6 $\mathrm{M}^{-1}\mathrm{s}^{-1}$
k_{rs}	=	0.5 s^{-1}
k_{rf}	=	10 s^{-1}
k_l	=	1 $\mathrm{M}^{-1}\mathrm{s}^{-1}$

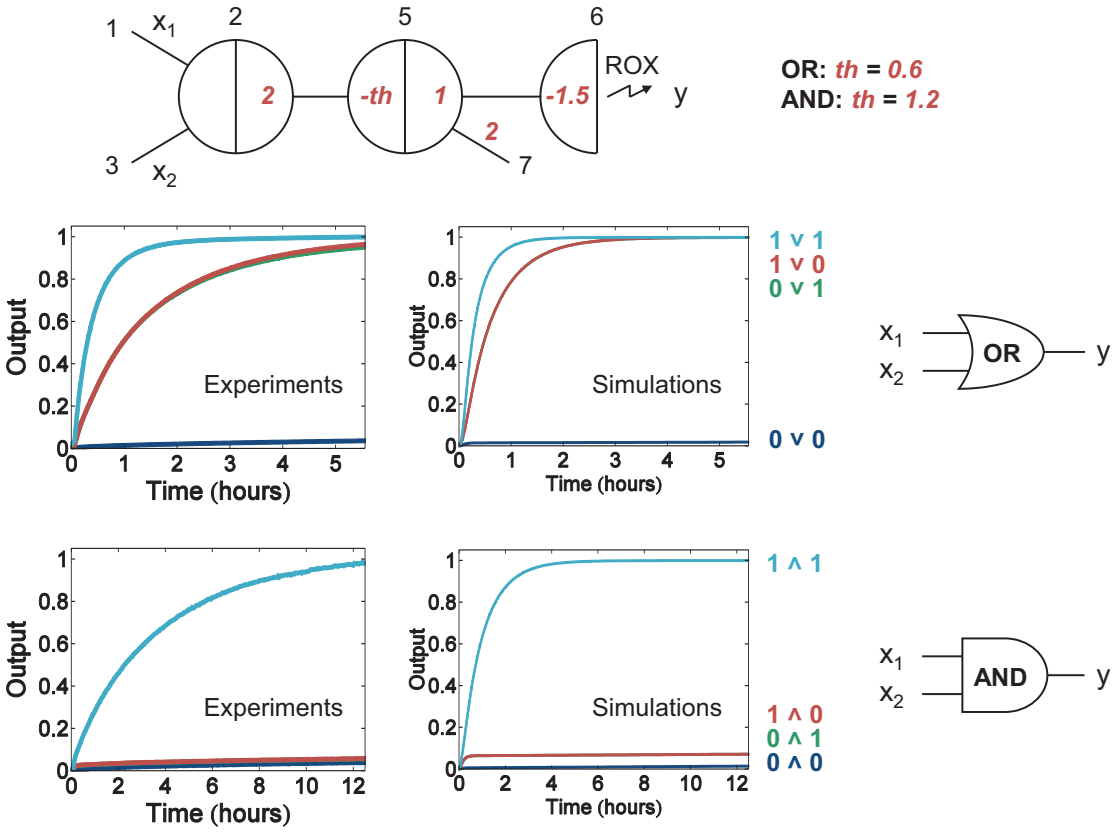

Figure S 24: Simulations of the two-input AND and OR gates. (Experimental data is from Fig. 2.) Standard concentration $c = 100 \times 10^{-9}$ M. Rate parameters are set according to 20 °C. Inputs x_1 and x_2 are either 0.1 (0, logic OFF) or 0.9 (1, logic ON).

$$
\begin{aligned}
&\mathrm{seesawOR}[2,5,\{1,3\},\{6\}] \\
&\quad \mathrm{reporter}[6,5] \\
&\quad \mathrm{conc}[w_{1,2}] = x_1 \times c \\
&\quad \mathrm{conc}[w_{3,2}] = x_2 \times c \\
&\quad \mathrm{conc}[W] = (2 + x_1 + x_2) \times c \\
&\quad \mathrm{conc}[G] = 4.5 \times c \\
&\quad \mathrm{conc}[TH] = 1.1 \times 0.6 \times c \\
&\quad y = Fluor_6
\end{aligned}
$$

$$
\begin{aligned}
&\mathrm{seesawAND}[2,5,\{1,3\},\{6\}] \\
&\quad \mathrm{reporter}[6,5] \\
&\quad \mathrm{conc}[w_{1,2}] = x_1 \times c \\
&\quad \mathrm{conc}[w_{3,2}] = x_2 \times c \\
&\quad \mathrm{conc}[W] = (2 + x_1 + x_2) \times c \\
&\quad \mathrm{conc}[G] = 4.5 \times c \\
&\quad \mathrm{conc}[TH] = 1.1 \times 1.2 \times c \\
&\quad y = Fluor_6
\end{aligned}
$$

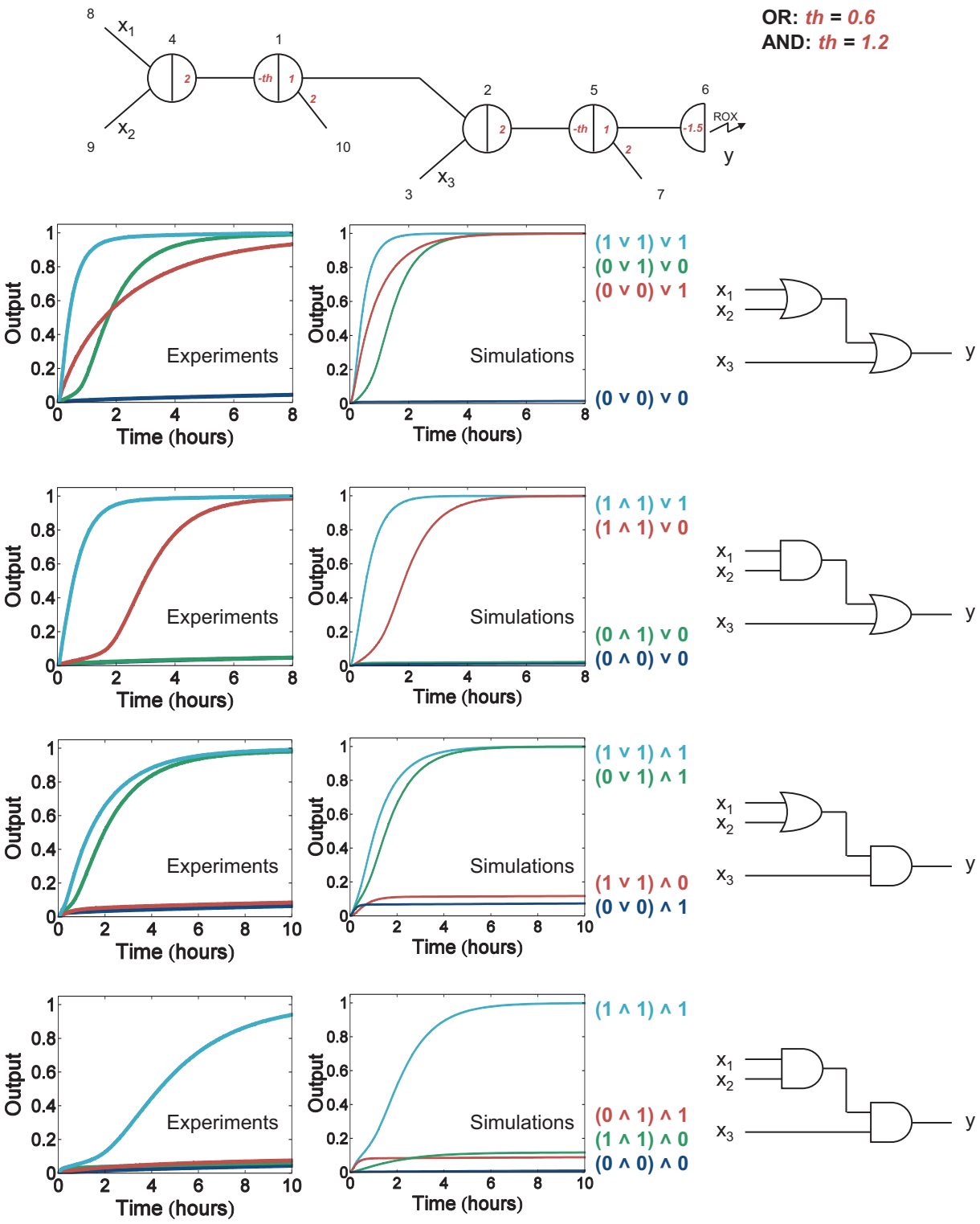

Figure S 25: Simulations of the two-layer AND/OR cascades. (Experimental data is from Fig. S5.) Standard concentration $c = 100 \times 10^{-9}$ M. Rate parameters are set according to 20 °C. Inputs x_1, x_2 and x_3 are either 0.1 (0, logic OFF) or 0.9 (1, logic ON).

$$
\begin{aligned}
&\text{seesawOR}[2,5,\{1,3\},\{6\}]\\
&\text{seesawOR}[4,1,\{8,9\},\{2\}]\\
&\text{reporter}[6,5]\\
\text{conc}[w_{8,4}] &= x_1 \times c\\
\text{conc}[w_{9,4}] &= x_2 \times c\\
\text{conc}[w_{3,2}] &= x_3 \times c\\
\text{conc}[W] &= (4 + x_1 + x_2 + x_3) \times c\\
\text{conc}[G] &= 7.5 \times c\\
\text{conc}[TH] &= 1.1 \times 1.2 \times c\\
y &= Fluor_6
\end{aligned}
$$

$$
\begin{aligned}
&\text{seesawOR}[2,5,\{1,3\},\{6\}]\\
&\text{seesawAND}[4,1,\{8,9\},\{2\}]\\
&\text{reporter}[6,5]\\
\text{conc}[w_{8,4}] &= x_1 \times c\\
\text{conc}[w_{9,4}] &= x_2 \times c\\
\text{conc}[w_{3,2}] &= x_3 \times c\\
\text{conc}[W] &= (4 + x_1 + x_2 + x_3) \times c\\
\text{conc}[G] &= 7.5 \times c\\
\text{conc}[TH] &= 1.1 \times 1.8 \times c\\
y &= Fluor_6
\end{aligned}
$$

$$
\begin{aligned}
&\text{seesawAND}[2,5,\{1,3\},\{6\}]\\
&\text{seesawOR}[4,1,\{8,9\},\{2\}]\\
&\text{reporter}[6,5]\\
\text{conc}[w_{8,4}] &= x_1 \times c\\
\text{conc}[w_{9,4}] &= x_2 \times c\\
\text{conc}[w_{3,2}] &= x_3 \times c\\
\text{conc}[W] &= (4 + x_1 + x_2 + x_3) \times c\\
\text{conc}[G] &= 7.5 \times c\\
\text{conc}[TH] &= 1.1 \times 1.8 \times c\\
y &= Fluor_6
\end{aligned}
$$

$$
\begin{aligned}
&\text{seesawAND}[2,5,\{1,3\},\{6\}]\\
&\text{seesawAND}[4,1,\{8,9\},\{2\}]\\
&\text{reporter}[6,5]\\
\text{conc}[w_{8,4}] &= x_1 \times c\\
\text{conc}[w_{9,4}] &= x_2 \times c\\
\text{conc}[w_{3,2}] &= x_3 \times c\\
\text{conc}[W] &= (4 + x_1 + x_2 + x_3) \times c\\
\text{conc}[G] &= 7.5 \times c\\
\text{conc}[TH] &= 1.1 \times 2.4 \times c\\
y &= Fluor_6
\end{aligned}
$$

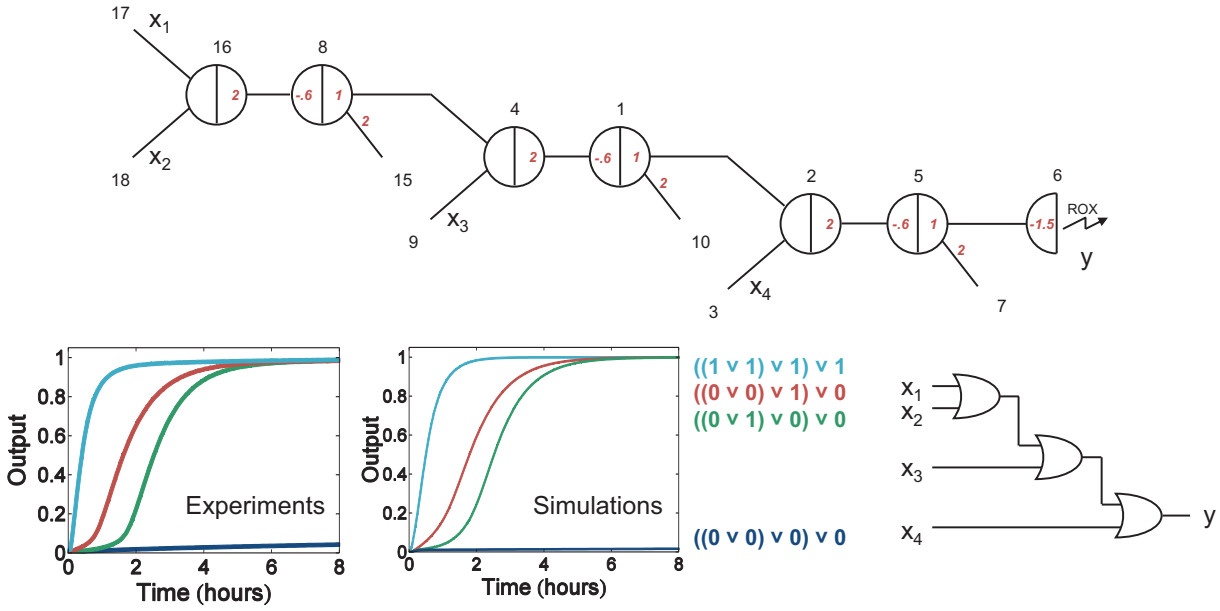

Figure S26: Simulations of the three-layer OR cascade. (Experimental data is from Fig. S6B.) Standard concentration $c = 100 \times 10^{-9}$ M. Rate parameters are set according to 20 °C. Inputs x_1 to x_4 are either 0.1 (0, logic OFF) or 0.9 (1, logic ON).

$$
\begin{aligned}
\text{seesawOR}[2, 5, \{1, 3\}, \{6\}] & \\
\text{seesawOR}[4, 1, \{8, 9\}, \{2\}] & \\
\text{seesawOR}[16, 8, \{17, 18\}, \{4\}] & \\
\text{reporter}[6, 5] & \\
\text{conc}[w_{17,16}] &= x_1 \times c \\
\text{conc}[w_{18,16}] &= x_2 \times c \\
\text{conc}[w_{9,4}] &= x_3 \times c \\
\text{conc}[w_{3,2}] &= x_4 \times c \\
\text{conc}[W] &= (6 + x_1 + x_2 + x_3 + x_4) \times c \\
\text{conc}[G] &= 10.5 \times c \\
\text{conc}[TH] &= 1.1 \times 1.8 \times c \\
y &= Fluor_6
\end{aligned}
$$

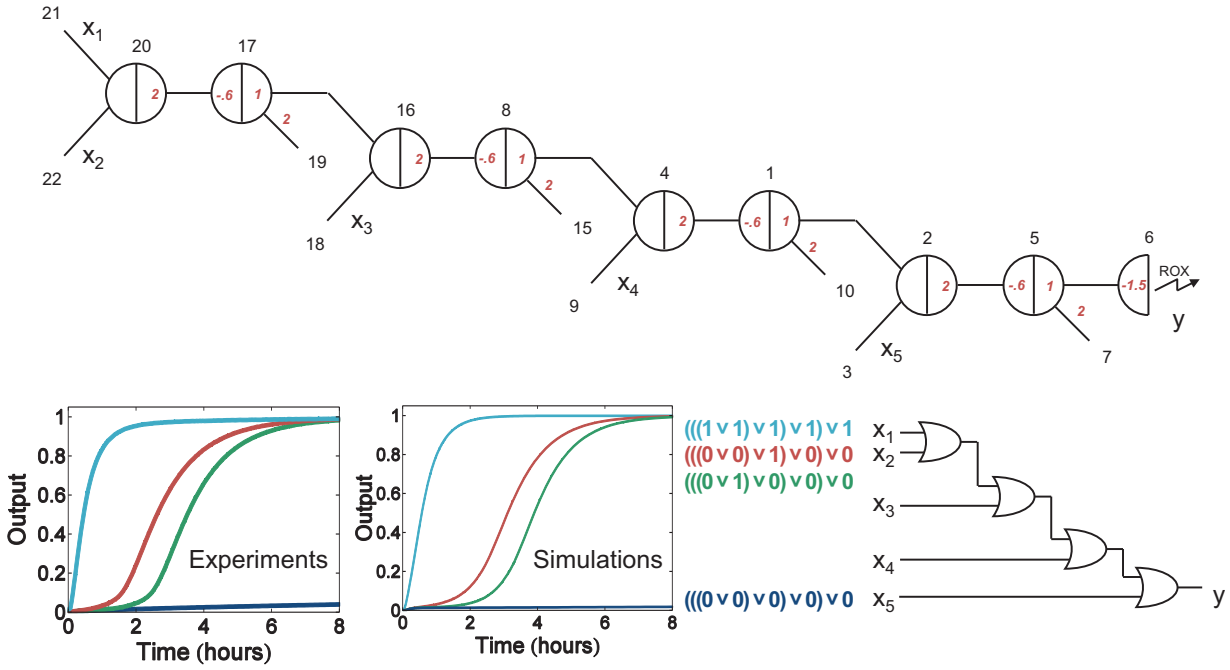

Figure S27: Simulations of the four-layer OR cascade. (Experimental data is from Fig. S6D.) Standard concentration $c = 100 \times 10^{-9}$ M. Rate parameters are set according to 20 °C. Inputs x_1 to x_5 are either 0.1 (0, logic OFF) or 0.9 (1, logic ON).

$$
\begin{aligned}
&\text{seesawOR}[2,5,\{1,3\},\{6\}] \\
&\text{seesawOR}[4,1,\{8,9\},\{2\}] \\
&\text{seesawOR}[16,8,\{17,18\},\{4\}] \\
&\text{seesawOR}[20,17,\{21,22\},\{16\}] \\
&\text{reporter}[6,5] \\
\text{conc}[w_{21,20}] &= x_1 \times c \\
\text{conc}[w_{22,20}] &= x_2 \times c \\
\text{conc}[w_{18,16}] &= x_3 \times c \\
\text{conc}[w_{9,4}] &= x_4 \times c \\
\text{conc}[w_{3,2}] &= x_5 \times c \\
\text{conc}[W] &= (8 + x_1 + x_2 + x_3 + x_4 + x_5) \times c \\
\text{conc}[G] &= 13.5 \times c \\
\text{conc}[TH] &= 1.1 \times 2.4 \times c \\
y &= Fluor_6
\end{aligned}
$$

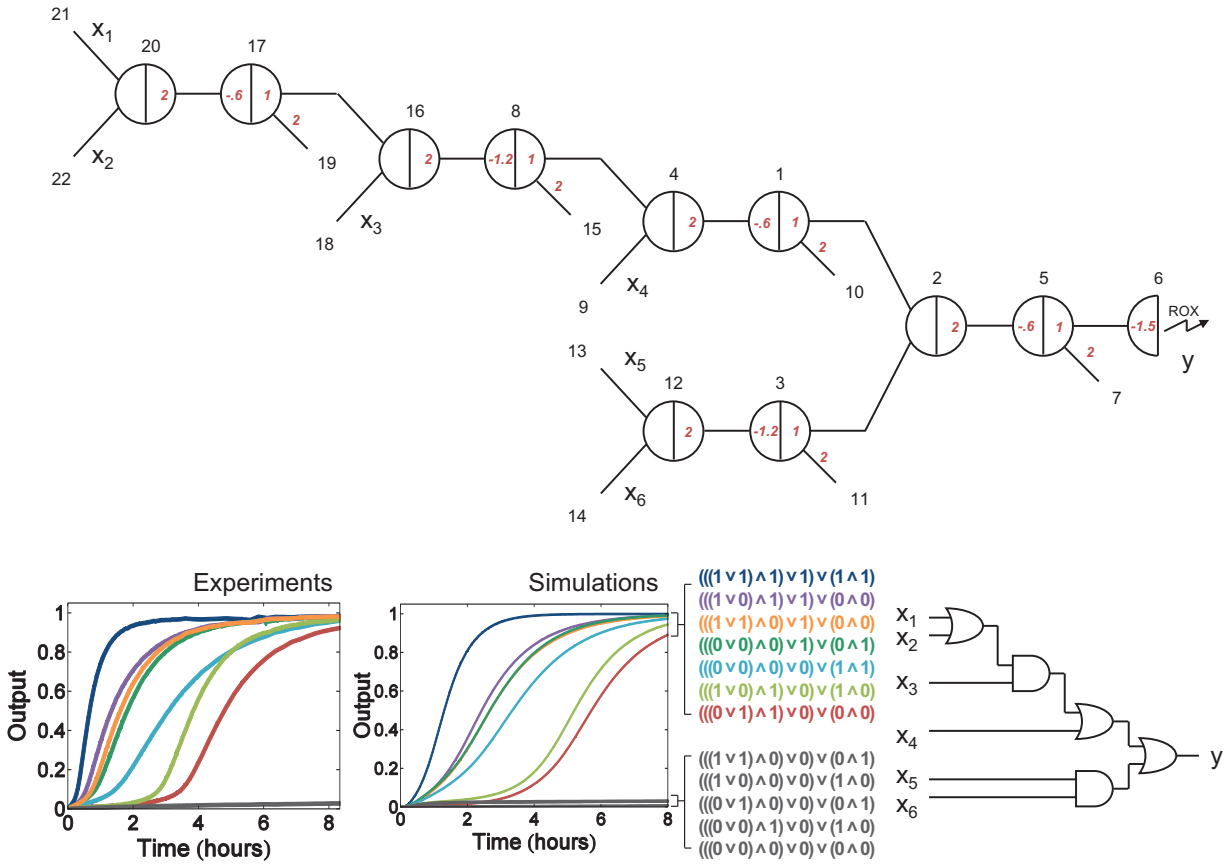

Figure S28: Simulations of the circuit with five AND/OR gates and four layers. (Experimental data is from Fig. 3C and Fig. S7.) Standard concentration $c = 100 \times 10^{-9}$ M. Rate parameters are set according to 20 °C. Inputs x_1 to x_6 are either 0.1 (0, logic OFF) or 0.9 (1, logic ON).

$$
\begin{aligned}
\text{seesawOR}[2, 5, \{1, 3\}, \{6\}] & \\
\text{seesawAND}[12, 3, \{13, 14\}, \{2\}] & \\
\text{seesawOR}[4, 1, \{8, 9\}, \{2\}] & \\
\text{seesawAND}[16, 8, \{17, 18\}, \{4\}] & \\
\text{seesawOR}[20, 17, \{21, 22\}, \{16\}] & \\
\text{reporter}[6, 5] & \\
\text{conc}[w_{21,20}] &= x_1 \times c \\
\text{conc}[w_{22,20}] &= x_2 \times c \\
\text{conc}[w_{18,16}] &= x_3 \times c \\
\text{conc}[w_{9,4}] &= x_4 \times c \\
\text{conc}[w_{13,12}] &= x_5 \times c \\
\text{conc}[w_{14,12}] &= x_6 \times c \\
\text{conc}[W] &= (10 + x_1 + x_2 + x_3 + x_4 + x_5 + x_6) \times c \\
\text{conc}[G] &= 16.5 \times c \\
\text{conc}[TH] &= 1.1 \times 4.2 \times c \\
y &= Fluor_6
\end{aligned}
$$

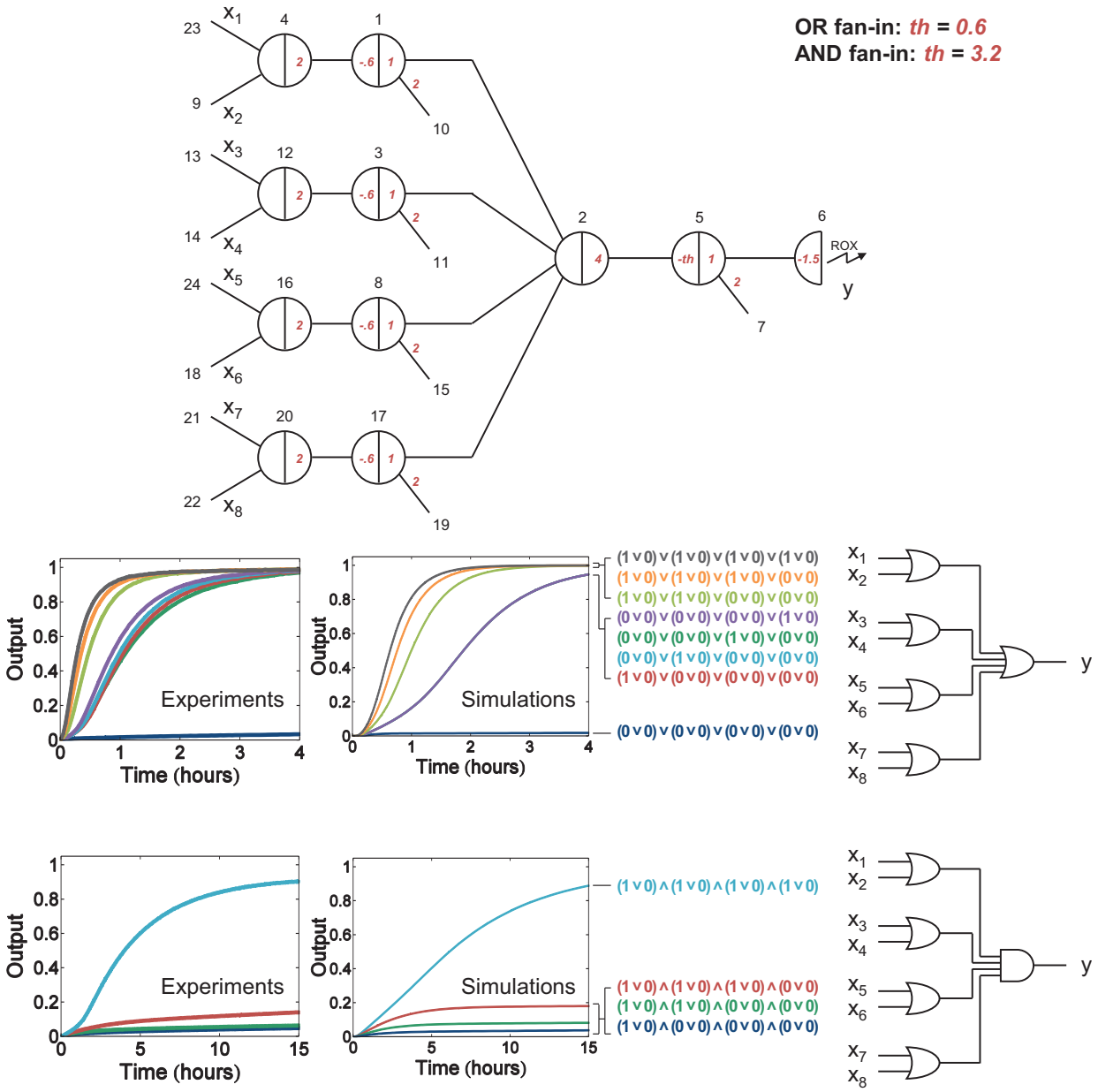

Figure S29: Simulations of the circuits with four-input AND or OR gates. (Experimental data is from Fig. 3D and Fig. S8.) Standard concentration $c = 100 \times 10^{-9}$ M. Rate parameters are set according to 20 °C. Inputs x_1 to x_8 are either 0.1 (0, logic OFF) or 0.9 (1, logic ON).

$$
\begin{aligned}
\text{seesawOR}[2,5,\{1,3,8,17\},\{6\}] & \\
\text{seesawOR}[4,1,\{23,9\},\{2\}] & \\
\text{seesawOR}[12,3,\{13,14\},\{2\}] & \\
\text{seesawOR}[16,8,\{24,18\},\{2\}] & \\
\text{seesawOR}[20,17,\{21,22\},\{2\}] & \\
\text{reporter}[6,5] & \\
\text{conc}[w_{23,4}] &= x_1 \times c \\
\text{conc}[w_{9,4}] &= x_2 \times c \\
\text{conc}[w_{13,12}] &= x_3 \times c \\
\text{conc}[w_{14,12}] &= x_4 \times c \\
\text{conc}[w_{24,16}] &= x_5 \times c \\
\text{conc}[w_{18,16}] &= x_6 \times c \\
\text{conc}[w_{21,20}] &= x_7 \times c \\
\text{conc}[w_{22,20}] &= x_8 \times c \\
\text{conc}[W] &= (10 + x_1 + x_2 + x_3 + x_4 + x_5 + x_6 + x_7 + x_8) \times c \\
\text{conc}[G] &= 18.5 \times c \\
\text{conc}[TH] &= 1.1 \times 3 \times c \\
y &= Fluor_6
\end{aligned}
$$

$$
\begin{aligned}
\text{seesawAND}[2,5,\{1,3,8,17\},\{6\}] & \\
\text{seesawOR}[4,1,\{23,9\},\{2\}] & \\
\text{seesawOR}[12,3,\{13,14\},\{2\}] & \\
\text{seesawOR}[16,8,\{24,18\},\{2\}] & \\
\text{seesawOR}[20,17,\{21,22\},\{2\}] & \\
\text{reporter}[6,5] & \\
\text{conc}[w_{23,4}] &= x_1 \times c \\
\text{conc}[w_{9,4}] &= x_2 \times c \\
\text{conc}[w_{13,12}] &= x_3 \times c \\
\text{conc}[w_{14,12}] &= x_4 \times c \\
\text{conc}[w_{24,16}] &= x_5 \times c \\
\text{conc}[w_{18,16}] &= x_6 \times c \\
\text{conc}[w_{21,20}] &= x_7 \times c \\
\text{conc}[w_{22,20}] &= x_8 \times c \\
\text{conc}[W] &= (10 + x_1 + x_2 + x_3 + x_4 + x_5 + x_6 + x_7 + x_8) \times c \\
\text{conc}[G] &= 18.5 \times c \\
\text{conc}[TH] &= 1.1 \times 5.6 \times c \\
y &= Fluor_6
\end{aligned}
$$

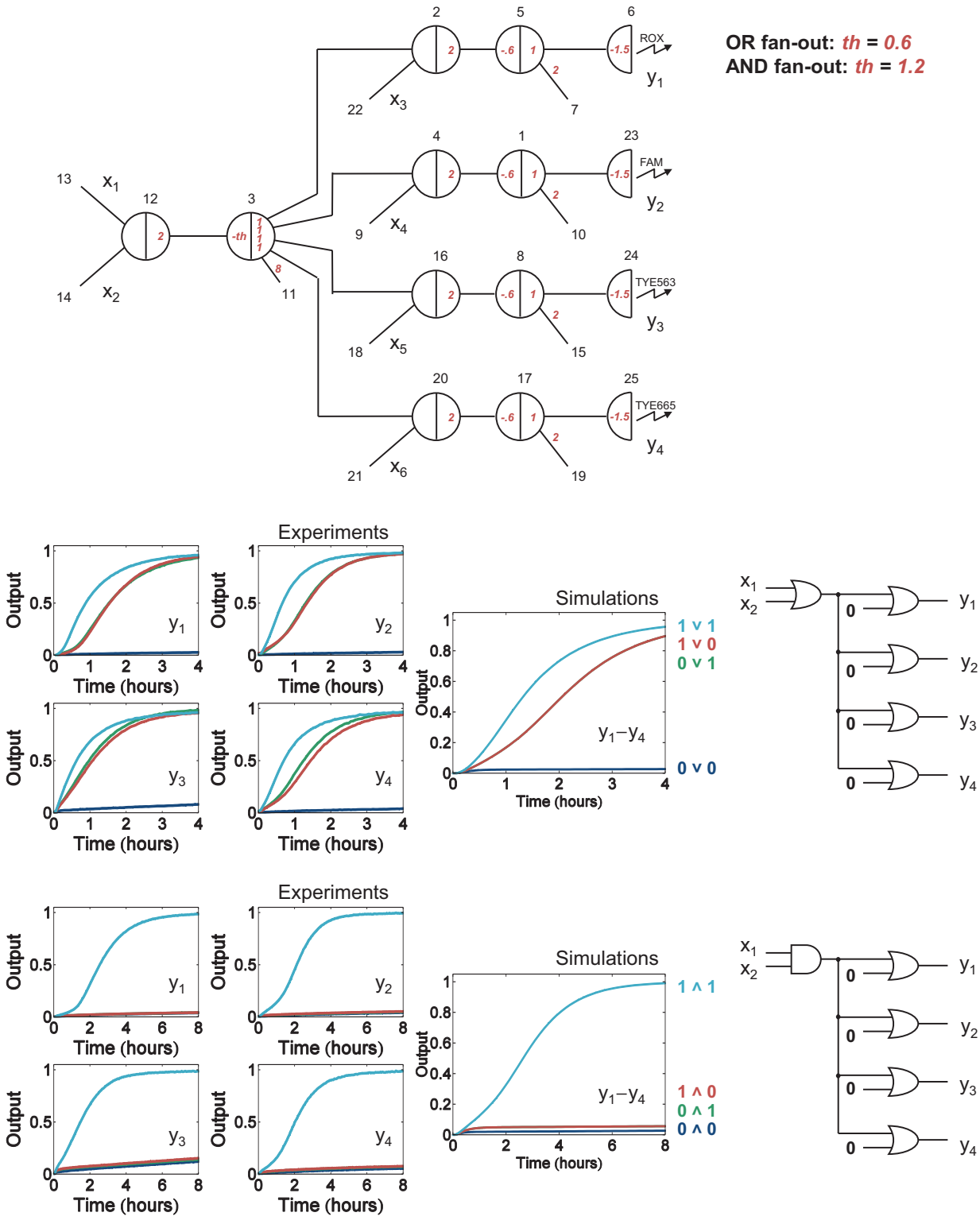

Figure S30: Simulations of the circuits with four-output AND or OR gates. (Experimental data is from Fig. 3E and Fig. S9.) Standard concentration $c = 100 \times 10^{-9}$ M. Rate parameters are set according to 20 °C. Inputs x_1 and x_2 are either 0.1 (0, logic OFF) or 0.9 (1, logic ON).

$$
\begin{aligned}
&\text{seesawOR}[12, 3, \{13, 14\}, \{2, 4, 16, 20\}] \\
&\text{seesawOR}[2, 5, \{3, 22\}, \{6\}] \\
&\text{seesawOR}[4, 1, \{3, 9\}, \{23\}] \\
&\text{seesawOR}[16, 8, \{3, 18\}, \{24\}] \\
&\text{seesawOR}[20, 17, \{3, 21\}, \{25\}] \\
&\text{reporter}[6, 5] \\
&\text{reporter}[23, 1] \\
&\text{reporter}[24, 8] \\
&\text{reporter}[25, 17] \\
\text{conc}[w_{13,12}] &= x_1 \times c \\
\text{conc}[w_{14,12}] &= x_2 \times c \\
\text{conc}[w_{22,2}] &= 0.1 \times c \\
\text{conc}[w_{9,4}] &= 0.1 \times c \\
\text{conc}[w_{18,16}] &= 0.1 \times c \\
\text{conc}[w_{21,20}] &= 0.1 \times c \\
\text{conc}[W] &= (16.4 + x_1 + x_2) \times c \\
\text{conc}[G] &= 19.5 \times c \\
\text{conc}[TH] &= 1.1 \times 3 \times c \\
y_1 &= Fluor_6 \\
y_2 &= Fluor_{23} \\
y_3 &= Fluor_{24} \\
y_4 &= Fluor_{25}
\end{aligned}
$$

$$
\begin{aligned}
&\text{seesawAND}[12, 3, \{13, 14\}, \{2, 4, 16, 20\}] \\
&\text{seesawOR}[2, 5, \{3, 22\}, \{6\}] \\
&\text{seesawOR}[4, 1, \{3, 9\}, \{23\}] \\
&\text{seesawOR}[16, 8, \{3, 18\}, \{24\}] \\
&\text{seesawOR}[20, 17, \{3, 21\}, \{25\}] \\
&\text{reporter}[6, 5] \\
&\text{reporter}[23, 1] \\
&\text{reporter}[24, 8] \\
&\text{reporter}[25, 17] \\
\text{conc}[w_{13,12}] &= x_1 \times c \\
\text{conc}[w_{14,12}] &= x_2 \times c \\
\text{conc}[w_{22,2}] &= 0.1 \times c \\
\text{conc}[w_{9,4}] &= 0.1 \times c \\
\text{conc}[w_{18,16}] &= 0.1 \times c \\
\text{conc}[w_{21,20}] &= 0.1 \times c \\
\text{conc}[W] &= (16.4 + x_1 + x_2) \times c \\
\text{conc}[G] &= 19.5 \times c \\
\text{conc}[TH] &= 1.1 \times 3.6 \times c \\
y_1 &= Fluor_6 \\
y_2 &= Fluor_{23} \\
y_3 &= Fluor_{24} \\
y_4 &= Fluor_{25}
\end{aligned}
$$

Temperature: 25 °C		
k_s	=	5×10^4 $M^{-1}s^{-1}$
k_f	=	2×10^6 $M^{-1}s^{-1}$
k_{rs}	=	1.3 s^{-1}
k_{rf}	=	26 s^{-1}
k_l	=	10 $M^{-1}s^{-1}$

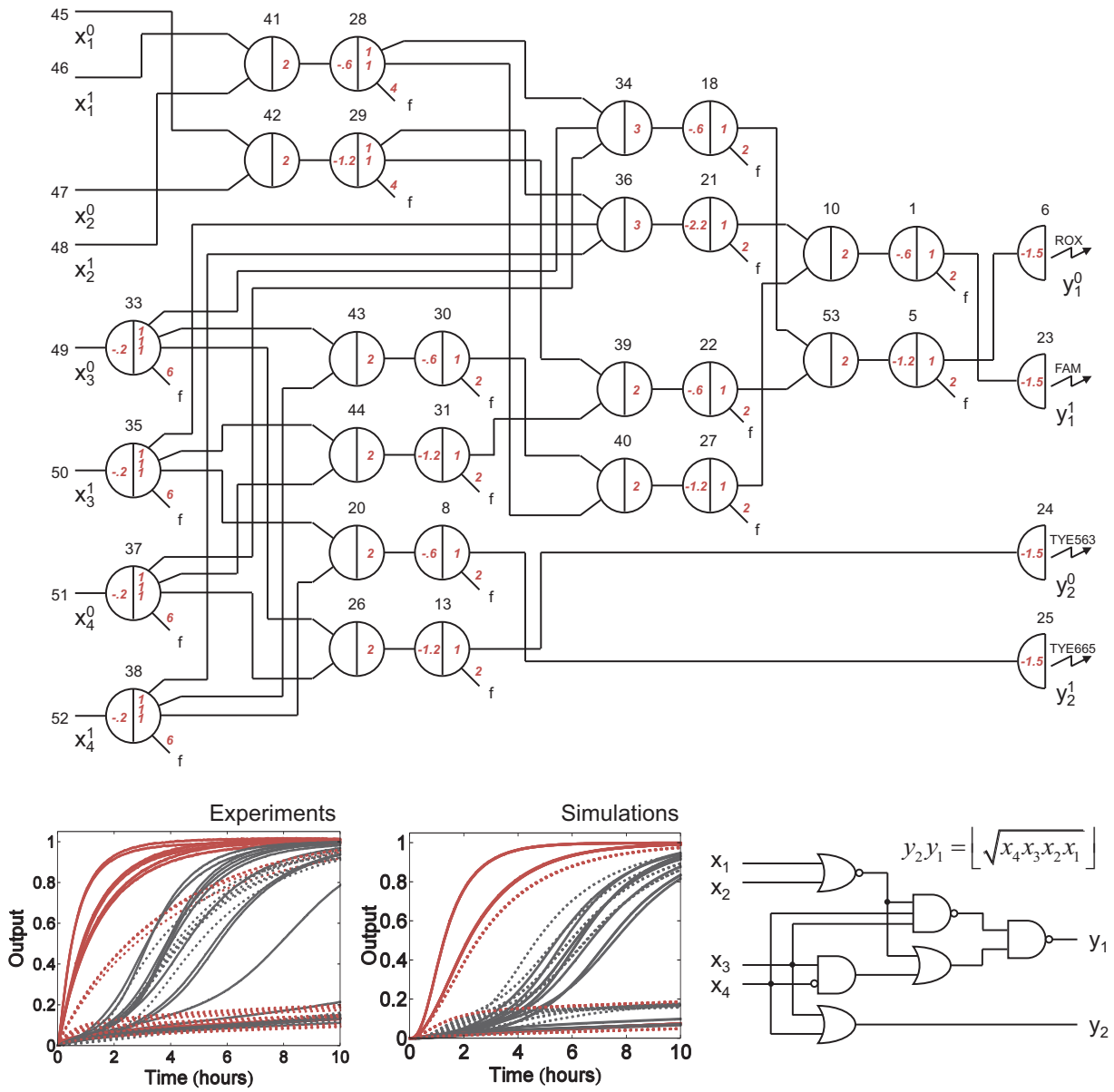

Figure S31: Simulations of the square root circuit. (Experimental data is from Fig. 4 and Fig. S11.) Standard concentration $c = 50 \times 10^{-9}$ M. Rate parameters are set according to 25 °C. Compared to rate parameters used for 20 °C experiments (Figs. S23 to S30), the reverse rates are increased by a factor of 2.6 and the leak is increased by a factor of 10, which are biophysically plausible. Inputs x_1 to x_4 are either 0.1 (0, logic OFF) or 0.9 (1, logic ON).

$$
\begin{aligned}
\text{seesawOR}[10, 1, \{21, 27\}, \{23\}] \\
\text{seesawAND}[53, 5, \{18, 22\}, \{6\}] \\
\text{seesawOR}[34, 18, \{28, 33, 37\}, \{53\}] \\
\text{seesawAND}[36, 21, \{29, 35, 38\}, \{10\}] \\
\text{seesawOR}[39, 22, \{29, 31\}, \{53\}] \\
\text{seesawAND}[40, 27, \{30, 28\}, \{10\}] \\
\text{seesawOR}[41, 28, \{46, 48\}, \{34, 40\}] \\
\text{seesawAND}[42, 29, \{45, 47\}, \{36, 39\}] \\
\text{seesawOR}[43, 30, \{33, 38\}, \{40\}] \\
\text{seesawAND}[44, 31, \{35, 37\}, \{39\}] \\
\text{seesawOR}[20, 8, \{35, 38\}, \{25\}] \\
\text{seesawAND}[26, 13, \{33, 37\}, \{24\}] \\
\text{inputfanout}[33, 49, \{34, 43, 26\}] \\
\text{inputfanout}[35, 50, \{36, 44, 20\}] \\
\text{inputfanout}[37, 51, \{34, 44, 26\}] \\
\text{inputfanout}[38, 52, \{36, 43, 20\}] \\
\text{reporter}[6, 5] \\
\text{reporter}[23, 1] \\
\text{reporter}[24, 13] \\
\text{reporter}[25, 8]
\end{aligned}
$$

$$
\begin{aligned}
\text{conc}[w_{45,42}] &= (1 - x_1) \times c \\
\text{conc}[w_{46,41}] &= x_1 \times c \\
\text{conc}[w_{47,42}] &= (1 - x_2) \times c \\
\text{conc}[w_{48,41}] &= x_2 \times c \\
\text{conc}[w_{49,33}] &= (1 - x_3) \times c \\
\text{conc}[w_{50,35}] &= x_3 \times c \\
\text{conc}[w_{51,37}] &= (1 - x_4) \times c \\
\text{conc}[w_{52,38}] &= x_4 \times c \\
\text{conc}[W] &= 56 \times c \\
\text{conc}[G] &= 58 \times c \\
\text{conc}[TH] &= 1.1 \times 12.6 \times c \\
y_1^0 &= Fluor_6 \\
y_1^1 &= Fluor_{23} \\
y_2^0 &= Fluor_{24} \\
y_2^1 &= Fluor_{25}
\end{aligned}
$$

S14. A seesaw compiler

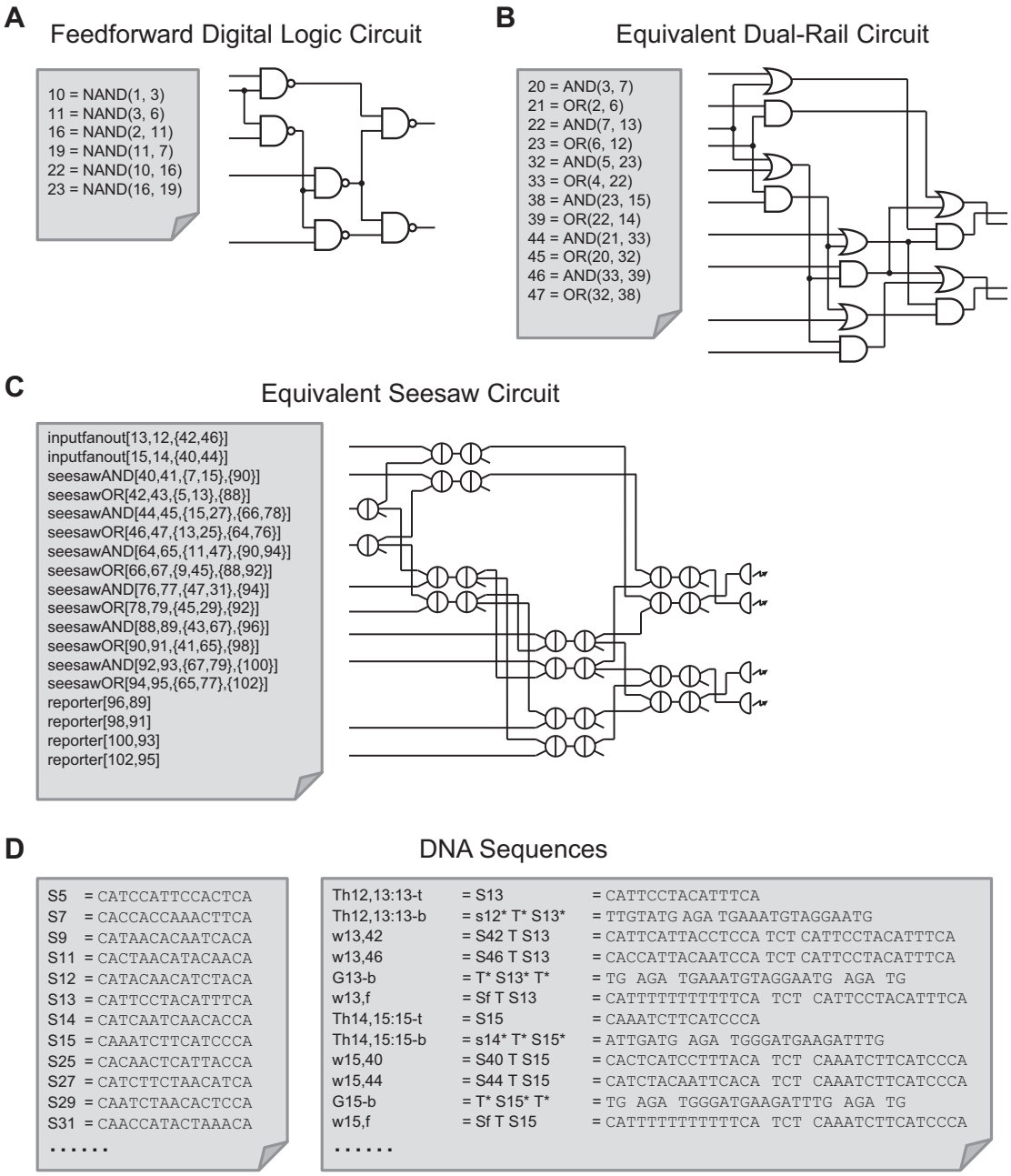

Figure S 32: Stages in a seesaw compiler (written in Perl, and online at [21]) that automatically translates an arbitrary feedforward digital logic circuit into its equivalent seesaw circuit. (A) It inputs a file containing a digital circuit netlist. (B) It then generates an equivalent dual-rail circuit file. (C) It then generates seesaw circuit files specifying gates and their connections, and relative concentrations of all initial species. (D) Finally, it generates DNA sequence files containing signal strands, top and bottom strands for threshold complexes, gate complexes and reporters.

Figure S33: The seesaw compiler automatically generates a Mathematica package file and an SBML file for simulations at the chemical reaction network level, and generates a DSD file for visualization and simulation at the domain level. (A) Simulating a seesaw circuit at the chemical reaction network level in Mathematica. (B) Simulating a seesaw circuit at the chemical reaction network level using software that supports SBML (here, COPASI [43]). (C) Visualizing and simulating a seesaw circuit at the domain level in Visual DSD [10].

S15. Discussion on scalability and speed

S15.1. Spurious binding and concentrations

How well seesaw circuits, or other strand displacement circuits, will scale is a difficult question that will require careful theoretical and experimental study to answer definitively. At this time we can provide only a few preliminary comments. We have estimated in previous theoretical work [17] that seesaw circuits involving thousands of logic gates may be practically synthesized and executed, based on the available sequence design space for typical DNA lengths, current synthesis technologies using parallel DNA microarrays, and plausible mass-action rates and concentrations. Here, after developing quantitative models based on experimental data, we see that a major challenge for scaling up is the spurious binding between signal strands and the exposed toeholds. We chose a universal toehold sequence for all toehold domains in seesaw circuits, because there were a limited number of sufficiently distinct sequences for short toeholds, and given our aim for scalability, we wanted to confront this limitation early on. This choice seemed suitable for desired circuit function because the uniqueness of the recognition domains ensures that the spurious toehold binding will not lead to branch migration. However, the unproductive spurious binding changed the effective reaction rates by temporarily disabling some fraction of gate:signal and threshold complexes and by reducing the signal strand concentrations. Furthermore, the effectiveness of thresholding was decreased due to the extended toehold having more severe spurious interaction with the signal strands compared to the gate:signal complex, which caused the threshold reaction rate to decrease more significantly than the seesawing reaction rate. These arguments were supported by our experiments.

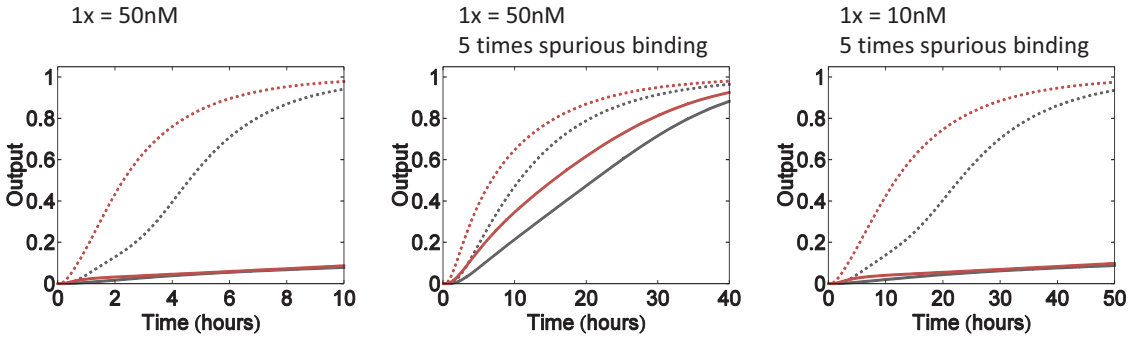

Figure S34: Simulations of the square root circuit with input 0000.

To examine how our model (which includes the spurious binding reactions) predicts these effects will influence larger circuits, we simulated a five times larger circuit where the spurious binding is five times worse (for convenience, we simulated five parallel copies of the four-bit square root circuit). As shown in Fig. S34, compared to the original square root circuit (left), the computation slowed down roughly by a factor of 4 and the expected OFF signals went ON (middle). However, decreasing the concentration by a factor of 5 recovered the correct computation while the slowdown remained about the same (right). This is consistent with theoretical expectations for the effect of spurious toehold binding: the $1\times$ concentration for a circuit with N gates should scale as $O(1/N)$ to retain a constant fraction of spuriously bound toeholds.

A related issue arises for the extended toeholds present in threshold complexes. In our model, we assume the slow toehold disassociation rate is 20 times slower than the fast toehold disassociation rate. (The fast toehold disassociation rate is the backward reaction rate of spurious toehold binding between signal strands and gate:signal complexes. The slow toehold disassociation rate is the backward reaction rate of spurious toehold binding between signal strands and threshold complexes – it is slower because threshold complexes have extended toeholds that are likely to bind to the signal strands by more than just the universal toehold domain.) In sequence design, we tried to avoid the similarity between the extended toeholds of threshold complexes and the signal strands that the thresholds are not suppose to absorb. However, this will become a challenge when the circuit scales up and the sequence space is more packed; in fact, for large circuits, it is inevitable that for any threshold complex, there will be some signal strands that spuriously interact by binding to the full extended toehold. In such cases, the slow toehold disassociation rate will not be preserved

– it will be even slower and thus lead to worse spurious binding. Again, this problem should be solved by using lower concentrations, with the same scaling principle as for spurious binding of universal toeholds.

A third factor (which is not explicitly enforced in our model, but was discussed in [17]) is simply the density of DNA molecules in solution. If we assume that there is a maximum total concentration of DNA nucleotides above which DNA interactions are no longer well modeled as well-mixed chemical reactions in a dilute solution, then it again follows that the $1\times$ concentration for a circuit with N gates should scale as $O(1/N)$ to keep the total nucleotide concentration bounded.

In summary, three independent arguments predict that scaling up seesaw circuits by a factor of N requires N-fold lower concentrations and thus N-fold slower reaction times. Further, due to more strenuous sequence design constraints and likely worse spurious binding will again require lower $1\times$ concentrations. These issues potentially could be ameliorated to a certain extent by (1) using multiple toehold sequences when possible, rather than a universal toehold sequence, (2) shortening the threshold toehold extension from 5 nt to 3 nt, and (3) increasing the temperature to reduce spurious binding.

S15.2. Architectural issues

The seesaw circuit architecture makes several different choices compared to previous experimentally demonstrated DNA strand displacement circuits [11, 12] that affect scalability and speed. We will briefly review the issues inherent in these systems, the choices and trade-offs made in the seesaw architecture, and the potential for improvements.

DNA strand displacement cascades capable of performing robust digital computation were introduced in Ref. [11]. In this architecture, a single multistranded DNA complex was used for each AND gate, for each threshold gate, and for each catalytic amplifying gate, while OR gates could be implemented implicitly without need for any DNA complexes. Furthermore, every strand displacement reaction was irreversible and could take place at the maximum strand displacement rate. However, multistranded complexes use longer strands and are more sensitive to synthesis errors than simpler complexes, the four-letter code (A, T, C, and G) used in single-stranded domain sequences makes it difficult to avoid spurious binding interactions [39], and signal restoration by thresholding and amplification was cumbersome and therefore employed only at the output of the largest circuit – rather than after every logical operation as is needed for fast [44] and robust operation in large circuits. Perhaps as a consequence of these issues, the largest circuit constructed (6 repeaters, 3 AND, 2 OR, 1 signal restoration) exhibited an unexplained slowdown by roughly a factor of 6 over what could be predicted from a characterization of the individual components ($t_{1/2}$ = 12 hr at 1×= 250 nM).

Ref. [12] introduced an improved catalysis mechanism that made use of reversible "toehold exchange" reactions in addition to irreversible strand displacement reactions. The use of a three-letter code (A, C, T) for single-stranded domains further improved the speed and facilitated accurate modeling [8, 39] by reducing spurious interactions. However, the catalysis mechanism still used multistranded complexes, did not standardize input and output strand sequence domain formats, and was not integrated with digital logic gates to articulate a full-fledged circuit architecture.

Our primary goals when developing seesaw circuits were to simplify the components to no more than two strands per gate and to articulate a systematic modular circuit architecture, in the hopes that this would facilitate the sequence design process and the experimental preparation and characterization of devices and systems. These hopes were realized, and additionally we found that three-letter codes could be used for sequence design and that seesaw circuits were sufficiently expressive and compact that it was possible to include signal restoration (thresholding and amplification) within every logical computation step. However, these advances came at a cost: the required roughly 20 times speed difference between threshold reactions and seesawing reactions implies that the seesawing reactions must be roughly 20 times slower than the maximal reaction rate for DNA strand displacement reactions, and additionally the reversible nature of the seesawing reactions introduces a backflow that inhibits completion of the net reaction. Even so, the largest circuit demonstrated here (4 repeaters, 6 AND, 6 OR, 12 signal restoration) computed faster than the smaller circuit of Ref. [11] despite 5× lower concentrations ($t_{1/2} < 8$ hr at 1×= 50 nM). Furthermore, it was accurately modeled using parameters consistent with prior characterization of the individual components.

It would be desirable to combine the best features of all these architectures. This calls for simple mechanisms capable of logic, thresholding, and catalysis using fast irreversible reactions, which may be difficult to achieve. On the other hand, seesaw circuits without thresholding have the potential to perform computation faster than the digital logic circuits demonstrated here, since they are free to use longer toeholds that yield maximal toehold exchange rate constants. Simple examples of analog time-domain circuits without thresholds were discussed in [17], but characterizing the computational power of seesaw circuits without thresholding remains an important open question.

There are also techniques to speed up hybridization itself, which might help strand displacement circuits in general. For example, the phenol emulsion reassociation technique (PERT) has been reported to speed up hybridization dynamics by four orders of magnitude. If the exponential dependence on toehold lengths is preserved under these conditions, this technique would reduce the seesaw AND or OR computation to seconds.

Table S1: Seesaw domain level sequences. Here and elsewhere all sequences start from the 5' end.

c	= CA	t	= TCT		
c*	= TG	t*	= AGA		
S1	= CATCCATTCCACTCA	S2	= CAAAACAAAACCTCA	S3	= CACCCTAAAATCTCA
S1*	= TGAGTGGAATGGATG	S2*	= TGAGGTTTTGTTTTG	S3*	= TGAGATTTTAGGGTG
S4	= CACATAACAACCACA	S5	= CACCACCAAACTTCA	S6	= CATAACACAATCACA
S4*	= TGTGGTTGTTATGTG	S5*	= TGAAGTTTGGTGGTG	S6*	= TGTGATTGTGTTATG
S7	= CAACATATCAATTCA	S8	= CACTAACATACAACA	S9	= CACCATCAAATAACA
S7*	= TGAATTGATATGTTG	S8*	= TGTTGTATGTTAGTG	S9*	= TGTTATTTGATGGTG
S10	= CATACAACATCTACA	S11	= CAATATCCATAACCA	S12	= CATCAATCAACACCA
S10*	= TGTAGATGTTGTATG	S11*	= TGGTTATGGATATTG	S12*	= TGGTGTTGATTGATG
S13	= CACAACTCATTACCA	S14	= CATTATTCAAACCCA	S15	= CACACTATAATTCCA
S13*	= TGGTAATGAGTTGTG	S14*	= TGGGTTTGAATAATG	S15*	= TGGAATTATAGTGTG
S16	= CACTTCATAAATCCA	S17	= CAACTCCTAATATCA	S18	= CATCTTCTAACATCA
S16*	= TGGATTTATGAAGTG	S17*	= TGATATTAGGAGTTG	S18*	= TGATGTTAGAAGATG
S19	= CACCTCTTAAACACA	S20	= CAATCTAACACTCCA	S21	= CAACCATACTAAACA
S19*	= TGTGTTTAAGAGGTG	S20*	= TGGAGTGTTAGATTG	S21*	= TGTTTAGTATGGTTG
S22	= CATTCCTACATTTCA	S23	= CAAATCTTCATCCCA	S24	= CACTCATCCTTTACA
S22*	= TGAAATGTAGGAATG	S23*	= TGGGATGAAGATTTG	S24*	= TGTAAAGGATGAGTG
S25	= CAATTCACTCAATCA	S26	= CATTCATTACCTCCA	S27	= CAAACACTCTATTCA
S25*	= TGATTGAGTGAATTG	S26*	= TGGAGGTAATGAATG	S27*	= TGAATAGAGTGTTTG
S28	= CATCTACAATTCACA	S29	= CACCAATACTCCTCA	S30	= CACCATTACAATCCA
S28*	= TGTGAATTGTAGATG	S29*	= TGAGGAGTATTGGTG	S30*	= TGGATTGTAATGGTG
S31	= CAATCCACACTTCCA	S32	= CACACTTCAAACTCA	S33	= CAACTCAAACATACA
S31*	= TGGAAGTGTGGATTG	S32*	= TGAGTTTGAAGTGTG	S33*	= TGTATGTTTGAGTTG
S34	= CACATAACAAAACCA	S35	= CACTCTCCATCACCA	S36	= CAAACTAAACAACCA
S34*	= TGGTTTTGTTATGTG	S35*	= TGGTGATGGAGAGTG	S36*	= TGGTTGTTTAGTTTG
S37	= CACCTCTTCCCTTCA	S38	= CATACCCTTTTCTCA	S39	= CACTATACACACCCA
S37*	= TGAAGGGAAGAGGTG	S38*	= TGAGAAAAGGGTATG	S39*	= TGGGTGTGTATAGTG
S40	= CAATACAAATCCACA	S41	= CAACAAACCATTACA	S42	= CACTTTTCACTATCA
S40*	= TGTGGATTTGTATTG	S41*	= TGTAATGGTTTGTTG	S42*	= TGATAGTGAAAAGTG
S43	= CATCATACCTACTCA	S44	= CAAAACTCTCTCTCA	S45	= CACCCAAAACCCACA
S43*	= TGAGTAGGTATGATG	S44*	= TGAGAGAGAGTTTTG	S45*	= TGTGGGTTTTGGGTG
S46	= CAAACCCAACTCACA	S47	= CATTCTCCCACCTCA	S48	= CATCACCACTATACA
S46*	= TGTGAGTTGGGTTTG	S47*	= TGAGGTGGGAGAATG	S48*	= TGTATAGTGGTGATG
S49	= CATCCTTAACTCCCA	S50	= CATTACCAACCACCA	S51	= CACAAACTACATCCA
S49*	= TGGGAGTTAAGGATG	S50*	= TGGTGGTTGGTAATG	S51*	= TGGATGTAGTTTGTG
S52	= CACTTCACAACTACA	S53	= CATATCTAATCTCCA	Sf	= CATTTTTTTTTTTCA
S52*	= TGTAGTTGTGAAGTG	S53*	= TGGAGATTAGATATG		

Table S2: Seesaw small circuit sequences (part one). Shading indicates which strands were used in which circuits. P indicates PAGE purification by IDT, used only for input strands. H indicates HPLC purification by IDT, used only for reporter strand with fluorophores or quenchers. All other strands were ordered without any purification. See Fig. S16 for details of the clamp design that modifies the toehold T implementation.

		Circuit number	1	2	3	4	5	6	7	8	9
$w_{5,6}$	= S6 T S5	= CATAACACAATCACA TCT CACCACCAAACTTCA									
G_5-b	= T* S5* T*	= TG AGA TGAAGTTTGGTGGTG AGA TG									
$w_{5,7}$	= S7 T S5	= CAACATATCAATTCA TCT CACCACCAAACTTCA									
$Th_{2,5:5}$-t	= S5	= CACCACCAAACTTCA									
$Th_{2,5:5}$-b	= s2* T* S5*	= TGTTTTG AGA TGAAGTTTGGTGGTG									
$w_{2,5}$	= S5 T S2	= CACCACCAAACTTCA TCT CAAAACAAAACCTCA	P	P							
G_2-b	= T* S2* T*	= TG AGA TGAGGTTTTGTTTTG AGA TG									
$w_{1,2}$	= S2 T S1	= CAAAACAAAACCTCA TCT CATCCATTCCACTCA			P						
G_1-b	= T* S1* T*	= TG AGA TGAGTGGAATGGATG AGA TG									
$w_{1,10}$	= S10 T S1	= CATACAACATCTACA TCT CATCCATTCCACTCA									
$Th_{4,1:1}$-t	= S1	= CATCCATTCCACTCA									
$Th_{4,1:1}$-b	= s4* T* S1*	= TTATGTG AGA TGAGTGGAATGGATG									
$w_{4,1}$	= S1 T S4	= CATCCATTCCACTCA TCT CACATAACAACCACA									
G_4-b	= T* S4* T*	= TG AGA TGTGGTTGTTATGTG AGA TG									
$w_{3,2}$	= S2 T S3	= CAAAACAAAACCTCA TCT CACCCTAAAATCTCA			P	P	P	P			
G_3-b	= T* S3* T*	= TG AGA TGAGATTTTAGGGTG AGA TG									
$w_{3,11}$	= S11 T S3	= CAATATCCATAACCA TCT CACCCTAAAATCTCA									
$Th_{12,3:3}$-t	= S3	= CACCCTAAAATCTCA									
$Th_{12,3:3}$-b	= s12* T* S3*	= ATTGATG AGA TGAGATTTTAGGGTG									
$w_{12,3}$	= S3 T S12	= CACCCTAAAATCTCA TCT CATCAATCAACACCA									
G_{12}-b	= T* S12* T*	= TG AGA TGGTGTTGATTGATG AGA TG									
$w_{8,4}$	= S4 T S8	= CACATAACAACCACA TCT CACTAACATACAACA				P					
G_8-b	= T* S8* T*	= TG AGA TGTTGTATGTTAGTG AGA TG									
$w_{8,15}$	= S15 T S8	= CACACTATAATTCCA TCT CACTAACATACAACA									
$Th_{16,8:8}$-t	= S8	= CACTAACATACAACA									
$Th_{16,8:8}$-b	= s16* T* S8*	= TGAAGTG AGA TGTTGTATGTTAGTG									
$w_{16,8}$	= S8 T S16	= CACTAACATACAACA TCT CACTTCATAAATCCA									
G_{16}-b	= T* S16* T*	= TG AGA TGGATTTATGAAGTG AGA TG									
$w_{17,16}$	= S16 T S17	= CACTTCATAAATCCA TCT CAACTCCTAATATCA					P				
G_{17}-b	= T* S17* T*	= TG AGA TGATATTAGGAGTTG AGA TG									
$w_{17,19}$	= S19 T S17	= CACCTCTTAAACACA TCT CAACTCCTAATATCA									
$Th_{20,17:17}$-t	= S17	= CAACTCCTAATATCA									
$Th_{20,17:17}$-b	= s20* T* S17*	= TAGATTG AGA TGATATTAGGAGTTG									
$w_{20,17}$	= S17 T S20	= CAACTCCTAATATCA TCT CAATCTAACACTCCA									
G_{20}-b	= T* S20* T*	= TG AGA TGGAGTGTTAGATTG AGA TG									

Table S3: Seesaw small circuit sequences (part two). Shading indicates which strands were used in which circuits. P indicates PAGE purification by IDT, used only for input strands. H indicates HPLC purification by IDT, used only for reporter strand with fluorophores or quenchers. All other strands were ordered without any purification. See Fig. S16 for details of the clamp design that modifies the toehold T implementation.

		Circuit number	1	2	3	4	5	6	7	8	9
$w_{21,20}$	= S20 T S21	= CAATCTAACACTCCA TCT CAACCATACTAAACA						P	P	P	P
$w_{22,20}$	= S20 T S22	= CAATCTAACACTCCA TCT CATTCCTACATTTCA						P	P	P	
$w_{18,16}$	= S16 T S18	= CACTTCATAAATCCA TCT CATCTTCTAACATCA					P	P	P	P	P
$w_{9,4}$	= S4 T S9	= CACATAACAACCACA TCT CACCATCAAATAACA				P	P	P	P	P	P
$w_{13,12}$	= S12 T S13	= CATCAATCAACACCA TCT CACAACTCATTACCA							P	P	P
$w_{14,12}$	= S12 T S14	= CATCAATCAACACCA TCT CATTATTCAAACCCA							P	P	P
$w_{8,2}$	= S2 T S8	= CAAAACAAAACCTCA TCT CACTAACATACAACA									
$w_{17,2}$	= S2 T S17	= CAAAACAAAACCTCA TCT CAACTCCTAATATCA									
$w_{23,4}$	= S4 T S23	= CACATAACAACCACA TCT CAAATCTTCATCCCA								P	
$w_{24,16}$	= S16 T S24	= CACTTCATAAATCCA TCT CACTCATCCTTTACA								P	
$w_{3,4}$	= S4 T S3	= CACATAACAACCACA TCT CACCCTAAAATCTCA									
$w_{3,16}$	= S16 T S3	= CACTTCATAAATCCA TCT CACCCTAAAATCTCA									
$w_{3,20}$	= S20 T S3	= CAATCTAACACTCCA TCT CACCCTAAAATCTCA									
$w_{1,23}$	= S23 T S1	= CAAATCTTCATCCCA TCT CATCCATTCCACTCA									
$w_{8,24}$	= S24 T S8	= CACTCATCCTTTACA TCT CACTAACATACAACA									
$w_{17,25}$	= S25 T S17	= CAATTCACTCAATCA TCT CAACTCCTAATATCA									
$w_{22,2}$	= S2 T S22	= CAAAACAAAACCTCA TCT CATTCCTACATTTCA									P
Rep_6-t	= RQ S6	= /5IAbRQ/ CATAACACAATCACA	H	H	H	H	H	H	H	H	H
Rep_6-b	= T* S6* ROX	= TG AGA TGTGATTGTGTTATG /3ROXN/	H	H	H	H	H	H	H	H	H
Rep_{23}-t	= FQ S23	= /5IAbFQ/ CAAATCTTCATCCCA									H
Rep_{23}-b	= T* S23* FAM	= TG AGA TGGGATGAAGATTTG /36-FAM/									H
Rep_{24}-t	= RQ S24	= /5IAbRQ/ CACTCATCCTTTACA									H
Rep_{24}-b	= T* S24* TYE563	= TG AGA TGTAAAGGATGAGTG /3TYE563/									H
Rep_{25}-t	= RQ S25	= /5IAbRQ/ CAATTCACTCAATCA									H
Rep_{25}-b	= T* S25* TYE665	= TG AGA TGATTGAGTGAATTG /3TYE665/									H

Table S4: Seesaw square root circuit sequences (part one).

Gate strands (IDT unpurified)		
$w_{1,23}$	= S23 T S1	= CAAATCTTCATCCCA TCT CATCCATTCCACTCA
$w_{1,f}$	= Sf T S1	= CATTTTTTTTTTTCA TCT CATCCATTCCACTCA
G_1-b	= T* S1* T*	= TG AGA TGAGTGGAATGGATG AGA TG
$Th_{10,1:1}$-t	= S1	= CATCCATTCCACTCA
$Th_{10,1:1}$-b	= s10* T* S1*	= TTGTATG AGA TGAGTGGAATGGATG
$w_{10,1}$	= S1 T S10	= CATCCATTCCACTCA TCT CATACAACATCTACA
G_{10}-b	= T* S10* T*	= TG AGA TGTAGATGTTGTATG AGA TG
$w_{5,6}$	= S6 T S5	= CATAACACAATCACA TCT CACCACCAAACTTCA
$w_{5,f}$	= Sf T S5	= CATTTTTTTTTTTCA TCT CACCACCAAACTTCA
G_5-b	= T* S5* T*	= TG AGA TGAAGTTTGGTGGTG AGA TG
$Th_{53,5:5}$-t	= S5	= CACCACCAAACTTCA
$Th_{53,5:5}$-b	= s53* T* S5*	= AGATATG AGA TGAAGTTTGGTGGTG
$w_{53,5}$	= S5 T S53	= CACCACCAAACTTCA TCT CATATCTAATCTCCA
G_{53}-b	= T* S53* T*	= TG AGA TGGAGATTAGATATG AGA TG
$w_{8,25}$	= S25 T S8	= CAATTCACTCAATCA TCT CACTAACATACAACA
$w_{8,f}$	= Sf T S8	= CATTTTTTTTTTTCA TCT CACTAACATACAACA
G_8-b	= T* S8* T*	= TG AGA TGTTGTATGTTAGTG AGA TG
$Th_{20,8:8}$-t	= S8	= CACTAACATACAACA
$Th_{20,8:8}$-b	= s20* T* S8*	= TAGATTG AGA TGTTGTATGTTAGTG
$w_{20,8}$	= S8 T S20	= CACTAACATACAACA TCT CAATCTAACACTCCA
G_{20}-b	= T* S20* T*	= TG AGA TGGAGTGTTAGATTG AGA TG
$w_{13,24}$	= S24 T S13	= CACTCATCCTTTACA TCT CACAACTCATTACCA
$w_{13,f}$	= Sf T S13	= CATTTTTTTTTTTCA TCT CACAACTCATTACCA
G_{13}-b	= T* S13* T*	= TG AGA TGGTAATGAGTTGTG AGA TG
$Th_{26,13:13}$-t	= S13	= CACAACTCATTACCA
$Th_{26,13:13}$-b	= s26* T* S13*	= ATGAATG AGA TGGTAATGAGTTGTG
$w_{26,13}$	= S13 T S26	= CACAACTCATTACCA TCT CATTCATTACCTCCA
G_{26}-b	= T* S26* T*	= TG AGA TGGAGGTAATGAATG AGA TG
$w_{18,53}$	= S53 T S18	= CATATCTAATCTCCA TCT CATCTTCTAACATCA
$w_{18,f}$	= Sf T S18	= CATTTTTTTTTTTCA TCT CATCTTCTAACATCA
G_{18}-b	= T* S18* T*	= TG AGA TGATGTTAGAAGATG AGA TG
$Th_{34,18:18}$-t	= S18	= CATCTTCTAACATCA
$Th_{34,18:18}$-b	= s34* T* S18*	= TTATGTG AGA TGATGTTAGAAGATG
$w_{34,18}$	= S18 T S34	= CATCTTCTAACATCA TCT CACATAACAAAACCA
G_{34}-b	= T* S34* T*	= TG AGA TGGTTTTGTTATGTG AGA TG

Table S5: Seesaw square root circuit sequences (part two).

$w_{21,10}$	= S10 T S21	= CATACAACATCTACA TCT CAACCATACTAAACA
$w_{21,f}$	= Sf T S21	= CATTTTTTTTTTTCA TCT CAACCATACTAAACA
G_{21}-b	= T* S21* T*	= TG AGA TGTTTAGTATGGTTG AGA TG
$Th_{36,21:21}$-t	= S21	= CAACCATACTAAACA
$Th_{36,21:21}$-b	= s36* T* S21*	= TAGTTTG AGA TGTTTAGTATGGTTG
$w_{36,21}$	= S21 T S36	= CAACCATACTAAACA TCT CAAACTAAACAACCA
G_{36}-b	= T* S36* T*	= TG AGA TGGTTGTTTAGTTTG AGA TG
$w_{22,53}$	= S53 T S22	= CATATCTAATCTCCA TCT CATTCCTACATTTCA
$w_{22,f}$	= Sf T S22	= CATTTTTTTTTTTCA TCT CATTCCTACATTTCA
G_{22}-b	= T* S22* T*	= TG AGA TGAAATGTAGGAATG AGA TG
$Th_{39,22:22}$-t	= S22	= CATTCCTACATTTCA
$Th_{39,22:22}$-b	= s39* T* S22*	= TATAGTG AGA TGAAATGTAGGAATG
$w_{39,22}$	= S22 T S39	= CATTCCTACATTTCA TCT CACTATACACACCCA
G_{39}-b	= T* S39* T*	= TG AGA TGGGTGTGTATAGTG AGA TG
$w_{27,10}$	= S10 T S27	= CATACAACATCTACA TCT CAAACACTCTATTCA
$w_{27,f}$	= Sf T S27	= CATTTTTTTTTTTCA TCT CAAACACTCTATTCA
G_{27}-b	= T* S27* T*	= TG AGA TGAATAGAGTGTTTG AGA TG
$Th_{40,27:27}$-t	= S27	= CAAACACTCTATTCA
$Th_{40,27:27}$-b	= s40* T* S27*	= TGTATTG AGA TGAATAGAGTGTTTG
$w_{40,27}$	= S27 T S40	= CAAACACTCTATTCA TCT CAATACAAATCCACA
G_{40}-b	= T* S40* T*	= TG AGA TGTGGATTTGTATTG AGA TG
$w_{28,34}$	= S34 T S28	= CACATAACAAAACCA TCT CATCTACAATTCACA
$w_{28,40}$	= S40 T S28	= CAATACAAATCCACA TCT CATCTACAATTCACA
$w_{28,f}$	= Sf T S28	= CATTTTTTTTTTTCA TCT CATCTACAATTCACA
G_{28}-b	= T* S28* T*	= TG AGA TGTGAATTGTAGATG AGA TG
$Th_{41,28:28}$-t	= S28	= CATCTACAATTCACA
$Th_{41,28:28}$-b	= s41* T* S28*	= TTTGTTG AGA TGTGAATTGTAGATG
$w_{41,28}$	= S28 T S41	= CATCTACAATTCACA TCT CAACAAACCATTACA
G_{41}-b	= T* S41* T*	= TG AGA TGTAATGGTTTGTTG AGA TG
$w_{29,36}$	= S36 T S29	= CAAACTAAACAACCA TCT CACCAATACTCCTCA
$w_{29,39}$	= S39 T S29	= CACTATACACACCCA TCT CACCAATACTCCTCA
$w_{29,f}$	= Sf T S29	= CATTTTTTTTTTTCA TCT CACCAATACTCCTCA
G_{29}-b	= T* S29* T*	= TG AGA TGAGGAGTATTGGTG AGA TG
$Th_{42,29:29}$-t	= S29	= CACCAATACTCCTCA
$Th_{42,29:29}$-b	= s42* T* S29*	= AAAAGTG AGA TGAGGAGTATTGGTG
$w_{42,29}$	= S29 T S42	= CACCAATACTCCTCA TCT CACTTTTCACTATCA
G_{42}-b	= T* S42* T*	= TG AGA TGATAGTGAAAAGTG AGA TG

Table S6: Seesaw square root circuit sequences (part three).

$w_{30,40}$	= S40 T S30	= CAATACAAATCCACA TCT CACCATTACAATCCA
$w_{30,f}$	= Sf T S30	= CATTTTTTTTTTTCA TCT CACCATTACAATCCA
G_{30}-b	= T* S30* T*	= TG AGA TGGATTGTAATGGTG AGA TG
$Th_{43,30:30}$-t	= S30	= CACCATTACAATCCA
$Th_{43,30:30}$-b	= s43* T* S30*	= TATGATG AGA TGGATTGTAATGGTG
$w_{43,30}$	= S30 T S43	= CACCATTACAATCCA TCT CATCATACCTACTCA
G_{43}-b	= T* S43* T*	= TG AGA TGAGTAGGTATGATG AGA TG
$w_{31,39}$	= S39 T S31	= CACTATACACACCCA TCT CAATCCACACTTCCA
$w_{31,f}$	= Sf T S31	= CATTTTTTTTTTTCA TCT CAATCCACACTTCCA
G_{31}-b	= T* S31* T*	= TG AGA TGGAAGTGTGGATTG AGA TG
$Th_{44,31:31}$-t	= S31	= CAATCCACACTTCCA
$Th_{44,31:31}$-b	= s44* T* S31*	= AGTTTTG AGA TGGAAGTGTGGATTG
$w_{44,31}$	= S31 T S44	= CAATCCACACTTCCA TCT CAAAACTCTCTCTCA
G_{44}-b	= T* S44* T*	= TG AGA TGAGAGAGAGTTTTG AGA TG
$w_{33,34}$	= S34 T S33	= CACATAACAAAACCA TCT CAACTCAAACATACA
$w_{33,43}$	= S43 T S33	= CATCATACCTACTCA TCT CAACTCAAACATACA
$w_{33,26}$	= S26 T S33	= CATTCATTACCTCCA TCT CAACTCAAACATACA
$w_{33,f}$	= Sf T S33	= CATTTTTTTTTTTCA TCT CAACTCAAACATACA
G_{33}-b	= T* S33* T*	= TG AGA TGTATGTTTGAGTTG AGA TG
$Th_{49,33:33}$-t	= S33	= CAACTCAAACATACA
$Th_{49,33:33}$-b	= s49* T* S33*	= AAGGATG AGA TGTATGTTTGAGTTG
$w_{35,36}$	= S36 T S35	= CAAACTAAACAACCA TCT CACTCTCCATCACCA
$w_{35,44}$	= S44 T S35	= CAAAACTCTCTCTCA TCT CACTCTCCATCACCA
$w_{35,20}$	= S20 T S35	= CAATCTAACACTCCA TCT CACTCTCCATCACCA
$w_{35,f}$	= Sf T S35	= CATTTTTTTTTTTCA TCT CACTCTCCATCACCA
G_{35}-b	= T* S35* T*	= TG AGA TGGTGATGGAGAGTG AGA TG
$Th_{50,35:35}$-t	= S35	= CACTCTCCATCACCA
$Th_{50,35:35}$-b	= s50* T* S35*	= GGTAATG AGA TGGTGATGGAGAGTG
$w_{37,34}$	= S34 T S37	= CACATAACAAAACCA TCT CACCTCTTCCCTTCA
$w_{37,44}$	= S44 T S37	= CAAAACTCTCTCTCA TCT CACCTCTTCCCTTCA
$w_{37,26}$	= S26 T S37	= CATTCATTACCTCCA TCT CACCTCTTCCCTTCA
$w_{37,f}$	= Sf T S37	= CATTTTTTTTTTTCA TCT CACCTCTTCCCTTCA
G_{37}-b	= T* S37* T*	= TG AGA TGAAGGGAAGAGGTG AGA TG
$Th_{51,37:37}$-t	= S37	= CACCTCTTCCCTTCA
$Th_{51,37:37}$-b	= s51* T* S37*	= GTTTGTG AGA TGAAGGGAAGAGGTG

Table S7: Seesaw square root circuit sequences (part four).

$w_{38,36}$	= S36 T S38	= CAAACTAAACAACCA TCT CATACCCTTTTCTCA
$w_{38,43}$	= S43 T S38	= CATCATACCTACTCA TCT CATACCCTTTTCTCA
$w_{38,20}$	= S20 T S38	= CAATCTAACACTCCA TCT CATACCCTTTTCTCA
$w_{38,f}$	= Sf T S38	= CATTTTTTTTTTTCA TCT CATACCCTTTTCTCA
G_{38}-b	= T* S38* T*	= TG AGA TGAGAAAAGGGTATG AGA TG
$Th_{52,38:38}$-t	= S38	= CATACCCTTTTCTCA
$Th_{52,38:38}$-b	= s52* T* S38*	= TGAAGTG AGA TGAGAAAAGGGTATG
Reporter strands (IDT HPLC purified)		
Rep_6-t	= RQ S6	= /5IAbRQ/ CATAACACAATCACA
Rep_6-b	= T* S6* ROX	= TG AGA TGTGATTGTGTTATG /3ROXN/
Rep_{23}-t	= FQ S23	= /5IAbFQ/ CAAATCTTCATCCCA
Rep_{23}-b	= T* S23* FAM	= TG AGA TGGGATGAAGATTTG /36-FAM/
Rep_{24}-t	= RQ S24	= /5IAbRQ/ CACTCATCCTTTACA
Rep_{24}-b	= T* S24* TYE563	= TG AGA TGTAAAGGATGAGTG /3TYE563/
Rep_{25}-t	= RQ S25	= /5IAbRQ/ CAATTCACTCAATCA
Rep_{25}-b	= T* S25* TYE665	= TG AGA TGATTGAGTGAATTG /3TYE665/
Input strands (IDT PAGE purified)		
$x_1^0 : w_{45,42}$	= S42 T S45	= CACTTTTCACTATCA TCT CACCCAAAACCCACA
$x_1^1 : w_{46,41}$	= S41 T S46	= CAACAAACCATTACA TCT CAAACCCAACTCACA
$x_2^0 : w_{47,42}$	= S42 T S47	= CACTTTTCACTATCA TCT CATTCTCCCACCTCA
$x_2^1 : w_{48,41}$	= S41 T S48	= CAACAAACCATTACA TCT CATCACCACTATACA
$x_3^0 : w_{49,33}$	= S33 T S49	= CAACTCAAACATACA TCT CATCCTTAACTCCCA
$x_3^1 : w_{50,35}$	= S35 T S50	= CACTCTCCATCACCA TCT CATTACCAACCACCA
$x_4^0 : w_{51,37}$	= S37 T S51	= CACCTCTTCCCTTCA TCT CACAAACTACATCCA
$x_4^1 : w_{52,38}$	= S38 T S52	= CATACCCTTTTCTCA TCT CACTTCACAACTACA
Internal fan-out strands for readout (IDT unpurified)		
$w_{21,32}$	= S32 T S21	= CACACTTCAAACTCA TCT CAACCATACTAAACA
$w_{28,32}$	= S32 T S28	= CACACTTCAAACTCA TCT CATCTACAATTCACA
$w_{31,32}$	= S32 T S32	= CACACTTCAAACTCA TCT CAATCCACACTTCCA
Internal readout reporter strands (IDT HPLC purified)		
Rep_{32}-t	= RQ S32	= /5IAbRQ/ CACACTTCAAACTCA
Rep_{32}-b	= T* S32* Cy5.5	= TG AGA TGAGTTTGAAGTGTG /3Cy55Sp/

Table S8: Seesaw sequences without clamps.

Domain level sequences					
T	= CTCT	T*	= AGAG		
S1	= CATCCATTCCACTAT	S2	= CCAAACAAAACCTAT	S3	= CACCCTAAAATCTAT
S1*	= ATAGTGGAATGGATG	S2*	= ATAGGTTTTGTTTGG		
S4	= AACAAAACAACCACT	S5	= AACCACCAAACTTAT	S6	= CCTAACACAATCACT
S4*	= AGTGGTTGTTTTGTT	S5*	= ATAAGTTTGGTGGTT	S6*	= AGTGATTGTGTTAGG
S7	= CCACAAAACAAAACT	S8	= CCCAAATAAACAACT	S9	= CACCATCAAATAACT
S10	= TCAAAACCAACTACT				

Gate strands (IDT unpurified)		
$w_{5,6}$	= S6 T S5	= CCTAACACAATCACT CTCT AACCACCAAACTTAT
G_5-b	= T* S5* T*	= AGAG ATAAGTTTGGTGGTT AGAG
$w_{5,7}$	= S7 T S5	= CCACAAAACAAAACT CTCT AACCACCAAACTTAT
$Th_{2,5:5}$-t	= S5	= AACCACCAAACTTAT
$Th_{2,5:5}$-b	= s2* T* S5*	= TTTGG AGAG ATAAGTTTGGTGGTT
$w_{2,5}$	= S5 T S2	= AACCACCAAACTTAT CTCT CCAAACAAAACCTAT
G_2-b	= T* S2* T*	= AGAG ATAGGTTTTGTTTGG AGAG
$w_{1,2}$	= S2 T S1	= CCAAACAAAACCTAT CTCT CATCCATTCCACTAT
G_1-b	= T* S1* T*	= AGAG ATAGTGGAATGGATG AGAG
$w_{1,10}$	= S10 T S1	= TCAAAACCAACTACT CTCT CATCCATTCCACTAT
$Th_{4,1:1}$-t	= S1	= CATCCATTCCACTAT
$Th_{4,1:1}$-b	= s4* T* S1*	= TTGTT AGAG ATAGTGGAATGGATG
$w_{4,1}$	= S1 T S4	= CATCCATTCCACTAT CTCT AACAAAACAACCACT
G_4-b	= T* S4* T*	= AGAG AGTGGTTGTTTTGTT AGAG
Reporter strands (IDT HPLC purified)		
$Rep_{5,6}$-t	= RQ S6 T	= /5IAbRQ/ CCTAACACAATCACT CTCT
$Rep_{5,6}$-b	= s5* T* S6* ROX	= TGGTT AGAG AGTGATTGTGTTAGG/3ROXN/
Input strands (IDT PAGE purified)		
$w_{3,2}$	= S2 T S3	= CCAAACAAAACCTAT CTCT CACCCTAAAATCTAT
$w_{8,4}$	= S4 T S8	= AACAAAACAACCACT CTCT CCCAAATAAACAACT
$w_{9,4}$	= S4 T S9	= AACAAAACAACCACT CTCT CACCATCAAATAACT

Table S9: Seesaw hairpin sequences.

Domain level sequences					
T	= TGAGG	T*	= CCTCA		
S1	= TAGTTGGAAGAGGGC	S3	= GATGTAAGTATTTGC	S4	= AGTATGTAGTGTGGC
S1*	= GCCCTCTTCCAACTA	S3*	= GCAAATACTTACATC	S4*	= GCCACACTACATACT
S2	= GGATTAGGGGGTAGC				
Excised hairpin sequences with restriction enzyme recognition sites					
EH-HgaI	= NNNNNNNNNNGCGTCNTTTTNGACGCNNNNN				
EH-MlyI	= NNNNNGACTCNTTTTNGAGTCNNNNN				
Gate strands (IDT unpurified)					
$G_{3:3,1}$-h	= S1 T S3 EH-HgaI T* S3* T*	= TAGTTGGAAGAGGGC TGAGG GATGTAAGTATTTGC TGAGGCGCTGGCGTCGTTTTCGACGCCAGCG CCTCA GCAAATACTTACATC CCTCA			
$w_{3,2}$	= S2 T S3	= GGATTAGGGGGTAGC TGAGG GATGTAAGTATTTGC			
$Th_{4,3:3}$-h	= s4* T* S3* EH-MlyI S3	= ACT CCTCA GCAAATACTTACATC AACCAGACTCGTTTTCGAGTCTGGTT GATGTAAGTATTTGC			
Reporter strands (IDT HPLC purified)					
Rep_1-t	= TET S1	= /5TET/ TAGTTGGAAGAGGGC			
Rep_1-b	= T* S1* BHQ	= CCTCA GCCCTCTTCCAACTA /3BHQ_1/			
Input strands (IDT unpurified)					
$w_{4,3}$	= S3 T S4	= GATGTAAGTATTTGC TGAGG AGTATGTAGTGTGGC			

References

[1] L. M. Adleman. Molecular computation of solutions to combinatorial problems. *Science*, 266:1021–1024, 1994.

[2] M. N. Stojanovic and D. Stefanovic. A deoxyribozyme-based molecular automaton. *Nature Biotechnology*, 21:1069–1074, 2003.

[3] J. Elbaz, O. Lioubashevski, F. Wang, F. Remacle, R. D. Levine, and I. Willner. DNA computing circuits using libraries of DNAzyme subunits. *Nature Nanotechnology*, 5:417–422, 2010.

[4] Y. Benenson, B. Gil, U. Ben-Dor, R. Adar, and E. Shapiro. An autonomous molecular computer for logical control of gene expression. *Nature*, 429:423–429, 2004.

[5] B. Yurke, A. J. Turberfield, A. P. Mills, F. C. Simmel, and J. L. Neumann. A DNA-fuelled molecular machine made of DNA. *Nature*, 406:605–608, 2000.

[6] A. J. Turberfield, J. C. Mitchell, B. Yurke, A. P. Mills Jr, M. I. Blakey, and F. C. Simmel. DNA fuel for free-running nanomachines. *Physical Review Letters*, 90:118102, 2003.

[7] B. Yurke and A. P. Mills Jr. Using DNA to power nanostructures. *Genetic Programming and Evolvable Machines*, 4:111–122, 2003.

[8] D. Y. Zhang and E. Winfree. Control of DNA strand displacement kinetics using toehold exchange. *Journal of the American Chemical Society*, 131:17303–17314, 2009.

[9] D. Soloveichik, G. Seelig, and E. Winfree. DNA as a universal substrate for chemical kinetics. *Proceedings of the National Academy of Sciences USA*, 107:5393–5398, 2010.

[10] A. Phillips and L. Cardelli. A programming language for composable DNA circuits. *Journal of The Royal Society Interface*, 6:S419–S436, 2009.

[11] G. Seelig, D. Soloveichik, D. Y. Zhang, and E. Winfree. Enzyme-free nucleic acid logic circuits. *Science*, 314:1585–1588, 2006.

[12] D. Y. Zhang, A. J. Turberfield, B. Yurke, and E. Winfree. Engineering entropy-driven reactions and networks catalyzed by DNA. *Science*, 318:1121–1125, 2007.

[13] P. Yin, H. M. T. Choi, C. R. Calvert, and N. A. Pierce. Programming biomolecular self-assembly pathways. *Nature*, 451:318–322, 2008.

[14] S. Venkataraman, R. M. Dirks, C. T. Ueda, and N. A. Pierce. Selective cell death mediated by small conditional RNAs. *Proceedings of the National Academy of Sciences USA*, 107:16777–16782, 2010.

[15] H. M. T. Choi, J. Y. Chang, L. A. Trinh, J. E. Padilla, S. E. Fraser, and N. A. Pierce. Programmable in situ amplification for multiplexed imaging of mRNA expression. *Nature Biotechnology*, 28:1208–1212, 2010.

[16] G. Eckhoff, V. Codrea, A. D. Ellington, and X. Chen. Beyond allostery: Catalytic regulation of a deoxyribozyme through an entropy-driven DNA amplifier. *Journal of Systems Chemistry*, 1:13, 2010.

[17] L. Qian and E. Winfree. A simple DNA gate motif for synthesizing large-scale circuits. *Journal of the Royal Society Interface*. Published online February 4, 2011 [doi: 10.1098/rsif.2010.0729].

[18] D. E. Muller. Asynchronous logics and application to information processing. In *Symposium on the Application of Switching Theory to Space Technology*, pages 289–297. Stanford University Press, Stanford, California, 1963.

[19] J. Tian, K. Ma, and I. Saaem. Advancing high-throughput gene synthesis technology. *Molecular BioSystems*, 5:714–722, 2009.

[20] Justin S. Bois. *Analysis of interacting nucleic acids in dilute solutions*. PhD thesis, California Institute of Technology, 2007.

[21] `http://www.dna.caltech.edu/SeesawCompiler/`.

[22] M. Hucka, A. Finney, H. M. Sauro, H. Bolouri, J. C. Doyle, H. Kitano, A. P. Arkin, B. J. Bornstein, D. Bray, A. Cornish-Bowden, et al. The systems biology markup language (SBML): a medium for representation and exchange of biochemical network models. *Bioinformatics*, 19:524–531, 2003.

[23] P. W. K. Rothemund. Folding DNA to create nanoscale shapes and patterns. *Nature*, 440:297–302, 2006.

[24] H. Gu, J. Chao, S. J. Xiao, and N. C. Seeman. A proximity-based programmable DNA nanoscale assembly line. *Nature*, 465:202–205, 2010.

[25] K. Lund, A. J. Manzo, N. Dabby, N. Michelotti, A. Johnson-Buck, J. Nangreave, S. Taylor, R. Pei, M. N. Stojanovic, N. G. Walter, E. Winfree, and H. Yan. Molecular robots guided by prescriptive landscapes. *Nature*, 465:206–210, 2010.

[26] L. Qian, D. Solovechik, and E. Winfree. Efficient Turing-universal computation with DNA polymers. In Y. Sakakibara and Y. Mi, editors, *DNA Computing and Molecular Programming 16*, volume LNCS 6518, pages 123–140. Springer, 2011.

[27] E. Chiniforooshan, D. Doty, L. Kari, and S. Seki. Scalable, time-responsive, digital, energy-efficient molecular circuits using DNA strand displacement. In Y. Sakakibara and Y. Mi, editors, *DNA Computing and Molecular Programming 16*, volume LNCS 6518, pages 25–36. Springer, 2011.

[28] A. Goel and M. Ibrahimi. Renewable, time-responsive DNA logic gates for scalable digital circuits. In R. Deaton and A. Suyama, editors, *DNA Computing and Molecular Programming 15*, volume LNCS 5877, pages 67–77. Springer, 2009.

[29] E. B. Baum. Building an associative memory vastly larger than the brain. *Science*, 268:583–585, 1995.

[30] R. M. Dirks and N. A. Pierce. Triggered amplification by hybridization chain reaction. *Proceedings of the National Academy of Sciences USA*, 101:15275–15278, 2004.

[31] W. U. Dittmer, A. Reuter, and F. C. Simmel. A DNA-based machine that can cyclically bind and release thrombin. *Angewandte Chemie International Edition*, 43:3550–3553, 2004.

[32] V. N. Kim. MicroRNA biogenesis: coordinated cropping and dicing. *Nature Reviews Molecular Cell Biology*, 6:376–385, 2005.

[33] R. W. Carthew and E. J. Sontheimer. Origins and mechanisms of miRNAs and siRNAs. *Cell*, 136:642–655, 2009.

[34] Sequences for all DNA molecules used in this work are provided in the supporting online material.

[35] K. U. Mir. A restricted genetic alphabet for DNA computing. *DNA based computers 2*, pages 243–246, 1999.

[36] R. S. Braich, N. Chelyapov, C. Johnson, P. W. K. Rothemund, and L. M. Adleman. Solution of a 20-variable 3-SAT problem on a DNA computer. *Science*, 296:499–502, 2002.

[37] D. Faulhammer, A. R. Cukras, R. J. Lipton, and L. F. Landweber. Molecular computation: RNA solutions to chess problems. *Proceedings of the National Academy of Sciences USA*, 97:1385–1389, 2000.

[38] M. Y. Kao, M. Sanghi, and R. Schweller. Randomized fast design of short DNA words. *ACM Transactions on Algorithms (TALG)*, 5:1–24, 2009.

[39] D. Y. Zhang and E. Winfree. Robustness and modularity properties of a non-covalent DNA catalytic reaction. *Nucleic Acids Research*, 38:4182–4197, 2010.

[40] J. N. Zadeh, C. D. Steenberg, J. S. Bois, B. R. Wolfe, M. B. Pierce, A. R. Khan, R. M. Dirks, and N. A. Pierce. NUPACK: Analysis and design of nucleic acid systems. *Journal of Computational Chemistry*, 32:170–173, 2010.

[41] J. D. Puglisi and I. Tinoco, Jr. Absorbance Melting Curves of RNA. In J. E. Dahlberg and J. N. Abelson, editors, *Methods in Enzymology*, volume 180, pages 304–325, San Diego, 1989. Academic Press.

[42] J. G. Wetmur. Applications of the principles of nucleic acid hybridization. *Critical Review in Biochemistry and Molecular Biology*, 36:227–259, 1991.

[43] S. Hoops, S. Sahle, R. Gauges, C. Lee, J. Pahle, N. Simus, M. Singhal, L. Xu, P. Mendes, and U. Kummer. COPASI–a COmplex PAthway SImulator. *Bioinformatics*, 22:3067–3074, 2006.

[44] G. Seelig and D. Soloveichik. Time-complexity of multilayered DNA strand displacement circuits. In R. Deaton and A. Suyama, editors, *DNA Computing and Molecular Programming 15*, volume LNCS 5877, pages 144–153. Springer, 2009.